Aus dem

Department für Anatomie

Institut für Klinische Anatomie und Zellanalytik

der Universität Tübingen

# Aquaporin-4 in the Human Choroid Plexus – Histological and *in vitro* Studies in Newly Established Human Primary Culture Models

Inaugural-Dissertation
zur Erlangung des Doktorgrades
der Medizin

der Medizinischen Fakultät
der Eberhard Karls Universität
zu Tübingen

vorgelegt von
Bihlmaier, Ronja

2024

Dekan: Professor Dr. rer. nat. Bernd Pichler

1. Berichterstatter: Professor Dr. med. Bernhard Hirt
2. Berichterstatter: Professor Dr. rer. nat. Peter Loskill

Tag der Disputation: 21.02.2025

Diese Arbeit ist meinen Eltern Ruth und Christof gewidmet, die mich mit ihrer grenzenlosen Unterstützung und ihrem Vertrauen in mich und meine Entscheidungen da hingebracht haben, wo ich heute bin.

## Table of contents

I. List of figures 4

II. List of tables 6

III. Abbreviations 7

1 Introduction 8

1.1 The cerebrospinal fluid system 9

1.2 The choroid plexus 11

1.3 Choroid plexus culture models 12

1.4 Aquaporins 13

1.4.1 AQP4 14

1.4.2 AQP4 regulation 15

1.4.3 AQP4 polarity 16

1.5 Physiology of CSF secretion 18

1.6 Ageing and disease 19

1.7 Aim of this research 20

2 Material 21

2.1 Mice 21

2.2 Human body donors 21

2.3 Chemicals and reagents 22

2.4 Buffer and solutions 24

2.5 Consumables 25

2.6 Antibodies for immunohistochemical stainings 26

2.6.1 Primary antibodies 26

2.6.2 Secondary antibodies 27

2.7 Software 27

2.8 Devices 28

3 Methods 29

3.1 Preparation 29

3.1.1 Murine specimen 29

3.1.2 Human specimen 30

3.2 Cultivation 30
3.2.1 Tissue culture 30
3.2.2 Dissociation culture 31
3.2.3 Coatings 32
3.2.4 Passaging 32
3.2.5 Cryopreservation 33
3.3 Immunohistochemistry 33
3.4 Hypoxia experiments 34
3.5 Imaging 35
3.6 Statistics 35
4 Results 36
4.1 Structure of the human CP and its attachment zone 36
4.2 AQP4 and the dystrophin glycoprotein complex (DGC) 40
4.3 Overview of CP cultures and murine experiments 42
4.3.1 Murine CP explant culture 42
4.3.2 Murine primary CP dissociation culture 44
4.4 Human CP explant culture 46
4.5 Human primary CP dissociation culture 50
4.5.1 Establishing the culture protocol: 50
4.5.2 Growth properties of human primary dissociation cultures 53
4.5.3 Identification of cell types 57
4.5.4 Expression of functional proteins on CPECs in vitro 59
4.5.5 Effect of serum-free medium on protein expression 61
4.6 Effect of hypoxia on AQP4 expression 62
4.6.1 Hypoxia treatment of human CP explant cultures 62
4.6.2 Hypoxia treatment of human primary CP dissociation culture 66
5 Discussion 69
5.1 Establishment and characterization of the cultures 69
5.1.1 Cell proliferation 69
5.1.2 Characterization of CP cell types 70
5.1.3 Effects of collagen and laminin coating on the cultures 71
5.2 Advantages and challenges of primary cell cultures 72

5.3 Regulation of AQP4 expression in CPECs ____ 73
5.3.1 Regulation of AQP4 by the basal lamina and DGC anchoring ____ 74
5.3.2 Effect of hypoxia on AQP4 expression ____ 76
5.3.3 AQP4 on murine culture ____ 77
5.4 Functional implications of AQP4 in the ageing CP and *Taenia choroidea* ____ 78
5.5 Implications for Alzheimer's disease ____ 80
6 Conclusion ____ 81
7 Deutsche Zusammenfassung ____ 84
8 Literaturverzeichnis ____ 87
9 Erklärung zum Eigenanteil ____ 97
10 Veröffentlichungen ____ 99
11 Danksagung ____ 100

# I. List of figures

Figure 1: Updated schematic description of the glymphatic system (2022)..... 10
Figure 2: Diagram showing the presumed molecular basis for the enrichment of AQP4 in perivascular and subpial membranes. ..... 17
Figure 3: Overview of macroscopy and microscopy of the human choroid plexus (CP) and its attachment zone, including expression patterns of AQP1 and AQP4..... 37
Figure 4: Subependymal tissue in the transitional zone is formed by astrocytes. ..... 38
Figure 5: Identification of cell types in human CP tissue. ..... 39
Figure 6: Expression of AQP4 and the DGC components dystrophin (Dp) and β-dystroglycan (β-DG) in the human CP epithelium. ..... 40
Figure 7: Expression of AQP4 and the DGC components dystrophin (Dp) and β-dystroglycan (β-DG) in the human *Taenia choroidea.* ..... 41
Figure 8: Overview of the culture methods used for this study. ..... 42
Figure 9: Murine CP explant culture after 17 days *in vitro* (div) in serum-supplemented medium. ..... 43
Figure 10: Characterization of AQP4-positive CPECs in murine explant cultures. ..... 44
Figure 11: Murine primary CP dissociation culture – the effect of cytosine arabinoside (AraC) and immunofluorescence staining of ZO-1 and TTR. ..... 45
Figure 12: Transmitted light image of human CP explant culture after 19 div. . 46
Figure 13: ZO-1 and AQP4 expression in fixed human CP compared to human CP explant culture. ..... 47
Figure 14: AQP1 and AQP4 expression in fixed human CP tissue compared to human CP explant culture. ..... 48
Figure 15: NKA and AQP4 expression in fixed human CP tissue compared to human explant culture. ..... 49
Figure 16: Effect of AraC on human primary dissociation cultures on laminin coating. ..... 51
Figure 17: Iba-1-positive macrophages in primary human dissociation cultures without AraC. ..... 52

Figure 18: Timeline of steps and observations in human primary CP dissociation cultures. ..... 53
Figure 19: Human primary CP dissociation culture on collagen coating. ..... 55
Figure 20: Human primary CP dissociation culture on laminin coating. ..... 56
Figure 21: Identification of CPECs. ..... 58
Figure 22: Human primary dissociated CPECs cultured on both laminin and collagen express ZO-1 and AQP4 at cell-cell contact sites. ..... 60
Figure 23: Dissociated human primary CPECs cultured on both laminin and collagen coating express NKA and AQP1. ..... 61
Figure 24: Effect of hypoxia on AQP4 expression in human CP explant cultures. ..... 62
Figure 25: Effect of hypoxia on AQP4 expression in human CP explant cultures over time. ..... 64
Figure 26: Effect of hypoxia on AQP4 expression in human CP explant cultures of ID H102 and H103. ..... 65
Figure 27: Verification of hypoxic in vitro conditions in human primary CP dissociation culture. ..... 66
Figure 28: Comparison of AQP4 and ZO-1 expression on hypoxia-treated human primary CP dissociation culture with a control group. ..... 67
Figure 29: Effect of hypoxia on AQP4 expression in human CP dissociation culture. ..... 68
Figure 30: Schematic illustrations summarizing AQP expression in the ependyma, the CP and the trans-itional zone, in addition to changes that occur during ageing ..... 79

## II. List of tables

Table 1: Human specimen ..... 22
Table 2: Chemicals and reagents for tissue preparation and cell culture..... 22
Table 3: Chemicals and reagents for immunohistochemical stainings..... 23
Table 4: Buffer and media..... 24
Table 5: Consumables ..... 25
Table 6: Primary antibodies ..... 26
Table 7: Secondary antibodies..... 27
Table 8: Software ..... 27
Table 9: Devices..... 28
Table 10: Overview of the impact of different media tested on murine cultures. ..... 45
Table 11: Numbers of AQP4-positive CPECs (in % of total CPECs per region) in human CP explant cultures treated with hypoxia compared to a control group. 63
Table 12: Numbers of AQP4-positive CPECs (in % of total CPECs per region) in human primary CP dissociation cultures treated with hypoxia compared to a control group. ..... 68

## III. Abbreviations

| | |
|---|---|
| Aβ | β-amyloid |
| AD | Alzheimer's disease |
| AraC | cytosine arabinoside |
| AQP | aquaporin |
| BBB | blood-brain barrier |
| BCSFB | blood-CSF barrier |
| CHIP | channel-forming integral membrane protein |
| CSF | cerebrospinal fluid |
| CNS | central nervous system |
| CP | choroid plexus |
| CPEC | choroid plexus epithelial cell |
| DG | dystroglycan |
| DGC | dystrophin-glycoprotein complex |
| div | days *in vitro* |
| DMEM | Dulbecco's Modified Eagle Medium |
| Dp | dystrophin |
| hEGF | human epidermal growth factor |
| FCS | fetal calf serum |
| GFAP | glial fibrillary acidic protein |
| HBSS | Hanks' Balanced Salt Solution |
| IGF | insulin-like growth factor |
| NKA | $Na^+/K^+$-ATPase |
| NKCC1 | $Na^+/K^+/2Cl^-$ -cotransporter |
| OAP | orthogonal arrays of particles |
| (D)PBS | (Dulbecco's) phosphate buffered saline |
| PCNA | proliferating-cell-nuclear-antigen |
| SAS | subarachnoidal space |
| TTR | transthyretin |
| ZO-1 | zonula occludens 1 |

# 1 Introduction

The human brain is a highly complex and vulnerable organ that requires special protection from both mechanical and chemical stress. In addition to the protection provided by the skull, the brain has two unique features that fulfill this vital role. First, the central nervous system (CNS) is isolated from the bloodstream by the blood-brain barrier (BBB). The BBB is primarily maintained by two cell types, the tightly sealed endothelial cells of the cerebral vasculature and astrocytes [1]. Astrocytic endfeet almost completely envelop the capillaries of the brain, thus mediating between the neuronal circuit and the blood. This barrier protects the brain from harmful substances such as toxins, drugs, pathogens, and inflammation. It also allows the endothelial cells to tightly regulate CNS homeostasis, which is essential for optimal neuronal function [1]. Second, the brain has developed a unique fluid system, historically referred to as the 'third circulation' of the body (the first being the blood and the second the lymph system) [2]. This system contains a secreted fluid, called cerebrospinal fluid (CSF). Its composition is regulated by another barrier, the blood-cerebrospinal fluid barrier (BCSFB) [3]. Among the first functions of CSF to be described was its role in mechanically protecting the brain by acting as a cushion between the brain tissue and the rigid skull. In addition, the fluid provides buoyancy, reducing the effective weight of the brain by more than 60% [4]. In the early 20$^{th}$ century, Stern and Gautier proposed a nutritive role for CSF [5]. Further research has shown that CSF contains several essential substances such as micronutrients, ions, vitamins and peptides. While most nutrients enter from the blood under the strict regulation of the BBB, it has been shown that certain molecules cannot diffuse sufficiently across this barrier and are therefore dependent on CSF distribution [6]. A paradigm shift in the understanding of the importance of CSF occurred with the discovery that it recirculates into the brain's interstitial fluid and thus assists in the clearance of metabolic waste products and toxic protein aggregations [7]. This is particularly important because the brain lacks a lymphatic vasculature that would efficiently remove aggregates in peripheral tissues. Protein accumulation is one of the causes of many neurodegenerative diseases and brain function disorders. This clearance

system of the brain, referred to as the glymphatic system (recently reviewed in [8]), is therefore vital and could play an important role in understanding neurodegeneration and developing therapies.

### 1.1 The cerebrospinal fluid system

The human brain and spinal cord are surrounded by approximately 150 ml of CSF, about 20% of which are contained in the four ventricular cavities [9]. CSF secretion and clearance from the CNS is commonly reported to be a minimum of 500 ml per day, suggesting a replacement rate of 3 to 5 times per day [10, 11]. Interestingly, CSF secretion increases during the night, suggesting a circadian rhythm [12]. In addition, the glymphatic drainage pathway has also been shown to be primarily active during sleep, proposing a new restorative function for sleep [13]. The choroid plexus (CP) is generally accepted as the primary site of CSF production. Alternative sources such as the ependymal lining or the BBB have been proposed, but their contribution is estimated to be less than one third [14]. CP tissue is located in all four ventricles of the human brain. CSF produced in the lateral ventricles flows through the foramen of Monro into the third ventricle. The third and fourth ventricles are then connected by the aqueduct of Sylvius. CSF leaves the inner ventricular system through the foramina of Luschka and Magendie and enters into the subarachnoidal space (SAS) [15]. The SAS maintains direct communication with the perivascular space (also known as Virchow-Robin space), which in turn communicates with the perineuronal space (Figure 1A), [16, 17]. As astrocytes form a barrier between the perivascular space and the neuropil, bulk water flow into the neuronal interstitium is thought to be mediated by the water channel aquaporin-4 (AQP4), which is abundantly expressed on astrocytic endfeet (Figure 1A) [18]. The CSF reuptake pathway is being controversially discussed. While many textbooks still refer to specialized structures - called arachnoid granulations - that extend into the venous sinuses, Proulx [19] claims that there has never been solid evidence that tracers in vivo drain directly from the SAS into the blood. A widely supported theory is a dual outflow model with drainage in both meningeal lymphatic [20] and venous vessels (Figure 1C).

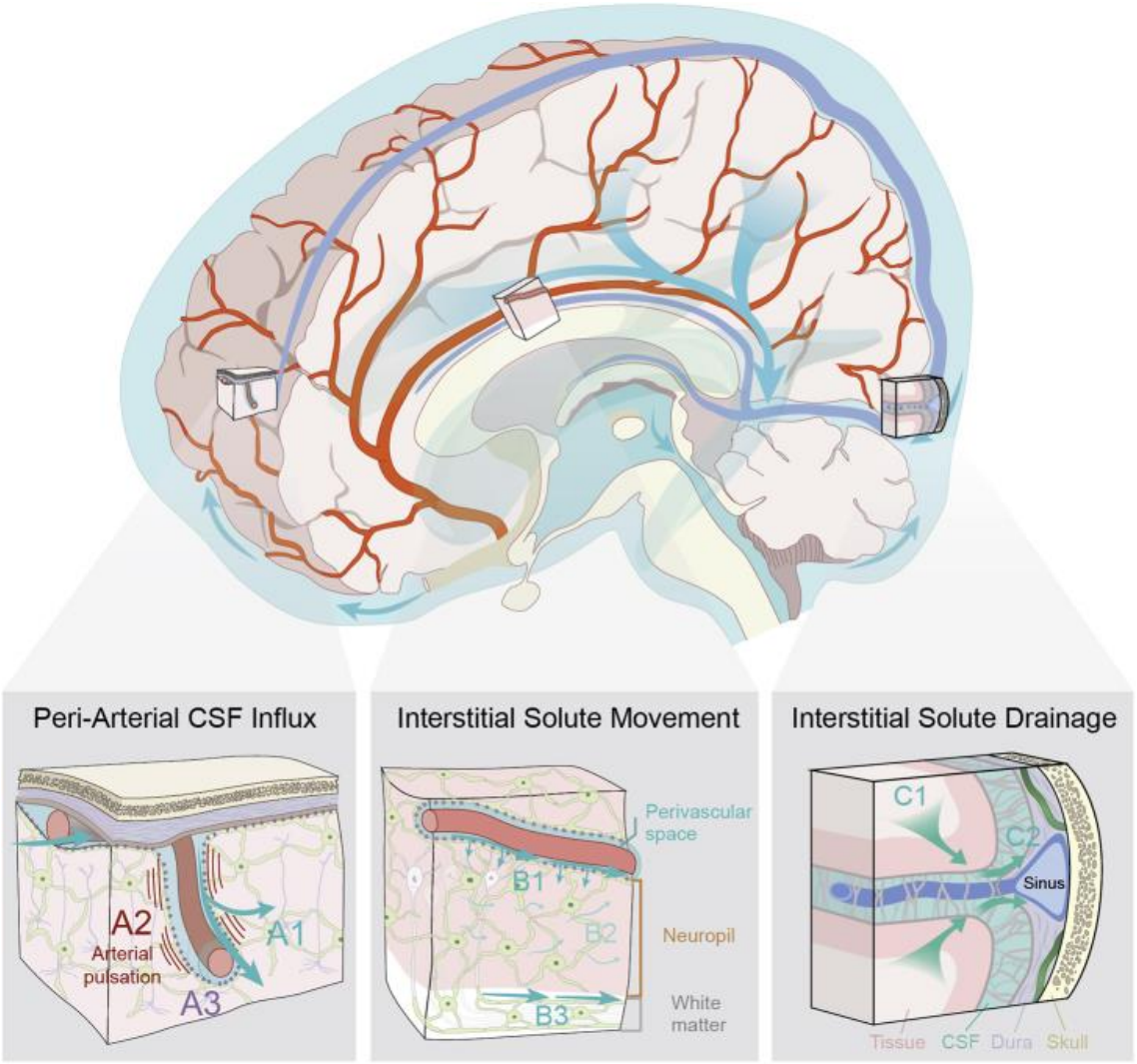


*Figure 1: Updated schematic description of the glymphatic system (2022)*

*The glymphatic system supports the perivascular exchange of CSF and interstitial solutes throughout the CNS. This process occurs over macroscopic anatomical scales, within the perivascular influx of subarachnoid CSF into brain tissue organized along the scaffold of the arterial vascular network, and the efflux of interstitial solutes occurring toward cisternal CSF compartments associated with dural sinuses.*

*(A) CSF influx into brain tissue occurs along perivascular pathway surrounding penetrating arteries (A1) and is driven in part by arterial pulsation (A2). Perivascular bulk flow and interstitial solute clearance are dependent upon the astroglial water channel AQP4 localized to perivascular astroglial endfeet surrounding the cerebral vasculature (A3).*

*(B) Interstitial solute movement occurs through the combined effects of diffusion and advection. Advection is most rapid along privileged anatomical pathways, including intraparenchymal perivascular spaces (B1) and white matter tracts (B3), and supports the movement of large molecular weight solutes. Diffusion dominates the movement of small molecules, particularly within the wider interstitium (B2).*

*(C) Interstitial solutes drain from the parenchyma along white matter tracts and draining veins towards sinus-associated cisternal CSF compartments (C1). CSF solutes are cleared from the cranium via uptake into meningeal lymphatic vessels, by efflux through dural arachnoid granulations, or through clearance along cranial or spinal nerve sheathes (C2).*

*With permission from [21].*

## 1.2 The choroid plexus

The choroid plexus (CP) is a highly specialized structure that extends into the ventricles of the brain. Its architecture is closely related to its functions. The organ consists of an extensive vascular plexus covered by a thin sheet of stroma and a single layer of epithelial cells [15]. The high vascularization of the CP tissue results in a blood flow 10 times higher than that of the cerebral cortex [22]. Unlike the rest of the brain, where capillaries are tightly closed, capillaries in the CP are fenestrated, sealed only by thin diaphragms. This feature allows the easy passage of ions, water and small molecules, facilitating CSF production [4]. Blood is supplied to the CP from the anterior and posterior choroidal arteries, which branch multiple times before entering the CP. Upon entry, these blood vessels are enveloped by meningeal tissue, which extends into the CP stroma. In addition, the connective tissue surrounding the CP capillaries contains fibroblasts and immune cells, predominantly macrophages. These macrophages play an important role in the response of the CNS to neuroinflammation [23]. The human CP of all four ventricles has numerous folds with prominent villi, which significantly increase the surface area of the organ. This surface is covered by an epithelial lamina that defines the boundary between the CP stroma and the ventricular cavities. As the BBB is interrupted within the CP, CP epithelial cells (CPECs) form a blood-cerebrospinal fluid barrier (BCSFB) by tightly interconnecting through junctional complexes consisting of tight junctions, adherens junctions and desmosomes [15]. This feature also creates and maintains apicobasal polarity, which is critical for many epithelial functions. Furthermore, CPECs demonstrate characteristic features of secretory cells [15]. They are rich in mitochondria, have abundant Golgi apparatus and vesicles, and display dense microvilli on their apical side, increasing the cell surface area [24]. This expansion provides space for abundant membrane proteins that are involved in the regulation of secretion and CSF composition, which will be described in more detail in a later section. At least 47 solute transporters have been identified in the CP epithelium, including numerous ion exchangers and transporters for amino acids, glucose, glutamate, transthyretin, transferrin, metal ions and fatty acids [25]. A variety of

efflux transporters and metabolizing enzymes contribute to the neuroprotective function of the BCSFB [25]. Furthermore, CPECs express a variety of receptors and interactive molecules. For example, cell adhesion molecules facilitate the migration of immune cells and are thus involved in the immunosurveillance of the CNS [26]. Several hormone receptors have also been identified, some of which directly influence CP functions, such as the modulation of circadian rhythms by sex hormones [27], while others facilitate the passage of hormones into the brain [28]. In addition to its role as a selective barrier, the CP epithelium also produces substrates that are secreted, such as growth factors, transcription factors and chemokines, and thus plays an important role throughout brain development [29].

The transition zone between CP tissue and the adjacent thalamic region, also referred to as *Taenia choroidea*, consists of a dense network of astrocytes. In the superficial region of the transition zone, the epithelial cell lining extends directly into the ependymal layer, which covers the rest of the ventricular surface [30]. Although both cell types are derived from neuroepithelium, they differ in their properties. CPECs rest on a basal lamina that disappears where the ependymal cell line begins. Ependymal cells share features with astrocytes, such as the expression of glial fibrillary acidic protein (GFAP) and AQP4 [30]. Cilia are rarely observed on CPECs, but frequently on ependymal cells [31].

### 1.3 Choroid plexus culture models

Culture models can generally be divided into primary cultures, which are obtained directly from the tissue of interest, and cell lines, which are immortalized and can be passaged infinite times [32]. Additionally, pluripotent stem cells can be used to generate organoids *in vitro* [33]. Each of these culture models has distinct advantages and disadvantages and their suitability depends on the specific research aim. Over time, numerous CP culture models have been established. An overview can be found in the reviews by Strazielle et al. [34] and Dabbagh et al. [35]. It is striking that there is a much greater abundance of animal CP culture models compared to human CP culture models, especially in the field of primary cultures. There have been previous

attempts to keep primary human CPECs in culture. In 1949, Hogue had access to and used human fetal brains to observe growth in explanted choroid plexus *in vitro* [36]. 26 years later, Wroblewska et al. isolated brain cells from various regions, including CP, and used tissue from patients' autopsies and biopsies, in an effort to study cells in culture [37]. The authors describe CP cells as 'bipolar spindle-shaped', and in a follow-up study as 'choroid plexus fibroblastic cells' since they were positive for fibronectin [38]. This indicates that these adult human CP cultures were dominated by fibroblasts with no specific identification of epithelial cells. These early approaches were not pursued, possibly because of the high variability between the cultures and because human primary CP tissue is difficult to obtain due to its central location in the brain and rare indications for surgical excision [39]. To overcome this challenge, human CPECs have later been cultured as cell lines, derived from CP carcinoma and papilloma [40-42]. Additionally, a stem cell derived human CP organoid model has recently been developed [43]. Primary cultures of CPECs have been established from a variety of animal species including rodents [44-49], bovine [50], porcine [51, 52] and non-human primate species [53]. These culture models have been a valuable tool for many studies. However, there are significant differences between animal and human CP, which can make the translation of results to humans challenging. For example, the murine lateral CP appears as a thin sheet, whereas the human lateral ventricular CP has a complex, three-dimensional structure with extensive stromal areas. Species related differences also extend to genetic expression in CP tissue [54], which emphasizes the need for a human model to study human phenomena.

### 1.4 Aquaporins

Water moves across epithelia by either paracellular or transcellular pathways, depending on the density of the epithelium. In the case of the CP epithelium, water movement is primarily transcellular due to the tight intercellular junctions that form the BCSFB [15]. The phospholipid bilayer of the cell membrane has low permeability to water molecules by simple diffusion. It was not until 1988 that Peter Agre discovered a channel-forming integral membrane protein (CHIP), which was proposed to explain the capacity for extremely rapid fluid

transport of most human tissues [55]. Subsequently, CHIP was renamed ‘aquaporin CHIP’ to align it with a group of structurally and functionally related proteins [56, 57]. Since then, thirteen human aquaporins have been characterized [58]. All aquaporins are small proteins of approximately 30 kDa, with a secondary protein structure consisting of six alpha-helices connected by five loops [59]. In the membrane, four monomers form a homotetrameric structure [60]. Aquaporins can be divided into three subgroups. They all share a high water permeability of up to 3 x $10^9$ water molecules per monomer per second [59]. Classical aquaporins differ from the group of aquaglyceroporins (AQP3, AQP7, AQP9 and AQP10) in their selectivity: aquaglyceroporins also allow glycerol and certain small neutral solutes to pass [61]. AQP11 and AQP12 form the superaquaporin subgroup, created because of their minimal homology with the previous subfamilies [62]. Among the aquaporins expressed in the CNS, AQP1, AQP4 and AQP9 are the most abundant ones. While AQP1 and AQP4 are primarily associated with CSF homeostasis, AQP9 is thought to be involved in the energy metabolism of the brain [63]. The first localization of AQP1 (then known as CHIP) was in the apical domain of rat CPECs [64], which was later confirmed for human CPECs with an additionally much weaker basolateral expression [65]. Several studies have suggested an important role for AQP1 in CSF formation. For example, Oshio et al. found a significantly reduced CSF production and intraventricular pressure in AQP1-deficient mice [66].

### *1.4.1 AQP4*

AQP4 was first discovered in the brain in 1994 and has been identified as the predominant water channel of this organ [67, 68]. AQP4 expression was subsequently localized in astrocytes, radial glia and ependymal cells, all of which can be classified as astroglial cells. In addition, Deffner et al. recently discovered AQP4 expression on human CPECs, while it has not been found on these cells in mice under physiological conditions [69]. Notably, AQP4 is the only aquaporin that forms a supramolecular structure within the cell membrane. In 1998, previously known structures called orthogonal arrays of particles (OAPs) were labeled with AQP4 antibodies for the first time [70]. These OAPs

were originally used as markers for astrocytes [71, 72]. In the murine brain, OAPs were also identified at high frequency on ependymal cells and some in the transition zone between ependyma and CP epithelium, whereas they were absent on CPECs [73]. Notably, the same study that recently reported AQP4 on human CPECs also found OAPs on these cells [69]. The arrangement of AQP4 molecules to these higher order aggregates has been suggested to depend on the composition of the different AQP4 isotypes. These isotypes result from distinct translational mechanisms. The first isoforms discovered were M1 and M23. A leaky scanning translational mechanism produces a shorter form (M23) that starts at Met-23 instead of Met-1 as in the full-length M1 isoform [72, 74]. Studies have shown that the M1 isoform does not form OAPs in contrast to the M23 isoform. In cells expressing both isotypes, the size of OAPs in rat cultures has been described to depend on the M1/M23 ratio [75, 76]. A more recently discovered AQP4 isoform is the extended AQP4, referred to as AQP4ex. AQP4ex is generated by translational readthrough, resulting in a C-terminal polypeptide extension. In experiments with transfected cells, the extended isoform M23ex formed clusters that were smaller and more uniform compared to M23 OAPs [77].

### *1.4.2 AQP4 regulation*

Many different endogenous mechanisms have been suggested to play a role in AQP4 regulation. This section will provide a brief overview using a few examples. Starting with the transcriptional level, several transcription factors have been identified in the regulation of AQP4. For example, the hypoxia-inducible factor-1α (HIF-1α) has been shown to increase both AQP4 mRNA and protein levels [78]. Physiologically, HIF-1α is significantly upregulated under conditions of hypoxia. Interestingly, Trillo et al. recently demonstrated an increase in AQP4 mRNA and protein levels in CP tissue under hypoxic conditions [58]. On the translational level, several studies have shown that different endogenous microRNAs specifically target AQP4 mRNA and thereby repress AQP4 translation [79]. Post-translationally, AQP4 expression in the plasma membrane can be regulated by protein trafficking between cellular compartments. AQP4 trafficking is affected by both direct and indirect

mechanisms. For example, direct binding of calmodulin induces a conformational change, promoting the localization of AQP4 to the cell surface [80]. Phosphorylation of AQP4 contributes directly or indirectly to AQP4 trafficking [81]. For example, protein kinase A [82] and C [83] have both been implicated in phosphorylation-induced internalization of AQP4. In addition to affecting the amount of AQP4 molecules in the membrane, phosphorylation and other mechanisms can also modulate the water transport capacities and functionality of AQP4 [84].

### *1.4.3 AQP4 polarity*

In their initial studies, Iliff et al. suggested a central role for astrocytic AQP4 in the glymphatic clearance pathway. Their studies with AQP4-deficient mice, also termed AQP4 knockout mice, showed approximately 70% reduced solute clearance in these animals' brains [7]. In most astrocytes, AQP4 shows polarized expression with increased density in the perivascular and subpial endfeet regions [7], whereas its presence in astrocytic somas and perineuronal processes remains low to undetectable [85, 86]. The functionality of AQP4 on these cells is dependent on this specific expression pattern, as a loss of polarization has been linked to several pathologies such as edema formation in tumors [87]. Various lines of evidence have been presented that the polar expression of AQP4 is mediated by an anchoring complex, called the dystrophin glycoprotein complex (DGC) [88-90], which is equally enriched in astrocytic endfeet [91]. For example, the absence of the DGC protein α1-syntrophin led to a 90% reduction of AQP4 in the astrocytic endfeet through redistribution without altering total AQP4 levels [92]. The DGC includes several proteins that link the cytoskeleton to the extracellular matrix. More specifically, laminin and agrin, which are components of the basal lamina are connected through α-dystroglycan (DG) to β-DG, a transmembrane protein that interacts with dystrophin (Dp) (Figure 2). On the intracellular side, Dp associates with dystrobrevin, which can bind up to four syntrophin molecules. Syntrophins are a group of five proteins that can recruit membrane proteins such as channels (including AQP4), receptors, kinases and more [92]. Figure 2 shows a schematic representation of the complex.

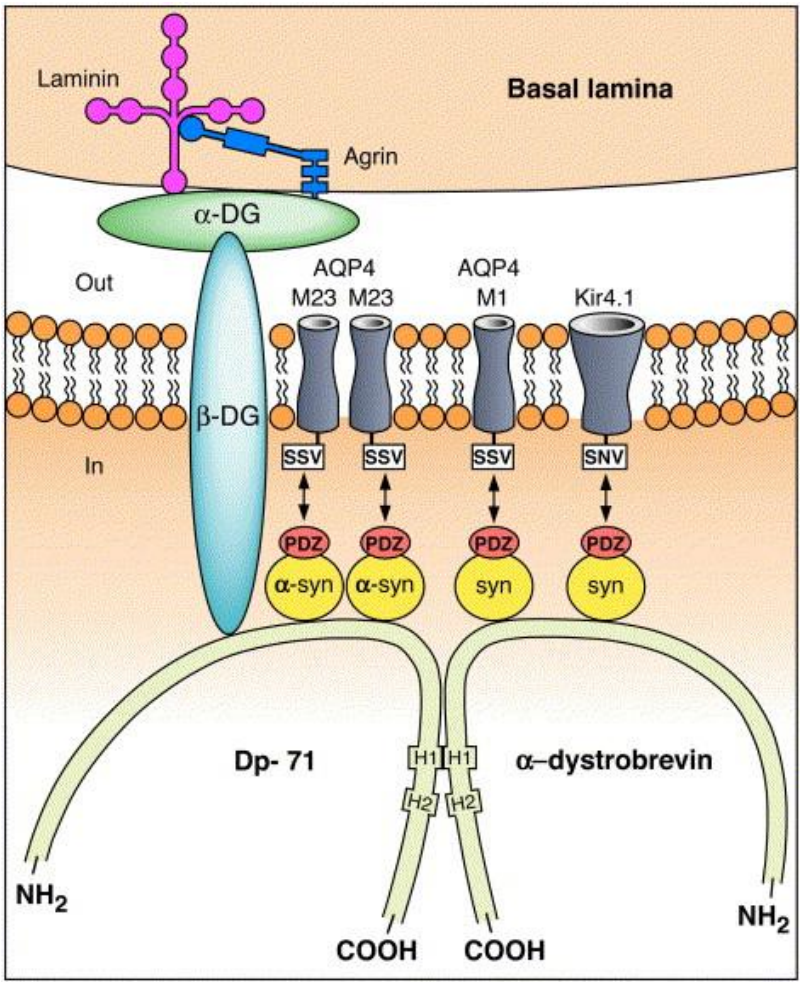


*Figure 2: Diagram showing the presumed molecular basis for the enrichment of AQP4 in perivascular and subpial membranes.*
*The dystrophin complex is anchored to the basal lamina through laminin and agrin and binds AQP4 (and possibly other molecules with a C-terminal SXV sequence like Kir4.1) by way of α-syntrophin (α-syn) or other syntrophins (syn). The coupling between AQP4 and syn may be indirect (indicated by double arrows). We assume that α-syn is crucially involved in the anchoring of the M23 isoform of AQP4 (as M23 is the isoform that forms orthogonal arrays of proteins, particularly enriched in endfeet membranes; Wolburg, 1995). Other syn may be primarily involved in the anchoring of the M1 isoform (which does not form OAPs; Furman et al., 2003). It should be understood that the identity and stoichiometry of the SXV-containing membrane molecules (SSV for AQP4; SNV for Kir4.1) may vary according to region, cell type, and membrane domain. α-DG and β-DG, α and β dystroglycan; Dp-71, major dystrophin isoform in brain. The PDZ binding domains of syn are indicated. H1 indicates the coiled-coil motif interaction between Dp71 (the major dystrophin isoform in brain) and α-dystrobrevin (Sadoulet-Puccio et al., 1997).*
*With licensed permission from [86]*

The regulation of AQP4 polarity has also been linked directly to laminin and agrin. For example, a loss of agrin has been shown to induce a redistribution of AQP4 [87]. Additionally, studies in astrocyte cultures have provided evidence that the addition of laminin induces AQP4 clustering *in vitro* through the assembling of DGC components [89].

## 1.5 Physiology of CSF secretion

The precise molecular mechanisms underlying CSF production by the CPECs remain the subject of ongoing and unresolved debate, despite decades of extensive research recently reviewed by Rasmussen et al. [2]. A possible reason for this may be that CP epithelium differs from all other secretory epithelia in two important ways. First, paracellular transport is largely inhibited by the maintenance of the BCSFB, which restricts water flow primarily to transcellular pathways. Second, the expression pattern of transport proteins on CPECs is different from any other secretory epithelia [2]. In particular, the $Na^+/K^+$-ATPase (NKA) and the $Na^+/K^+/2Cl^-$-cotransporter (NKCC1) are both located apically rather than at the typical basolateral position [93, 94]. In the classic model of CSF secretion proposed by Saito and Wright in 1983, NKA plays a central role by actively transporting $Na^+$ directly into the CSF [95]. In coordination with other transporters and channels, this process establishes an electrochemical gradient that either directly or indirectly moves $Na^+$, $HCO3^-$ and $Cl^-$ across the basolateral membrane into the CPECs. Subsequently, these ions also exit apically into the CSF [15]. Currently, two different theories of apical NKCC1 function are discussed [96, 97]. One model, advanced by Gregoriades et al. [94], suggests that under basal conditions NKCC1 functions in a net influx mode, which is critical for maintaining the water volume essential for CSF secretion. In coordination with other transporters, an osmotic gradient is established, which drives water through AQP1 in the apical membrane [65]. In addition, as early proposed by Husted & Reed in 1976, this model suggests that both apically expressed NKA and NKCC1 contribute to the uptake of $K^+$ from the CSF [22, 98, 99]. This is particularly important as maintaining a low $K^+$ concentration is essential for optimal neuronal function with deviations potentially increasing neuronal excitability and precipitating seizures [100]. In contrast to these findings, Steffens et al. present an alternative perspective, suggesting an outwardly directed transport of $N^+$, $K^+$, and $Cl^-$ ions by the apical NKCC1 transporter. They propose a comparatively minor role for AQP1 in water secretion and suspect that water movement occurs along the co-transporter NKCC1 instead [101]. Both theories report a lack of information on how water

enters CPECs basolaterally. Challenging the established view that CPECs exclusively express AQP1, Deffner et al. found significant basolateral AQP4 expression in a large number of CPECs in the human brain [69]. Evidence for the presence of AQP4 in the CP was provided years ago by studies using *in situ* hybridization and Western blot analysis [102, 103]. Recent investigations by Trillo-Contreras et al. also reported AQP4 expression in murine CPECs after hypoxia exposure [63, 104], and suggested, that if basolateral water influx was mediated by aquaporins, AQP4 would be a good candidate [58].

### 1.6 Ageing and disease

The CP undergoes age-related changes. Epithelial cells lose apical microvilli, experience a reduction in volume and a decrease in the expression of key proteins such as AQP1 and NKA, which together result in a reduced CSF production [105]. In addition, a thickening of the CP stroma is observed, caused by the accumulation of collagen fibers and aggregations such as hyaline and psammoma bodies and calcifications. The arterial walls also become thicker [106, 107]. Together, these changes lead to an increased and more complicated diffusion pathway from the capillaries to the CPECs. Another change that occurs with age is brain atrophy, which causes an expansion of the ventricular volume. Combined with the reduced production rate, this results in a significantly prolonged CSF turnover time [108]. In line with the glymphatic pathway hypothesis, an increased turnover time may lead to a reduced clearance of metabolic waste from the brain parenchyma. Consequently, these processes may contribute significantly to the progression of many neurological diseases, particularly those characterized by solute accumulation. For example, in Alzheimer's disease (AD), a protein called β-amyloid (Aβ) is deposited in the interstitial space of the brain [109]. Studies have demonstrated that a reduced glymphatic clearance is associated with the accumulation of Aβ. This correlation is evident in AQP4-knockout mice, where glymphatic clearance is significantly reduced, resulting in Aβ aggregation [7, 110, 111]. Interestingly, it has also been shown that in AD mouse models a decrease of glymphatic clearance occurs prior to the accumulation of Aβ, suggesting that this could serve as an early biomarker for AD [112].

## 1.7 Aim of this research

A central goal of this study was to establish human primary CP culture models as a tool to investigate functional mechanisms such as the regulation of channel and transport proteins. Therefore, two different methods, explant tissue cultures and dissociation cultures, were used. After the characterization of the cultures and the confirmation of the expression of typical CPEC proteins, the effect of different *in vitro* conditions on cell growth, morphology and protein expression was systematically evaluated.

Following the recent discovery of AQP4 expression on human CPECs [69], the newly established CP culture models were used to further investigate this phenomenon and the underlying regulatory mechanisms. We hypothesized that hypoxic conditions could induce AQP4 expression in these cells, as a recent study reported AQP4 in CPECs of mice that had been exposed to hypoxia [63]. Additionally, we examined whether AQP4 expression would differ between dissociated CPECs cultured on laminin coating compared to collagen coating, as laminin coating has previously been reported to induce AQP4 clustering in astrocyte cultures [89].

An additional aim of this study was to provide an extended histological characterization of the human CP and its attachment zone to the surrounding brain tissue, which is referred to as *Taenia choroidea*. Therefore, several immunofluorescence stainings were performed on the CP and adjacent tissues from 13 human body donors. Given the known interactions between AQP4, the DGC and laminin, we specifically investigated potential correlations between the expression patterns of these proteins.

With our work, we hope to contribute to a deeper understanding of alterations in CSF homeostasis in the human brain and their potential implications for impaired brain clearance. Such insights may contribute to the understanding of the cellular processes underlying neurodegenerative diseases.

# 2 Material

## 2.1 Mice

CP tissue from C57BL/6 x C3H (Charles River WIGA GmbH, Sulzfeld, Germany) mice was used for tissue and cell cultures. Dr. rer. nat. Peter Neckel's group kindly provided us with the heads of animals, which were otherwise used for their experiments. The care and handling of the animals was in accordance with national guidelines for the ethical treatment of animals in scientific research. The euthanasia of the animals was performed strictly according to §4 (3) (notification number AT 01/19 M) of the Animal Welfare Act, as part of experiments conducted by Dr. rer. nat. Peter Neckel. The ethical approval required for this study was granted by the *Regierungspräsidium* of Tübingen. After euthanasia, the mouse brains were either immediately dissected for cell culture or fixed for later study.

## 2.2 Human body donors

Human CP tissue was obtained from individuals who generously donated their body to the Institute of Clinical Anatomical and Cell Analysis in Tübingen. The donors gave explicit, informed consent in accordance with the Declaration of Helsinki, allowing their body to be used for research purposes. For the cell culture experiments, CP tissue from three different donors was used (H101-H103). CP material from an additional group of 10 body donors was included for the histological characterization studies (see Table 2). The procedures for processing the corpses complied with the requirements of §42 para. 1-4 of the Burial Law of the State of Baden-Württemberg of the 21$^{st}$ of July 1970. After the death of the body donors, the corpses were rapidly transported to the institute within less than 12 hours *post mortem* if the tissue was used for cell culture. Immediate dissection and tissue processing were carried out. To ensure confidentiality, the name of each body donor was changed to an anonymized ID number. Approval for this project was obtained from the Ethics Committee of the Medical Faculty of the University of Tübingen on the 18$^{th}$ of November 2010 and documented under the project number 237/2007BO1.

*Table 1: Human specimen*

| ID | Age | Sex | *Post mortem* time (in hours) | Cell culture | Cause of death* |
|---|---|---|---|---|---|
| H38 | 85 | m | 11 | No | Renal failure |
| H65 | 83 | f | 15 | No | Lung cancer |
| H70 | 89 | m | 12 | No | Renal failure |
| H74 | 91 | f | 19 | No | Exsiccosis, gastrointestinal bleeding |
| H75 | 93 | m | 11 | No | Pneumonia |
| H77 | 75 | f | 8 | No | Stroke |
| H78 | 74 | f | 9 | No | Multiorgan failure |
| H84 | 94 | f | 11 | No | Cardiac arrest |
| H85 | 85 | m | 8 | No | Pneumonia |
| H86 | 86 | m | 12 | No | Renal failure |
| H101 | 80 | w | 10 | Yes | Cardiac arrest |
| H102 | 92 | m | 8 | Yes | Acute abdomen |
| H103 | 79 | m | 12 | Yes | Pneumonia & heart failure |

** Cause of death taken from the medical death certificate*

## 2.3 Chemicals and reagents

*Table 2: Chemicals and reagents for tissue preparation and cell culture*

| Substance | Specification | Supplier |
|---|---|---|
| DMEM (Dulbecco's Modified Eagle Medium) / F12 Nutrient Mix (Ham) 1:1 | Ref. No.: 21331-020 | gibco® (Life Technologies) now: Thermo Fisher Scientific (Waltham, MA, USA) |
| HBSS (Hanks' Balanced Salt Solution) | Ref. No.: H9394 | Sigma Aldrich Chemie GmbH (Taufkirchen, Germany) |
| DPBS (Dulbecco`s Phosphate Buffered Saline) | Ref. No.: D8537 | Sigma Aldrich Chemie GmbH (Taufkirchen, Germany) |
| Penicillin / Streptomycin | Ref. No.: P0781, (v/v) | Sigma Aldrich Chemie GmbH (Taufkirchen, Germany) |
| L-Glutamine | Ref. No.: G7513 | Sigma Aldrich Chemie GmbH (Taufkirchen, Germany) |
| FCS (Fetal Calf Serum, 100 x) | Ref. No.: S0613 | Biochrom GmbH (Berlin, Germany) |
| DMSO (Dimethyl sulphoxide) | Ref. No.: A3672 | AppliChem GmbH (Darmstadt, Germany) |

| | | |
|---|---|---|
| Collagenase type XI | Ref. No.: C9407,<br>750 U/ml | Sigma Aldrich Chemie GmbH<br>(Taufkirchen, Germany) |
| Dispase type II | Ref. No.: D4693,<br>250 µg/ml | Sigma Aldrich Chemie GmbH<br>(Taufkirchen, Germany) |
| DNase I | Ref. No.: DN25,<br>0,05% (w/v) | Sigma Aldrich Chemie GmbH<br>(Taufkirchen, Germany) |
| Trypsin | Ref. No.: 25300-054 | gibco® (Life Technologies)<br>now: Thermo Fisher Scientific<br>(Waltham, MA, USA) |
| hEGF (human Epidermal Growth Factor) | Ref. No.: E9644<br>20 ng/ml | Sigma Aldrich Chemie GmbH<br>(Taufkirchen, Germany) |
| IGF-1 (Insulin-like Growth Factor) | Ref. No.: 791-MG<br>20 ng/ml | R&D Systems<br>(Minneapolis, MN, USA) |
| AraC (cytosine arabinoside) | Ref. No: 147-49-4<br>20 µM | Sigma Aldrich Chemie GmbH<br>(Taufkirchen, Germany) |
| Trypan blue | Ref. No.: T8154 | Sigma Aldrich Chemie GmbH<br>(Taufkirchen, Germany) |
| Collagen type I (rat tail) | Ref. No.: 354234<br>3,3 ug/ml | BD Biosciences<br>(Heidelberg, Germany) |
| Laminin | Ref. No.: L2020<br>2 ug/ml | Sigma Aldrich Chemie GmbH<br>(Taufkirchen, Germany) |
| Poly-D-Lysin | Ref. No.: A38904-01,<br>LOT: 959890A<br>50 ug/ml | gibco® (Life Technologies)<br>now: Thermo Fisher Scientific<br>(Waltham, MA, USA) |
| CellTracker™ CM-DiI Dye | Ref. No.: C7000 | Molecular Probes<br>now: Thermo Fisher Scientific<br>(Waltham, MA, USA) |
| Image-iT™ Green Hypoxia Reagent | Ref. No.: I14834 | Thermo Fisher Scientific<br>(Waltham, MA, USA) |

*Table 3: Chemicals and reagents for immunohistochemical stainings*

| **Chemical or reagent** | **Supplier** |
|---|---|
| 4% PFA (paraformaldehyde) | AppliChem (Darmstadt, Germany) |
| NaCl | VWR International (Darmstadt, Germany) |
| $Na_2HPO_4$ x $2H_2O$ | Merck Chemicals (Darmstadt, Germany) |
| $KH_2PO4$ | Merck Chemicals (Darmstadt, Germany) |
| Bovine serum albumin | Carl Roth GmbH & Co. KG (Karlsruhe, Germany |
| Triton® X-100 | Carl Roth GmbH & Co. KG (Karlsruhe, Germany) |

| | |
|---|---|
| Goat serum | Biochrom (Berlin, Germany) |
| Donkey serum | Biochrom (Berlin, Germany) |
| TissueTek® | Sakura (Staufen, Germany) |
| DAKO Pen | Dako Denmark (Glostrup, Denmark) |
| MOWIOL® 4-88 | Carl Roth GmbH & Co. KG (Karlsruhe, Germany) |
| DRAQ5 (use 1:1000) | Thermo Fisher Scientific (Waltham, MA, USA) |
| DAPI (use 1:5000) | Carl Roth GmbH & Co. KG (Karlsruhe, Germany) |
| Phalloidin (use 1:4000) | BioLegend (San Diego, CA, USA) |
| Immersion oil (Immersol™ 518F) | Carl Zeiss AG (Oberkochen, Germany) |

## 2.4 Buffer and solutions

*Table 4: Buffer and media*

| | |
|---|---|
| Preparation medium: | Hanks' Balanced Salt solution<br>(+) 1% Penicillin/Streptomycin (v/v)<br>(-) $Ca^{2+}$ / $Mg^{2+}$ |
| Cell culture medium: | Dulbecco's Modified Eagle Medium<br>(+) F12 Nutrient Mixture (HAM)<br>(+) 1% L-Glutamin<br>(+) 1% Penicillin/Streptomycin<br>(+) 10% FCS<br>(-) HEPES |
| Freezing medium for Cryopreservation: | Dulbecco's Modified Eagle Medium<br>(-) L-Glu<br>(+) 20% FCS<br>(+) 10% Dimethyl sulphoxide |
| Phosphate buffered salt solution (PBS): | Distilled water<br>(+) 7% NaCl (w/v)<br>(+) 2,86% $Na_2HPO_4$ x $2H_2O$ (w/v)<br>(+) 0,4% $KH_2PO4$ (w/v) |
| Blocking solution: | PBS<br>(+) 0.1% Bovine serum albumin (v/v)<br>(+) 0.1% Triton® X-100 (v/v)<br>(+) 4% goat or donkey serum (v/v) |
| 4% PFA solution: | PBS<br>(+) 4% Paraformaldehyde |
| Collagenase type XI / Dispase type II solution | HBSS<br>(+) $Ca^{2+}$ / $Mg^{2+}$<br>750 U/ml Collagenase type XI<br>250 µg/ml Dispase type II |

## 2.5 Consumables

*Table 5: Consumables*

| Consumable | Specification | Supplier |
|---|---|---|
| Cellstar® Petri Dish 94x 16 mm | Ref. No.: 633180 | Greiner Bio-One GmbH (Kremsmünster, Austria) |
| Cellstar® Petri Dish 145x20 mm | Ref. No.: 639102 | Greiner Bio-One GmbH (Kremsmünster, Austria) |
| Falcon® / Costar® 6-Well Dish | 9,6 $cm^2$ | Corning Inc. (Corning, NY, USA) |
| Costar® 12-Well Dish | 3.8 $cm^2$ | Corning Inc. (Corning, NY, USA) |
| Costar® 24-Well Dish | 2 $cm^2$ | Greiner Bio-One GmbH (Kremsmünster, Austria) |
| Cellstar® Cell Culture Flask | 75 $cm^2$ | Greiner Bio-One GmbH (Kremsmünster, Austria) |
| Cellstar® 4-Well 'Nocken' Dish | 1 $cm^2$ | Greiner Bio-One GmbH (Kremsmünster, Austria) |
| Ibidi® µ-Slide 8 Well (high glass bottom) | Ref. No.: 80807 | ibidi GmbH (Gräfelfing, Germany) |
| Ibidi® µ-Slide 8 Well Grid-500 | Ref. No.: 80826-G500 | ibidi GmbH (Gräfelfing, Germany) |
| Millicell® Cell Culture Inserts | Ref. No.: PICM 03050 | Merck Millipore (Billerica, MA, USA) |
| Falcon™ Cell Strainer ø100 µm | Ref. No.: 352350 | Becton, Dickinson and Company (Franklin Lakes, NJ, USA) |
| Cellstar® Tubes | 15, 50 ml | Greiner Bio-One GmbH (Kremsmünster, Austria) |
| Falcon® Pipette 'Spacesaver' | 5, 10, 25, 50 ml | Corning Inc. (Corning, NY, USA) |
| Cover slips | 0,13-0,17 mm | R. Langenbrinck GmbH, (Emmendingen, Germany) |
| SuperFrost® Microscope Slides Plus | | R. Langenbrinck GmbH, (Emmendingen, Germany) |
| TipOne Pipette Tips | | STARLAB GmbH (Hamburg, Germany) |

## 2.6 Antibodies for immunohistochemical stainings

### *2.6.1 Primary antibodies*

*Table 6: Primary antibodies*

| Antibody | Supplier | Specification | Host animal | Dilution |
|---|---|---|---|---|
| ZO-1 | Thermo Fisher Scientific (Waltham, MA, USA) | 33-9100 | Mouse | 1:50 |
| AQP-4 | Santa Cruz Biotechnology (Dallas, TX, USA) | sc-20812 | Rabbit | 1:100 |
| AQP-4 | Santa Cruz Biotechnology (Dallas, TX, USA) | sc-9888 | Goat | 1:100 |
| AQP-1 | Thermo Fisher Scientific (Waltham, MA, USA) | PA5-78805 | Rabbit | 1:100 |
| AQP-1 | Santa Cruz Biotechnology (Dallas, TX, USA) | sc-32737 | Mouse | 1:100 |
| PCNA | Sigma Aldrich Chemie GmbH (Taufkirchen, Germany) | P8825 | Mouse | 1:100 |
| TTR | Sigma Aldrich Chemie GmbH (Taufkirchen, Germany) | SAB3500378 | Chicken | 1:250 |
| CD-31 | Abcam (Cambridge, England) | abcam28364 | Rabbit | 1:100 |
| GFAP | Santa Cruz Biotechnology (Dallas, TX, USA) | sc-58755 | Mouse | 1:100 |
| NKA | Hybridoma Bank (Iowa, USA) | a6F | Mouse | 1:100 |
| Iba 1 | FUJIFILM Wako Chemicals Europe GmbH (Neuss, Germany) | 019-19741 | Rabbit | 1:100 |
| NKCC1 | Abcam (Cambridge, UK) | ab59791 | Rabbit | 1:100 |
| Dp | Abcam (Cambridge, UK) | ab15277 | Rabbit | 1:100 |
| ß-DG | Abcam (Cambridge, UK) | ab49515 | Mouse | 1:100 |
| Laminin | Abcam (Cambridge, UK) | ab11575 | Rabbit | 1:100 |
| Ki-67 | Dako (Hamburg, UK) | M 7248 | Rabbit | 1:400 |
| HuCD | Invitrogen (CA, USA) now: Thermo Fisher Scientific (Waltham, MA, USA) | A21271 | Mouse | 1:100 |
| Vimentin | Santa Cruz Biotechnology (Dallas, TX, USA) | ec-6260 | Mouse | 1:100 |

### 2.6.2 Secondary antibodies

*Table 7: Secondary antibodies*

| Antibody | Company | Host animal | Dilution |
|---|---|---|---|
| Anti-rabbit Alexa 546 | Invitrogen (CA, USA) * | Goat | 1:400 |
| Anti-rabbit Alexa 488 | Invitrogen (CA, USA) * | Goat | 1:400 |
| Anti-rabbit Alexa 660 | Invitrogen (CA, USA) * | Goat | 1:400 |
| Anti-mouse Alexa 488 | Invitrogen (CA, USA) * | Goat | 1:400 |
| Anti-mouse Alexa 546 | Invitrogen (CA, USA) * | Goat | 1:400 |
| Anti-mouse Alexa 660 | Invitrogen (CA, USA) * | Goat | 1:400 |
| Anti-Mouse Alexa 546 | Invitrogen (CA, USA) * | Donkey | 1:400 |
| Anti-Goat Alexa 488 | Invitrogen (CA, USA) * | Donkey | 1:400 |
| Anti-Rabbit Alexa 647 | Invitrogen (CA, USA) * | Donkey | 1:400 |
| Anti-Rabbit Alexa 546 | Invitrogen (CA, USA) * | Donkey | 1:400 |
| Anti-chicken Alexa 488 | Invitrogen (CA, USA) * | Goat | 1:400 |

** Now: Thermo Fisher Scientific (Waltham, MA, USA)*

## 2.7 Software

*Table 8: Software*

| Software | Supplier |
|---|---|
| Zen black 2009 | Carl Zeiss AG (Oberkochen, Germany) |
| Zen blue 2012 | Carl Zeiss AG (Oberkochen, Germany) |
| Adobe Photoshop CS2 | Adobe Inc. (Mountain View, CA, USA) |
| Microsoft Word | Microsoft Corporation (Redmond, WA, USA) |
| RStudio | Posit PBC (Boston, MA, USA) |
| BioRender (www.biorender.com) | Science Suite Inc. (Toronto, ON, Canada) |

## 2.8 Devices

*Table 9: Devices*

| Device | Supplier |
|---|---|
| Binocular loupe: Leica 125M | Leica Microsystems GmbH (Wetzlar, Germany) |
| Incubator: Thermo Scientific™, Heta Cell 150 | Thermo Fisher Scientific (Waltham, MA, USA) |
| Confocal microscope LSM510 Meta | Carl Zeiss AG (Oberkochen, Germany) |
| Confocal microscope LSM Exciter | Carl Zeiss AG (Oberkochen, Germany) |
| LSM 900 (with Airyscan2)* | Carl Zeiss AG (Oberkochen, Germany) |
| Lattice Lightsheet* | Carl Zeiss AG (Oberkochen, Germany) |
| Axio Imager Z1 | Carl Zeiss AG (Oberkochen, Germany) |
| Cryotome: Leica CM3050 S | Leica Biosystems Nussloch GmbH (Nussloch, Germany) |
| Vortex mixer: Vortex Genie® 2™ | Scientific Industries Inc. (Bohemia, NY, USA) |
| Centrifuge: Thermo Scientific™ Heraeus™ Fresco™ | Thermo Fisher Scientific (Waltham, MA, USA) |
| Pipette: ErgoOne | STARLAB GmbH (Hamburg, Germany) |
| Neubauer counting chamber | Carl Roth GmbH & Co. KG (Karlsruhe, Germany) |
| Preparation Set with tweezers, scissors and scalpels | Bruno Baya GmbH (Tuttlingen, Germany) |

** Provided in the context of a workshop*

# 3 Methods

## 3.1 Preparation

### *3.1.1 Murine specimen*

Mice were euthanized by $CO_2$ inhalation followed by cervical dislocation with rapid and forceful extension of the animal's neck or by gently bending the head backwards. Animals were decapitated with scissors and the heads were placed in a petri dish. This was carried out by members of Dr. Neckel's research group. The following procedures were performed under sterile conditions in a laminar flow hood and the surfaces and heads of the animals were disinfected with 70% ethanol prior to dissection. Using a binocular dissecting scope and a preparation set with tweezers, scissors, and scalpels, the scalp was carefully removed from the dorsal skull. The skull was then secured with forceps and carefully opened along the sagittal suture from the *Foramen magnum* to the nasal bone. Fragments of the skull were carefully removed until the entire brain could be extracted, assisted by placing a spatula or forceps under the brain and gently lifting it. The brain was immediately transferred to a petri dish containing preparation buffer which completely covered the organ. Two precise cuts were then made with a scalpel. The first cut separated the cerebellum, and the second cut separated the two cerebral hemispheres along the *Fissura longitudinalis cerebri.* The lateral ventricles were accessed medially, using the anterior part of the *Corpus callosum* as orientation. The CP tissue within the lateral ventricles, which is a thin sheet, was carefully isolated with fine forceps and excised with small scissors. Access to the fourth ventricle was gained through the *Apertura mediana ventriculi cuarti.* The CP of the fourth ventricle is significantly larger than that of the lateral ventricles and is attached to the ventricle walls in several places, requiring careful dissection. CP tissue samples were collected in pre-warmed HBSS.

### *3.1.2 Human specimen*

The *post mortem* interval before tissue collection was less than 12 hours. The donor body was placed in the supine position with the head resting on a headrest. First, the hair was removed from the scalp with a razor. A coronal incision was then made with a scalpel at the level of the sagittal suture. The tissue was cut down to the skull and pulled off dorsally to the lower end of the occipital bone. Next, the skull was opened with a bone saw and removed, carefully separating the bone from the dura mater. The *Medulla oblongata* and cranial nerves were dissected with a scalpel, allowing the brain to be completely removed from the calvaria. All previous steps were carried out with the help of the prosectional staff. For the dissection of the CP within the third and lateral ventricle, the brain was carefully sectioned along the *Fissura longitudinalis cerebri*, cutting the *Corpus callosum*, the *Septum pellucidum* and the *Fornix* with a scalpel. This exposed the third ventricle from above. Access to the lateral ventricles was gained through the interventricular foramen. The CP was carefully removed with a scalpel and transferred into a 50 ml tube filled with sterile preparation buffer. Then, the fourth ventricle CP was located and dissected at the *Aperturae laterales ventriculi quarti* where it builds a structure called *Bochdalek's flower basket*. All subsequent procedures were carried out under sterile laboratory conditions. Prior to dissection, all surfaces of the laminar flow hood were disinfected with 70% ethanol. CP tissue was transferred to petri dishes containing preparation buffer and dissected under a binocular loupe. A small piece of each CP was immediately fixed for histology.

## 3.2 Cultivation

### *3.2.1 Tissue culture*

For the explant cultures, 6-Well dishes with PTFE (polytetrafluoroethylene) membrane inserts were used. To maintain optimal conditions, 1.5 ml of culture medium was added to each well, ensuring that the medium level exceeded the height of the insert membrane to prevent the membrane from drying out. For murine explant cultures, the CPs were whole-mounted on the membranes. For

human explant cultures, small pieces of 2-3 mm in length were excised from epithelial regions and carefully placed on the membranes.

### *3.2.2 Dissociation culture*

For murine dissociation cultures, CP material was collected from 5 mice. In the case of human dissociation cultures, each CP was initially carefully dissected. The epithelial regions were separated from the stroma and vasculature, and only the epithelial regions were subsequently included in the dissociation process. The collected tissues from either murine or human specimens were transferred to HBSS solution containing $Ca^{2+}$ and $Mg^{2+}$ in a 50 ml tube. An enzyme mixture of collagenase (750 µg/ml), dispase (250 µg/ml) and DNase (10 µl/ml of 5% DNase solution) was then added and the tissues were incubated at 37°C for 20 minutes. During this incubation period, trituration was performed every 5 minutes and an additional 0.05% DNase solution was added. After 20 minutes of enzymatic digestion, the process was stopped by the addition of 10% FCS. The cells were then centrifuged at 200 g for 6 minutes in the tube. The supernatant was carefully removed and the cell pellet was resuspended in HBSS without $Ca^{2+}$ and $Mg^{2+}$. This washing step was repeated and, afterwards, cells were resuspended in culture medium. In the case of human tissue, the medium was additionally passed through a cell strainer. Cell density was counted using a Neubauer counting chamber and trypan blue stain exclusion. Murine cell suspensions were seeded at 10,000 cells/$cm^2$. Due to the extensive presence of cell fragments and aggregations in human *post mortem* samples, cell counting was not possible before the initial plating. Therefore, all cells were plated and cell counts were performed on subsequent passages. The cultures were maintained in culture medium at 37°C with 5% $CO_2$. The culture medium was renewed based on the cells' metabolic rates, typically every 3 to 5 days. Additional components, such as growth factors, were added as required for specific experiments.

### *3.2.3 Coatings*

3.2.3.1 Collagen coating

A collagen coating solution was prepared by mixing collagen type 1 at a concentration of 5 µg/cm$^2$ of dish surface with DMEM/F12. The solution was pipetted onto culture dishes and the plates were then incubated either for 1 hour at 37°C or overnight at room temperature. After incubation, the plates were washed three times with HBSS (without $Ca^{2+}$ & $Mg^{2+}$) and once with distilled water. The plates were then air-dried and used immediately.

3.2.3.2 Laminin coating

Plates coated with poly-D-lysine were used for laminin coating. First, poly-D-lysine (100 µg/ml) was dissolved in DPBS. This solution was applied to the plates for 1 hour at room temperature. The plates were then washed three times with distilled water. As a next step, laminin was thawed gently on ice. A working solution of 2 µg laminin per ml DPBS was then prepared. The distilled water was removed from the poly-D-lysine coated plates and they were allowed to dry. Then the laminin solution was applied rapidly in a circular motion using ice-cooled pipette tips. The plates were incubated at 37°C for 2 hours. The laminin solution was removed directly before cell plating and no washing step was performed in between.

### *3.2.4 Passaging*

Prior to the passaging of the cultures, DPBS and trypsin were preheated in a water bath at 37°C for 20 minutes. The medium was aspirated from the culture plates intended for passaging and the plates were rinsed with DPBS. After removing the DPBS, trypsin was pipetted over the plates, ensuring the complete coverage of the surface. The plates were then returned to the incubator. After 3 minutes of incubation, the plates were examined under a microscope to confirm cell detachment. After 6 to 8 minutes at the latest, trypsin digestion was stopped by the addition of an equal volume of culture medium to the trypsin solution. The cells were collected by transferring the entire suspension to a 50 ml tube. The tube was then centrifuged for 6 minutes at 200 g and the supernatant was carefully removed. The cells were resuspended in culture medium, and this step

was repeated twice. Next, cells were resuspended in 1 ml culture medium and counted using a Neubauer counting chamber with trypan blue exclusion. Subsequently, the required volume of culture medium was added to achieve a cellular concentration of approximately 10,000 cells per $cm^2$. The cells were then pipetted onto the new culture plates while the tube was continuously and gently swirled to ensure an even distribution of the resuspended cells in the solution.

### *3.2.5 Cryopreservation*

For cryopreservation, cells were first detached from the culture plates with the same procedure that was used for passaging. The resulting cell suspension was transferred into a tube and centrifuged at 200 g for 6 minutes. The supernatant was carefully aspirated and the cell pellet was resuspended in 1 ml of freezing medium. Cells were counted using a Neubauer counting chamber with trypan blue exclusion. Approximately one million cells were cryopreserved in 1 ml of freezing medium. The tubes were then placed in a freezing container and stored overnight at -80°C. On the following day, the tubes were transferred to a nitrogen tank for long-term storage.

## 3.3 Immunohistochemistry

For immunohistochemical staining, the cultures were fixed in 4% paraformaldehyde (PFA) for 20 minutes. They were then washed three times with PBS and stored at 4°C in PBS containing $NaN_3$ to prevent bacterial contamination. Uncultured tissue samples were fixed in 4% PFA overnight, directly after they had been carefully excised. Before cryosectioning, the samples were rinsed with PBS and immersed into a 30% sucrose solution for 24 hours for cryoprotection. The fixed samples were frozen in isopentane-nitrogen cooled TissueTek and stored at -80°C before cryosectioning at a thickness of 18 µm. To perform stainings on the cryostat sections, they were rehydrated, washed three times for 10 minutes in PBS and incubated for 90 minutes at room temperature in a blocking solution containing either goat serum or donkey serum, depending on the secondary antibodies for the specific staining. The sections were then incubated overnight with primary antibodies

(see Table 6 for a list that also includes the concentrations) diluted in preincubation solution at 4°C in a humidified chamber. After three 10-minute PBS washes, secondary antibodies (Table 7) were applied for 90 minutes at room temperature. Secondary antibodies (for concentrations see Table 7) were diluted in PBST and complemented with either the nuclear stain DRAQ5 (1:1000) or DAPI (1:2000). To remove the secondary antibodies, the sections were washed with PBS three times for 10 minutes before being mounted with Mowiol. This protocol was adapted for the staining of the cultures. The blocking solution was applied directly after removing the PBS from the dishes. In the modified protocol, 0.1% TritonX was added to the primary antibody solution to facilitate tissue penetration. Washes were performed four times instead of three and PBST (PBS with 0.1% TritonX) was used instead of PBS. Secondary antibodies were applied for 2 to 3 hours, depending on the size of the tissue. Subsequently, four additional changes of PBST were performed. Some culture stainings were fixed with Mowiol, while others were kept in PBS + $NaN_3$, taking care not to let them dry out.

### 3.4 Hypoxia experiments

Both explant and dissociation cultures were used for hypoxia experiments. The explant cultures were already divided into two experimental groups during the preparation process of the CP tissue. Therefore, pieces from the same region were divided in half and assigned to the groups. The experiments were initiated two days after obtaining the tissue from the body donors to minimize a potential decline in cell viability due to prolonged cultivation time. One group was exposed to hypoxic conditions (5% $O_2$), while the control group was maintained under normoxic conditions (approximately 20% $O_2$). Samples from each group were fixed after different periods of time. Fixation was performed immediately after removal from the hypoxic conditions and, subsequently, the samples were stained for AQP4 and ZO-1. In the explant cultures, at least two separate tissue pieces per group were used for the cell counts. Epithelial regions were randomly selected without knowledge of the treatment or AQP4 expression and subsequently scanned with a confocal system (LSM510 Meta). Specifically, using only the laser line for the ZO-1 immunofluorescence signal a total number

of viable epithelial cells was initially counted, including cells that could be clearly identified as epithelial by a positive, typical ZO-1 expression. Then, from these cells, AQP4 positive cells were counted, considering them positive if they showed a clearly specific AQP4 expression, independently of the localization (membranous or cytoplasmatic) and intensity. In the dissociation cultures, regions on the plates were randomly selected without knowledge of the treatment. Images were taken with an Apotome module on the Axio Imager Z1. First, the total number of cells was counted in the selected region. Next, all cells that showed a clearly specific AQP4 immunofluorescence signal were counted. Cell counts were performed on randomly selected regions and cells were considered to be positive if they had at least one clearly identified region of AQP4 at the membrane border. As AQP4 was often localized at cell-cell contact sites, both cells were considered positive in these cases. Hypoxia experiments on dissociation cultures were performed after the first passage with cells cultured on both laminin and collagen plating.

### 3.5 Imaging

Images of live cultures were taken on a Zeiss microscope using phase contrast optics. For fluorescence detection, either the Apotome module on the Axio Imager Z1 or a confocal system (LSM510 Meta or LSM Exciter) with laser lines at 488, 543 and 633 nm for excitation and appropriate filter sets was used.

All images were initially recorded with the installed Zeiss system software and image plates were assembled with Photoshop CS2.

### 3.6 Statistics

The blots were processed and analyzed using R Studio version 2023.12.1. For statistical analysis, Wilcoxon tests were performed within the same software.

# 4 Results

## 4.1 Structure of the human CP and its attachment zone

To further characterize the human CP and its transition zone to the brain parenchyma, tissues collected from 13 human body donors were investigated. Macroscopically, the human CP appears as a prominently folded structure located in the ventricles of the brain (Figure 3 a, b). Microscopically, the CP contains many blood vessels that are surrounded by a stromal sheet, and is covered by a single layer of epithelial cells (see Figure 3b for a schematic illustration). The cellular composition of the human CP stroma will be described subsequently in this part. The region where the epithelium transitions to ependyma and blood vessels enter the CP tissue is referred to as *Taenia choroidea* (arrows Figure 3c). We confirmed the established expression patterns of apical AQP1 in the CP epithelium and AQP4 in ependymal cells and astrocytes in the thalamic brain tissue (Figure 3c). Furthermore, we validated the recently described basolateral AQP4 expression on several CPECs (arrowheads in Figure 3c) in CP tissues of all body donors, including the ones that were also used for cultivation (ID H101-H103). AQP4 expression on the CP epithelium varied significantly both within different regions of the tissue and between different body donors, suggesting an underlying regulatory mechanism (Figure 3d). Interestingly, we observed that astrocytes in the transitional zone showed an increased and unpolarized immunofluorescence signal for AQP4 (arrows Figure 3c), different from the one on astrocytes in the adjacent thalamic brain tissue. We verified this staining pattern for AQP4 on the *Taenia choroidea* of six body donors.

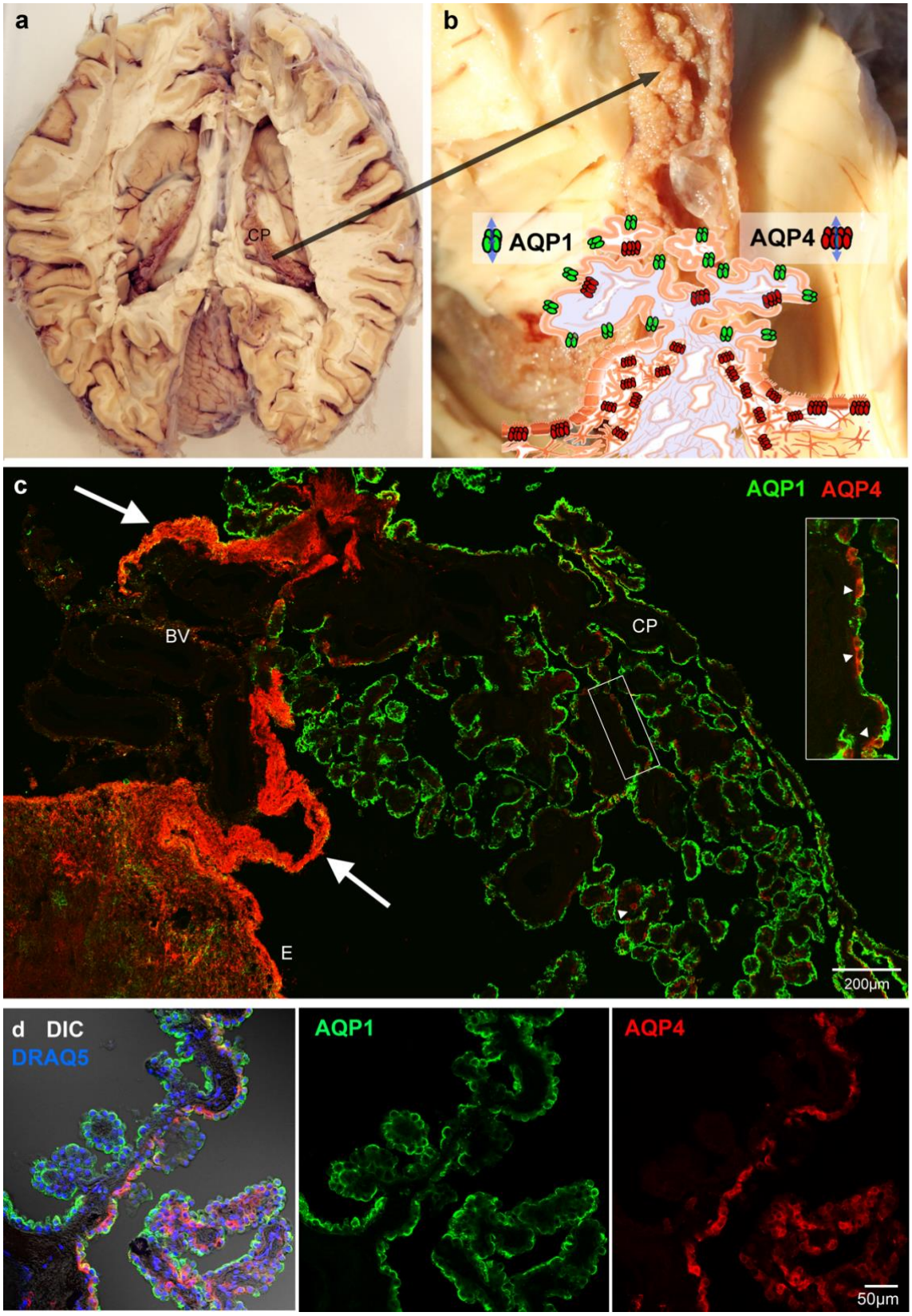


*Figure 3: Overview of macroscopy and microscopy of the human choroid plexus (CP) and its attachment zone, including expression patterns of AQP1 and AQP4.*
*a. Human brain transverse section showing open lateral ventricles, including the CP within the lateral ventricles. b. Magnification of the CP with a schematic illustration of a coronal section of the CP and its*

*transition zone, highlighting the expression patterns of AQP1 (green) and AQP4 (red). c. Cryostat section through the CP and the Taenia choroidea of the lateral ventricle stained for AQP1 and AQP4. The CP epithelium is positive for AQP1, while astrocytic endfeet in the brain parenchyma, ependyma (E), and some cells in the CP are positive for AQP4. The boxed area shows a higher magnification of these cells. Notably, the tissue in the transitional region between the CP and brain parenchyma is strongly immunopositive for AQP4 (arrows). BV blood vessels. d. Higher magnification of the CP epithelium showing a regular apical AQP1 expression and an irregular AQP4 expression pattern. Some regions show no AQP4-positive cells, while other regions show a high density of AQP4-positive cells. Nuclei are stained with DRAQ5 (blue). (a-c from [113])*

To confirm the identities of the AQP4-positive cells, we co-stained for the astrocytic marker glial fibrillary acidic protein (GFAP) (Figure 4a-c). While GFAP was absent on AQP4-positive CPECs, the two stains overlapped in the *Taenia choroidea*, verifying the astrocytic identity of the AQP4-positive cells in the transitional zone.

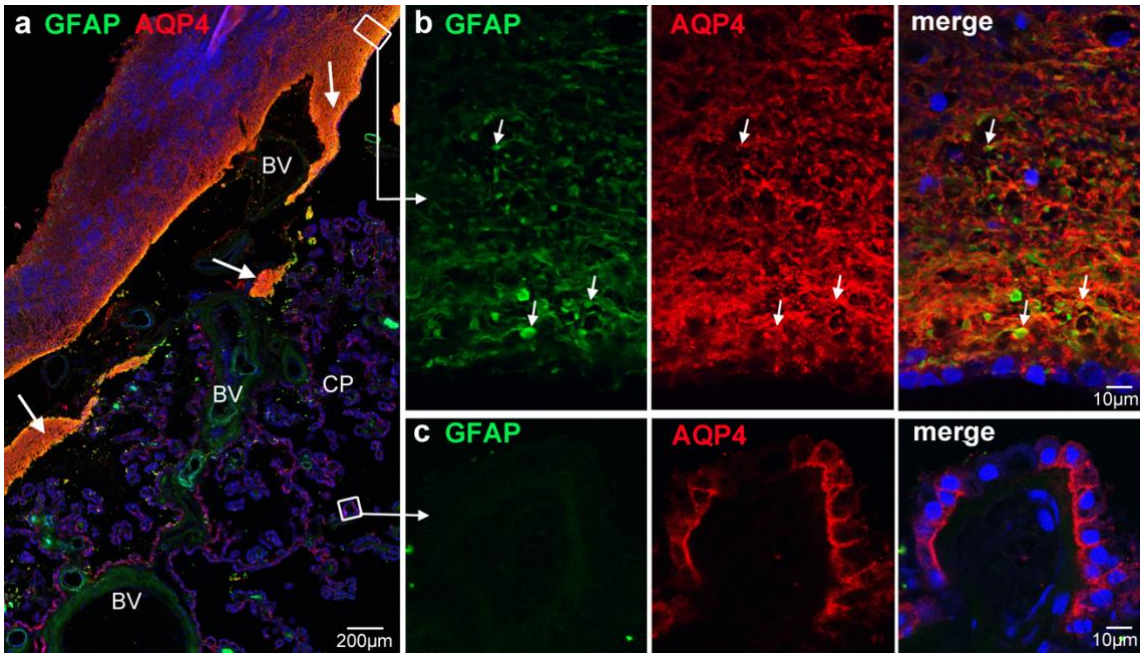


*Figure 4: Subependymal tissue in the transitional zone is formed by astrocytes.*
*a. At low magnification, GFAP immunoreactivity largely overlaps with AQP4 stain under the transitional ependyma (large arrows). b. Detailed view from the ependymal/subependymal region indicated by the white box shows a dense meshwork of GFAP positive processes and strong AQP4 immunoreactivity. The GFAP processes are often surrounded or associated with AQP4 staining (small arrows). The surface ependymal cells are only weakly positive for GFAP. c. GFAP stain is completely lacking in AQP4-positive CPECs. Nuclei are stained with DRAQ5. BV blood vessels.*
*(From [114])*

In a next step, the human CP stroma was closely investigated. Therefore, cryostat sections of fixed human CP tissue were stained with established markers of endothelial cells and macrophages. Notably, there is no specific marker for fibroblasts in CP tissue. Endothelial cells could be immunolabeled with a CD-31 antibody (Figure 5a) and macrophages with an antibody for Iba-1

(Figure 5b). Additionally, ZO-1 and phalloidin were used to mark the course of the epithelial cells in order to distinguish them from the stroma. Interestingly, the Iba-1 staining revealed a very high number of Iba-1-positive macrophages in the CP stroma of several body donors (Figure 5b). To quantify this observation, cell counts were performed on several regions. Depending on the region, the percentage of macrophages was between 56% and 70% of all non-epithelial cells.

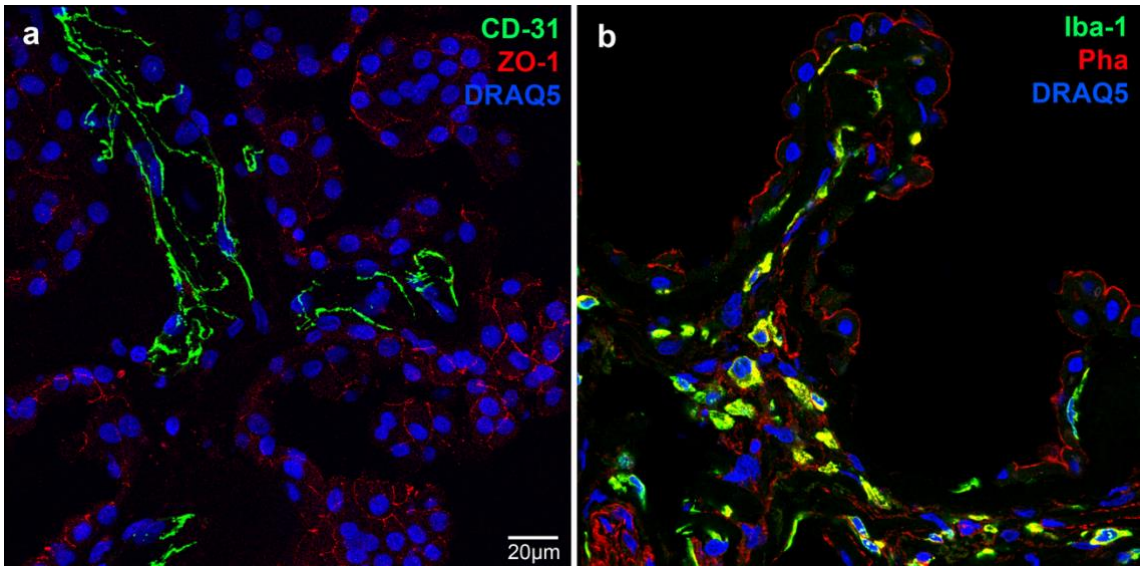


*Figure 5: Identification of cell types in human CP tissue.*
*a) ZO-1 (red) staining shows a high number of epithelial cells combined with several endothelial cells, marked by CD-31 staining (green) in the stromal part of the tissue. b) The cuboidal morphology of epithelial cells is highlighted by phalloidin staining. Notably, staining for Iba-1 (green) reveals high numbers of Iba-1-positive macrophages in the CP stroma. Nuclei are stained with DRAQ5 (blue).*

## 4.2 AQP4 and the dystrophin glycoprotein complex (DGC)

To investigate whether AQP4 in CPECs and astrocytes of the *Taenia choroidea* may be associated with the same anchoring molecules as AQP4 in perivascular astrocytic endfeet, we localized components of the DGC in CP tissue. Therefore, AQP4 was co-stained with the proteins dystrophin (Dp) and β-dystroglycan (DG). CPECs showed no detectable Dp immunoreactivity (Figure 6a). In contrast, β-DG was continuously expressed basolaterally on CPECs, where it aligned with the basal lamina (Figure 6b). Thus, neither the expression pattern of Dp nor that of β-DG correlated with AQP4 in CPECs.

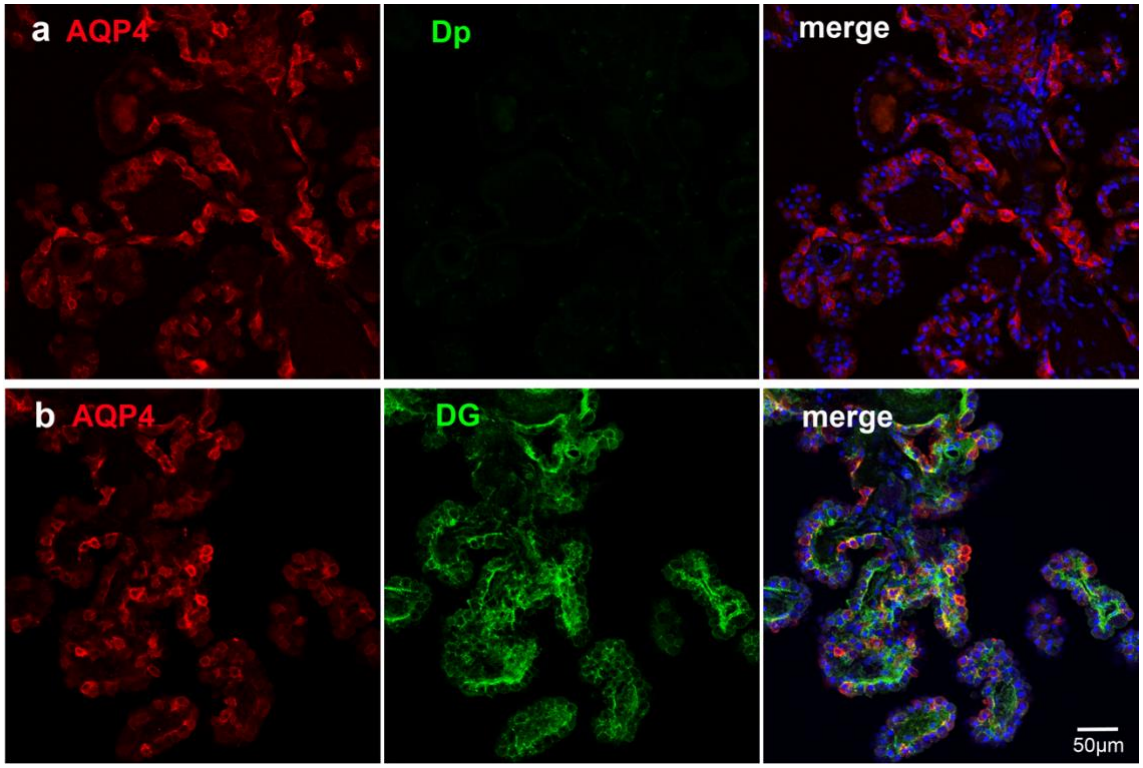


*Figure 6: Expression of AQP4 and the DGC components dystrophin (Dp) and β-dystroglycan (β-DG) in the human CP epithelium.*
a. *Dp staining (green) is negative in both AQP4-positive (red) and AQP4-negative CPECs. b. β-DG staining (green) is positive in all CPECs contacting the basal lamina, independently of AQP4 expression. Nuclei are stained with DRAQ5 (blue).*

Staining for laminin on the CP epithelium was also performed, showing a continuous expression on the basolateral side of both AQP4-positive and AQP4-negative CPECs (results published in [114]).

Interestingly, when Dp was stained on the *Taenia choroide*a, we found a similarly increased intensity as previously observed for AQP4 in these astrocytes (Figure 7a). Nevertheless, the expression pattern of β-DG was not consistently overlapping with AQP4 and Dp in astrocytic processes but was exclusively associated with astrocytic endfeet at blood vessels in the glial plate (Figure 7b).

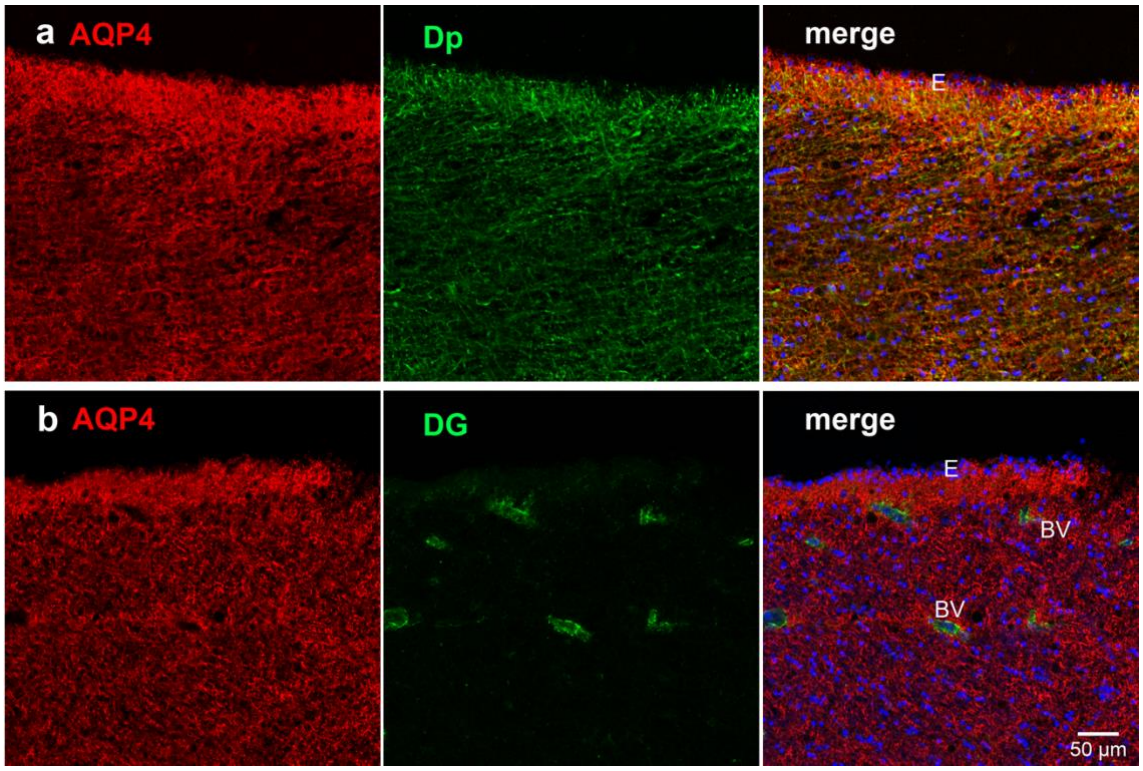


*Figure 7: Expression of AQP4 and the DGC components dystrophin (Dp) and β-dystroglycan (β-DG) in the human Taenia choroidea.*
a. *Astrocytes in the glial plate of the Taenia choroidea show strong immunoreactivity for Dp (green). Co-staining of AQP4 (red) and Dp shows an overlap of both stains. b. β-DG staining (green) on the Taenia choroidea shows that astrocytes in transitional zone are immunonegative for β-DG except in and around blood vessels. Nuclei are stained with DRAQ5 (blue). BV blood vessels, E ependyma.*

These findings suggest an AQP4 anchoring mechanism distinct from the perivascular astrocytic mechanism for both CPECs and astrocytes in the *Taenia choroidea.*

## 4.3 Overview of CP cultures and murine experiments

To investigate functional mechanisms such as the regulation of aquaporins, one major aim of this study was to establish a primary culture model of human body donor CP. Therefore, different cell and tissue culture approaches with varying conditions and time frames were tested. This included culturing small pieces of CP tissue as explants and two different approaches to obtain CP dissociation cultures. In addition, several media compositions and coating substrates were tested. Initially, murine CP was cultured as explant and dissociation cultures, which served two distinct purposes. Firstly, different culture conditions were evaluated using previously published protocols (see discussion) to investigate the behavior of these cells in our laboratory. Secondly, the expression of AQP4 in the murine cultures was briefly investigated. Subsequently, the human primary CP culture models were established and all following experiments focused on these cultures. Figure 8 shows an overview of the culture methods used for this study.

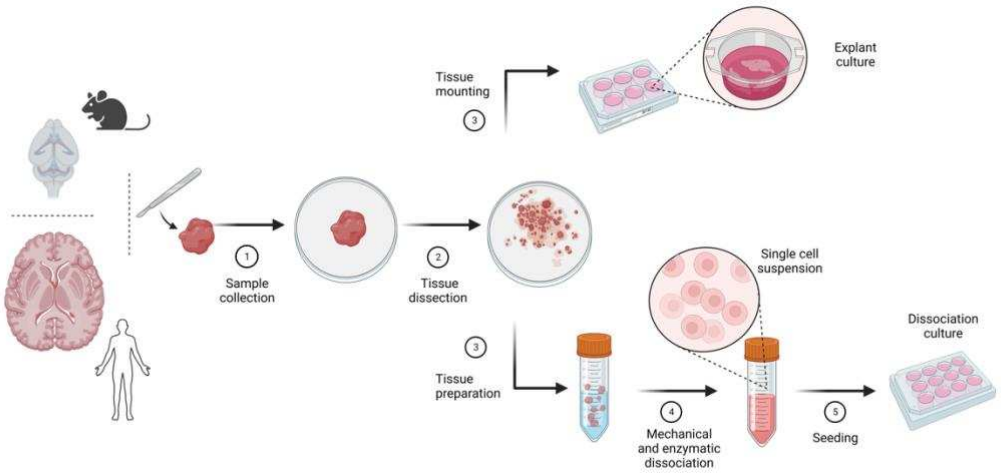


*Figure 8: Overview of the culture methods used for this study.*
*Both murine and human CP was cultured as explant cultures on PTFE membranes and dissociation cultures (for details see main text). Graphic created with BioRender.*

### *4.3.1 Murine CP explant culture*

Three separate experiments involved explanting and culturing CP from 5 mice on PTFE membrane inserts. Four different medium compositions were tested: medium containing 10% FCS and serum-free medium, each with and without the addition of growth factors (see Table 10 below). The explants were closely

monitored over time, and it was observed that groups of cells were growing at the border of the tissues (see boxed area in Figure 9a) cultured in FCS-supplemented medium with and without the addition of growth factors (see Table 10 below). The addition of IGF-1 (20 ng/ml) and EGF (20 ng/ml) was not sufficient to maintain this effect in serum-free medium (Table 10). The duration of cultivation was varied between tissues and ranged from 1 to 42 days *in vitro* (div) to explore the viability of the cultures. Throughout the different cultivation times and medium treatments, the integrity of the tissue remained remarkably intact, as evidenced by immunostaining for the characteristic proteins ZO-1 and AQP1 (Figure 9b). Surprisingly, AQP4 staining revealed several AQP4-positive cells in the cultured samples (Figure 9b).

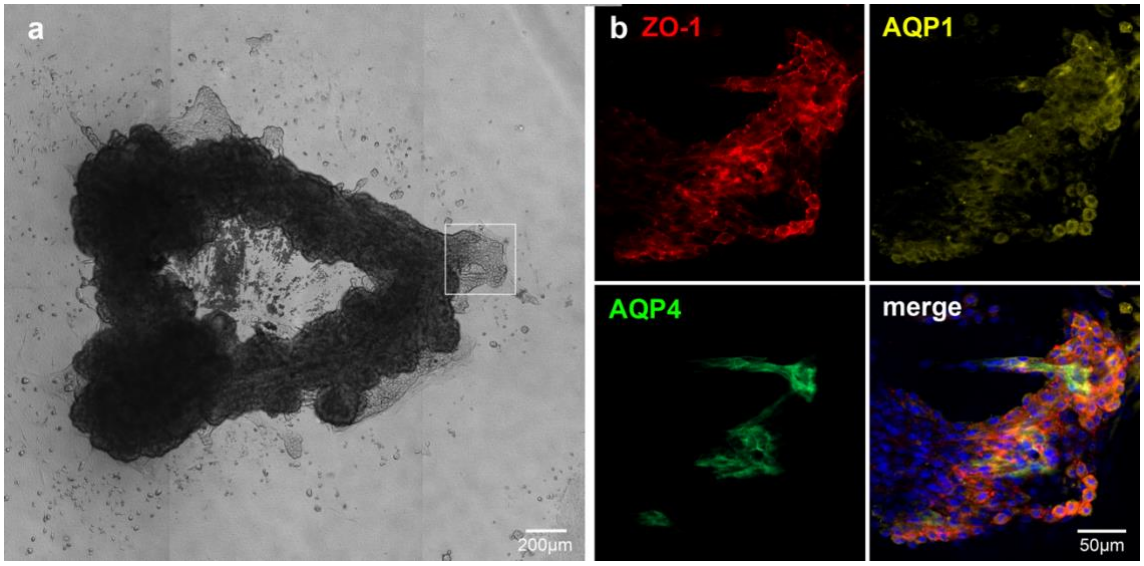


*Figure 9: Murine CP explant culture after 17 days in vitro (div) in serum-supplemented medium. a. Transmitted light image of murine CP of the fourth ventricle, cultured as explant culture on a PTFE membrane for 17 days in medium containing 10% FCS and growth factors. The boxed area shows groups of cells at the border of the explants, indicating cell growth on the PTFE membrane. b. High power view of the boxed area specifically immuno-stained: Cultured CPECs show a typical ZO-1 (red) expression pattern at cell borders, indicating epithelial integrity. The cells are positive for AQP1 (yellow), although the expression pattern appears to be cytoplasmatic rather than polarized to the apical cell pole. Note that in contrast to fixed CP tissue, AQP4 (green) is expressed by some CPECs with a heterogenous expression pattern. Nuclei are stained with DRAQ5 (blue).*

AQP4-positive cells were identified as epithelial cells by higher magnification of the co-staining with ZO-1 (Figure 10a). Some of the CPECs showed a polar, basolateral expression pattern of AQP4 (Figure 10a), while others showed a non-typical cytoplasmatic expression pattern (Figure 10b). In the last step, we tested for cell addition in the cultured tissue. For this purpose, it was stained

with the proliferation marker PCNA. Co-staining with AQP4 showed PCNA-positive CPECs that were also positive for AQP4, as well as cells that were positive for only one of the two markers (Figure 9b). This indicates that some of the AQP4-positive CPECs were proliferating in culture.

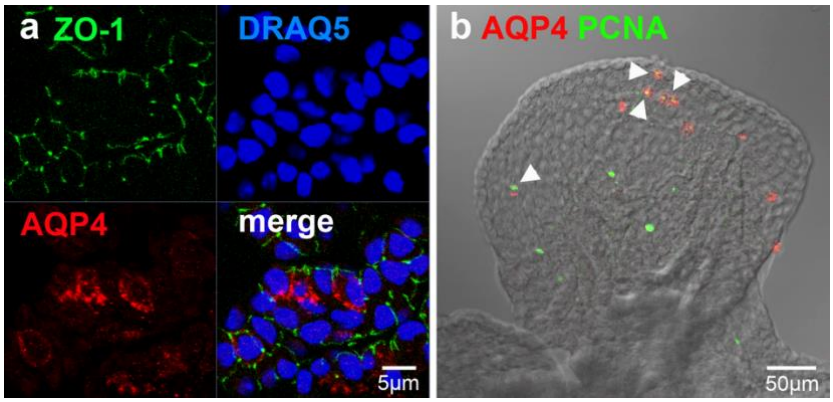


*Figure 10: Characterization of AQP4-positive CPECs in murine explant cultures.*
*Images of murine CP explants cultured for 19 div in medium containing 10% FCS without growth factors. a. High magnification image of AQP4-positive (red) murine CPECs exhibiting typical epithelial ZO-1 (green) expression at cell borders. Nuclei are stained with DRAQ5 (blue). b. Cultured murine CP epithelium shows PCNA-positive (PCNA in green) cells, indicating cell addition. Several PCNA-positive CPECs also show positive AQP4 staining (arrowheads).*

### *4.3.2 Murine primary CP dissociation culture*

CP from five mice were cultured as dissociation cultures on uncoated and laminin-coated culture plates. Cell growth was compared between groups treated with the same four medium compositions as the explant cultures (see Table 10). Additionally, the effect of cytosine arabinoside (AraC) as a fibroblast inhibitor was tested. Serum-free medium conditions drastically reduced cell numbers, showing only a small number of single cells. Supplementation of growth factors could not substitute for the lack of serum and showed no obvious additional effect in serum-containing medium (Table 10). Cultures treated with AraC exhibited fewer cells and a more homogenous morphology when compared to the control group (Figure 11a, b). Immunohistochemical staining revealed a typical membranous expression of ZO-1 and the presence of the CPEC-specific protein transthyretin (TTR) on the cells (Figure 11c).

*Table 10: Overview of the impact of different media tested on murine cultures.*

| **Medium** (DMEM + supplements) | **Serum-free** | **Serum-free + EGF/IGF-1 (20 ng/ml)** | **10% FCS** | **10% FCS + EGF/IGF-1** | **10% FCS + AraC** |
|---|---|---|---|---|---|
| **Explant culture** | tissue integrity | tissue integrity | tissue integrity, cell growth | tissue integrity, cell growth | / |
| **Dissociation culture** | no cell growth | no cell growth | cell growth | cell growth | reduced cell numbers, more heterogenous morphology |

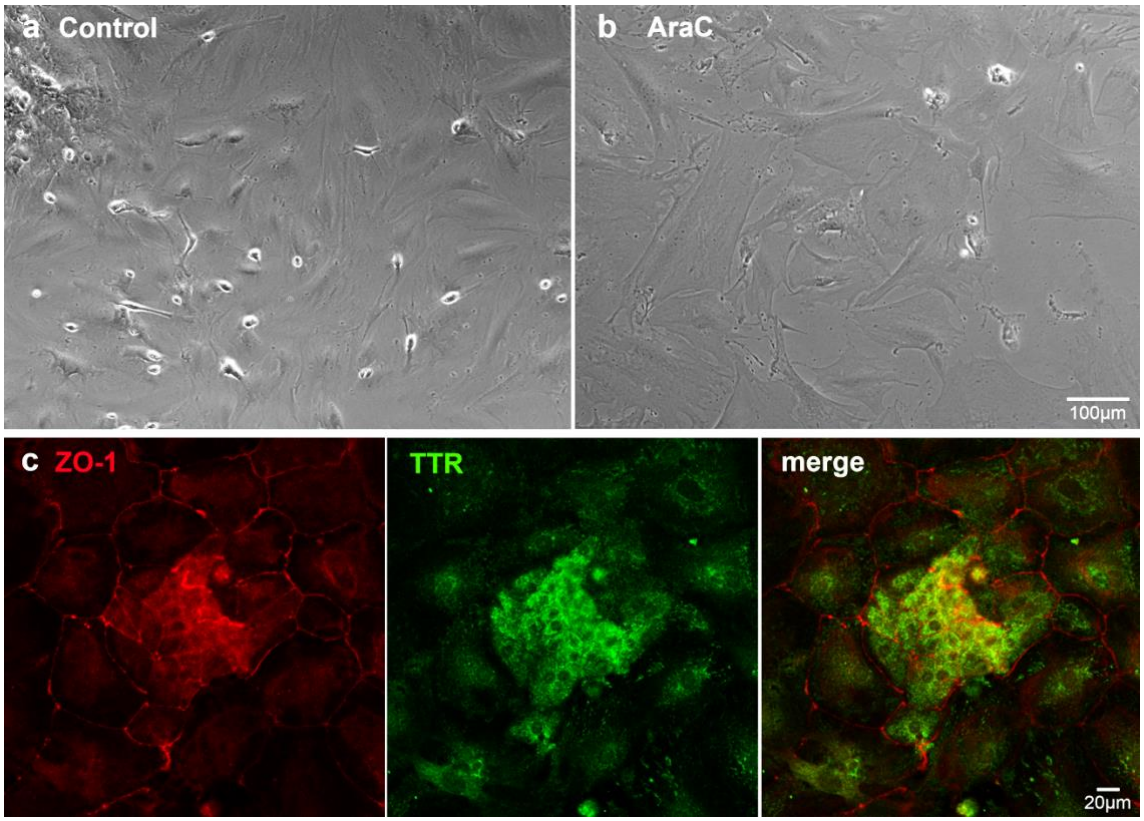


*Figure 11: Murine primary CP dissociation culture – the effect of cytosine arabinoside (AraC) and immunofluorescence staining of ZO-1 and TTR.*
*a,b. Transmitted light images of the cultures maintained in serum-supplemented medium without growth factors 5 days after the second passage. Control cultures (a) show increased heterogeneity in cell morphology and increased cell numbers compared to cultures treated with AraC (b), indicating the presence of additional cell types in the control group. c. Images of the AraC-treated group of the same culture, 13 days after the second passage. The cells show positive immunostaining for ZO-1 (red) at the cell borders and cytoplasmatic expression of TTR (green), indicating epithelial properties.*

### 4.4 Human CP explant culture

Human CP tissue from 3 different body donors (IDs: H101, H102, H103) was cultured on PTFE membrane inserts in medium containing 10% FCS. To allow optimal nutrient diffusion throughout the tissue, small pieces (2-3 mm) of epithelial regions were excised from the CP and placed on the membranes. Samples were fixed after different periods of cultivation. Similar to the murine explant cultures, cell groups observed at the edges of the explants were indicative of cell growth (Figure 12). ZO-1 immunostaining confirmed the epithelial origin of the cells on the filter membranes (data not shown).

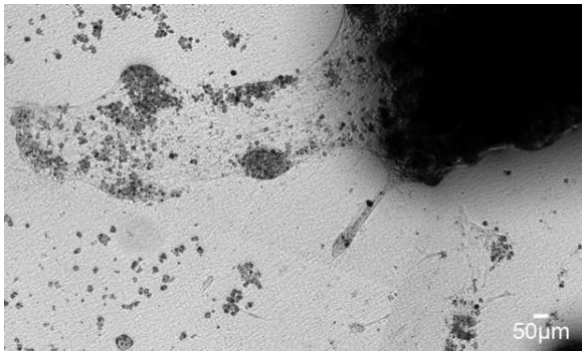


*Figure 12: Transmitted light image of human CP explant culture after 19 div.*
*Groups of cells at the border of the explanted tissue can be observed, which indicates cell growth.*

Before processing the human CP tissues for the cultures, a piece of each CP was fixed immediately for immunohistochemical analyses. Figure 13 shows ZO-1 staining on fixed CP tissue compared to CP tissue cultured for 5 days. In both fixed and cultured human CP tissues, the ZO-1 expression pattern showed heterogeneity across regions, with fragmented ZO-1 staining in some areas and continuous ZO-1 staining in others. Even after 19 days *in vitro* (div), most cultured samples showed cells with ZO-1 expression at cell-cell contacts, indicating polarization. However, the epithelial integrity of the cultured tissue varied substantially between regions and donors. Despite quantitative variations, all human body donor samples showed AQP4-positive CPECs in the fixed, uncultured tissue (Figure 13a). Remarkably, cultured CP tissue maintained this AQP4 expression (Figure 13b, c) up to 19 div (see Figures 14 and 15 below). Similar to AQP4 expression in fixed CP, the number of AQP4-positive cells and the intensity of the fluorescence signal in the cultured tissue varied substantially between regions and donors. In some CPECs, AQP4 was

exclusively expressed in the basolateral membrane (Figure 13b), whereas in others it remained membrane-associated but non-polar (Figure 13b). Additionally, several CPECs showed a cytoplasmatic AQP4 expression pattern (Figure 13c). Co-staining of AQP4 and ZO-1 was performed to investigate the possible influence of ZO-1 integrity on the AQP4 expression pattern, but no apparently visible correlation was observed.

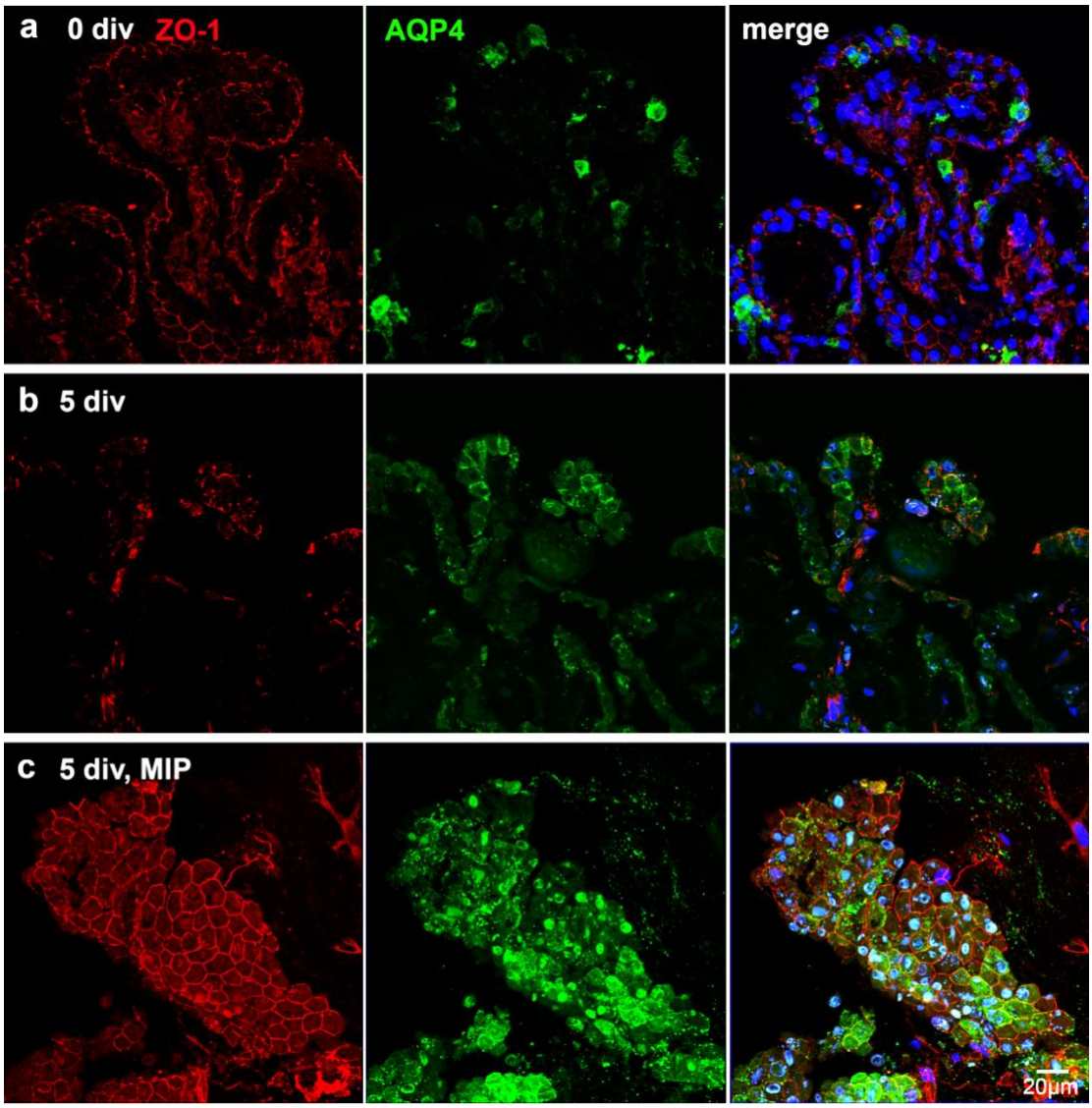


*Figure 13: ZO-1 and AQP4 expression in fixed human CP compared to human CP explant culture. a. Cryostat section of fixed human CP showing discontinuous ZO-1 staining (red) at epithelial cell borders and several AQP4-positive (green) CPECs. Nuclei are stained with DRAQ5 (blue). b. Cryostat section of human CP explant culture after 5 div, showing discontinuous ZO-1 expression and several AQP4-positive CPECs, displaying a membranous, basolateral expression pattern. Nuclei are stained with DRAQ5 (blue). c. An example of a cultured region exhibiting continuous ZO-1 expression after 5 div is shown, further highlighted by a maximum intensity projection (MIP). In addition, the region shows distinct AQP4 expression, with a higher number of AQP4-positive cells and varying expression patterns, showing membranous expression in some cells and cytoplasmatic expression in others. Nuclei are stained with DAPI (blue).*

Next, the expression of the functional proteins AQP1 (Figure 14) and NKA (Figure 15) was examined by comparing stainings on cryostat sections of uncultured and cultured CP tissue. CPECs in the tissue cultures maintained the cell-typical expression of AQP1 and NKA for up to 19 div, although the expression patterns became increasingly irregular and non-polar over time (Figure 14b, 15b). The immunohistochemical analyses were performed with AQP4-co-staining to investigate possible correlations in the development of these protein expressions *in vitro*. However, no staining pattern indicating a relationship between AQP4, NKA and AQP1 was observed.

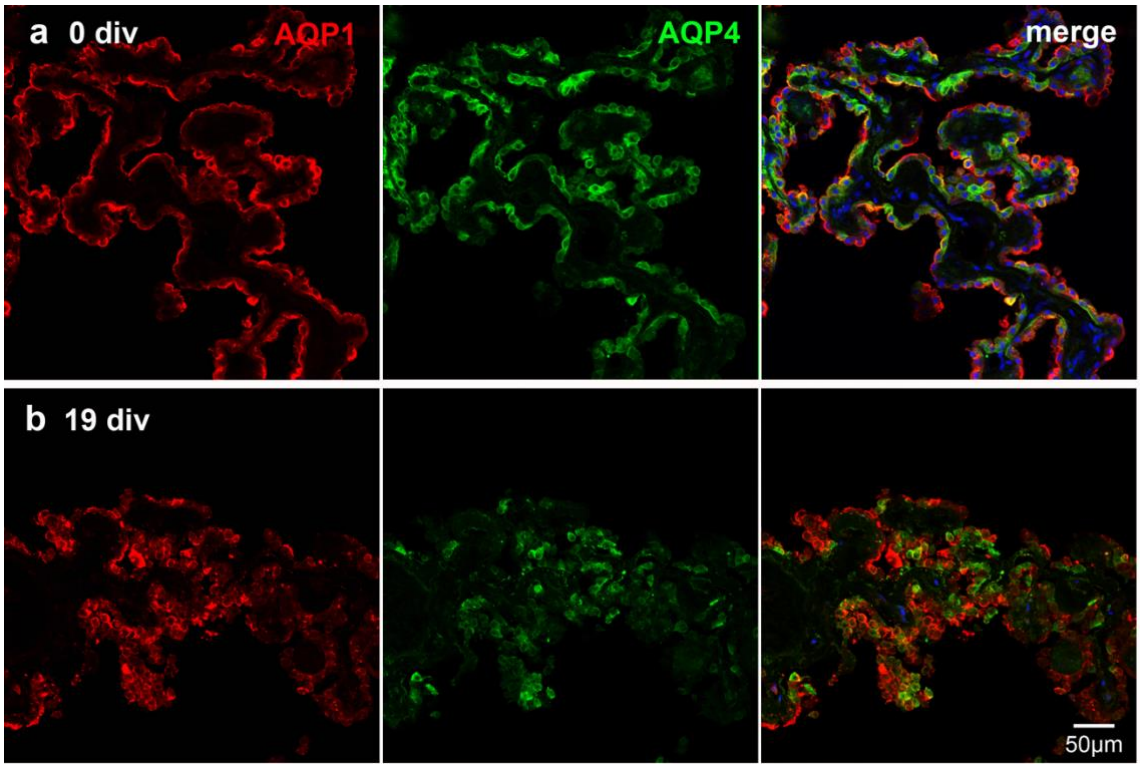


*Figure 14: AQP1 and AQP4 expression in fixed human CP tissue compared to human CP explant culture. a. Typical apical AQP1 (red) expression can be observed on CPECs of fixed human CP tissue. AQP4 (green) expression pattern varies between the CPECs. b. The expression of both proteins is maintained throughout the culture period of 19 div. In some CPECs, apical AQP1 expression is maintained, whereas in others, the polarity of the expression pattern is lost, similar to AQP4. Nuclei are stained with DRAQ5 (blue).*

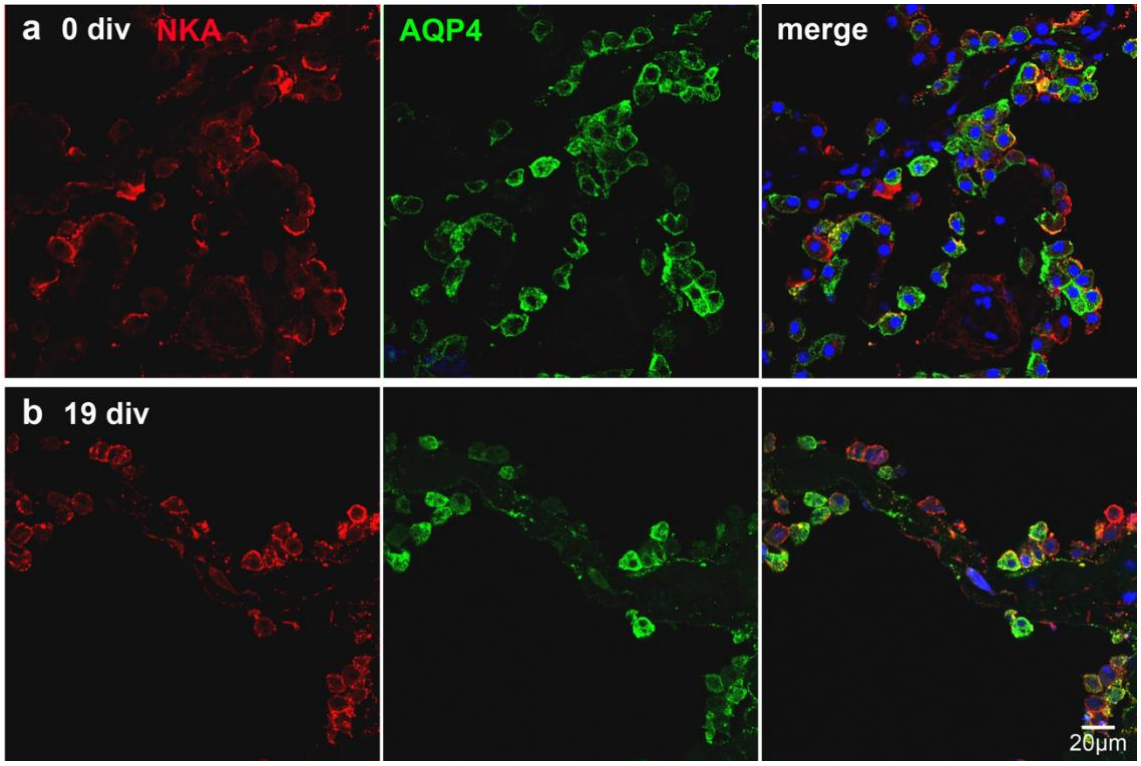


*Figure 15: NKA and AQP4 expression in fixed human CP tissue compared to human explant culture.* a. *Cell-typical apical NKA (red) expression pattern can be observed on CPECs of fixed human CP tissue. AQP4 (green) expression pattern varies between the CPECs. b. The expression of both proteins is maintained throughout the culture period. In some CPECs apical NKA expression is maintained, whereas in others the polarity of the expression pattern is lost, similar to AQP4. Nuclei are stained with DRAQ5 (blue).*

## 4.5 Human primary CP dissociation culture

Dissociation cultures of human primary CPECs were successfully established from three body donors (H101, H102, H103). Compared to murine cultures, dissociated cells from the human CP tissue needed much more time to adhere to the substrate (at least 4 days, see below) yet grew sufficiently to be passaged several times. Remarkably, the proliferative capacity of the cells was restored after cryopreservation at -80ºC. During the development of a reproducible and consistent cell culture model, many experiments were carried out to optimize conditions and test limitations of the models. Due to practical limitations, not all potential pathways could be pursued.

### *4.5.1 Establishing the culture protocol:*

Initially, CP tissue was obtained from the lateral, third, and fourth ventricles and cultured separately. It was observed that dissociation cultures from the lateral ventricle CP reached confluency significantly faster than those from the third and fourth ventricle CP (data not shown). Consequently, for subsequent cultures, the focus was on the lateral ventricle CP, which consistently produced comparable results. Two methods were employed to obtain dissociation cultures of lateral ventricle CP: enzymatic digestion and the acquisition of cells from floating CP tissue. While it was possible to obtain monolayer cultures with both methods, the floating culture gave inconsistent results in terms of duration and cell numbers. Since enzymatically digested human CPECs would survive and give consistent results, subsequent experiments focused on these cultures. The cells were cultured on two types of substrate coating: laminin and collagen. Substrate-specific results are reported in a later section.

Due to limited access to human material and the need to avoid loss of valuable samples, all human cultures were initially seeded in medium supplemented with 10% FCS, based on the observations from our murine experiments. The murine results and previous studies (see discussion) suggested a beneficial effect of AraC in preventing fibroblast contamination. Two groups of human dissociation cultures were compared, one group cultured in AraC-containing medium for 3 days and a control group without AraC. While only minimal differences were

observed at the beginning, after several weeks in culture, the control group showed a higher cell density and less homogeneous morphology (Figure 16). These observations indicated a selective inhibitory effect of AraC on the proliferation of specific cell types.

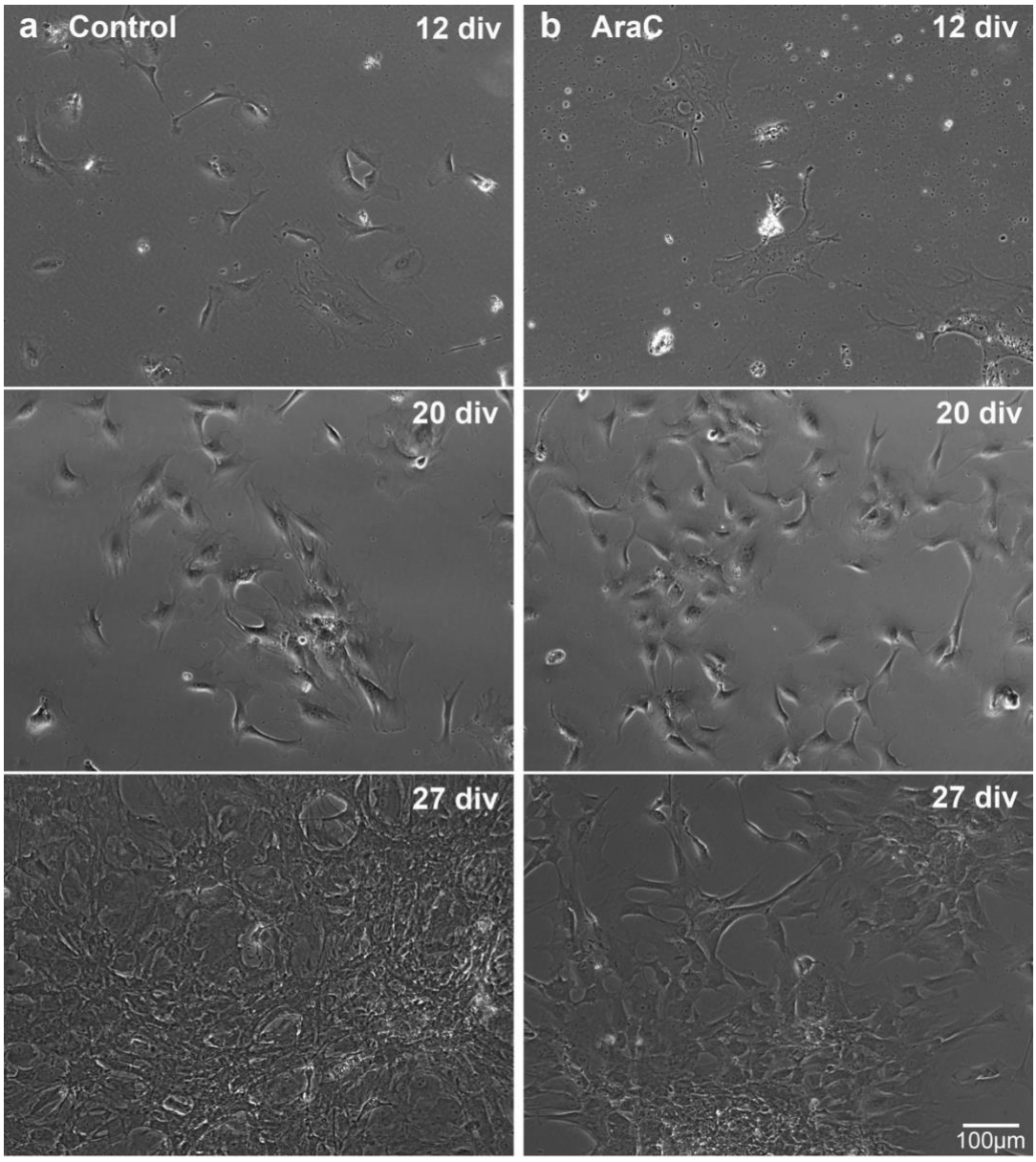


*Figure 16: Effect of AraC on human primary dissociation cultures on laminin coating.*
*a. Transmitted light images of the control group at 12, 20, and 27 div. In the early stages, the control group demonstrates a greater degree of heterogeneity in cell morphology, including small spindle-shaped cells. As the culture time progresses, the control group exhibits higher cell densities, with cells overgrowing each other. b. Cultures treated with AraC for 3 days show a development similar to the control group in the early stages. As the cultivation time progresses, AraC-treated cultures exhibit a more homogenous morphology and lower cell densities when compared to the control group.*

As an approach to identify additional cell types in the control culture, immunolabeling for astroglial (GFAP), endothelial (CD-31) and macrophage markers (Iba-1) was performed. GFAP and CD-31 staining showed no positive cells in the cultures. Interestingly, in cultures without AraC, several Iba-1-positive macrophages could be clearly identified (Figure 17a). However, no Iba-1-positive cells were observed in AraC treated cultures indicating an inhibitory effect on macrophages (Figure 17b).

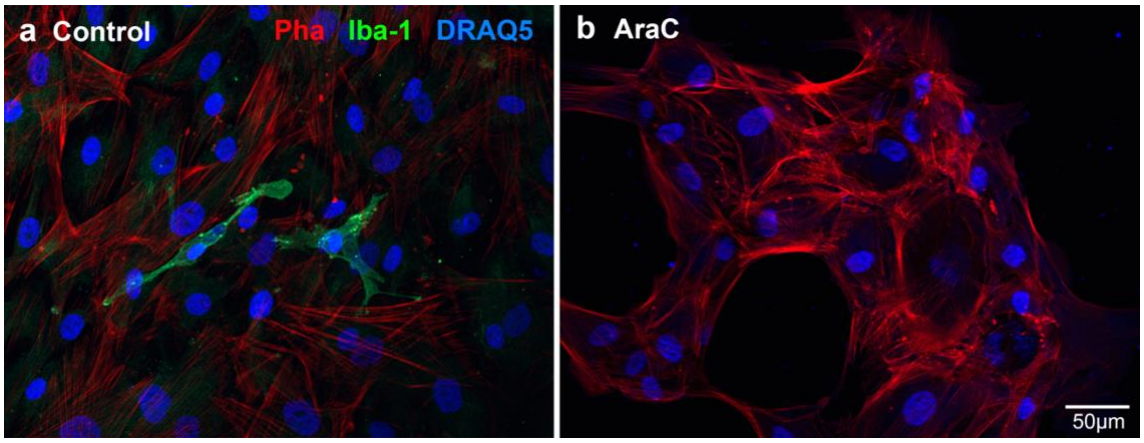


*Figure 17: Iba-1-positive macrophages in primary human dissociation cultures without AraC. a. Iba-1 (green)staining reveals the presence of several macrophages in human CP dissociation cultures that did not receive AraC treatment. b. AraC treatment effectively eliminates Iba-1-positive cells from human primary dissociation cultures. Nuclei are stained with DRAQ5 (blue).*

As the cultures could be passaged multiple times, the cell numbers were sufficient for experiments with serum-free medium. Cells were cultured in both serum-free medium and serum-free medium with IGF. As expected from the results of the murine experiments, the absence of FCS significantly reduced cell proliferation. The addition of IGF-1 (20 ng/ml) to the serum-free medium was unable to compensate for the absence of FCS. Nevertheless, it was possible to maintain cultures in serum-free medium for several days when the cells were seeded at high densities or initially cultivated in serum-supplemented medium. The results of the immunohistochemical investigations of these approaches will be reported in a subsequent section.

### 4.5.2 Growth properties of human primary dissociation cultures

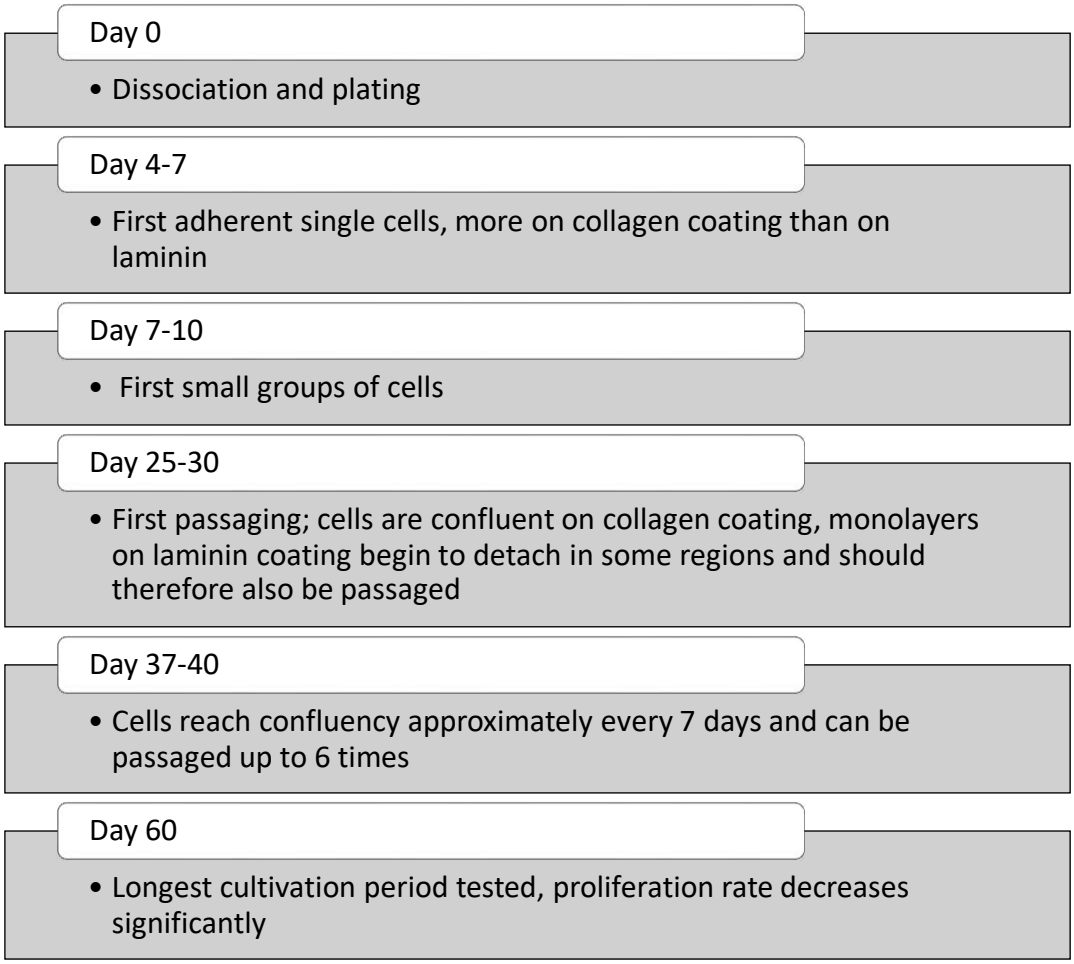


*Figure 18: Timeline of steps and observations in human primary CP dissociation cultures.*

Figure 18 shows a timeline of the observed steps occurring in the established human primary dissociation cultures. After tissue dissociation, it took approximately 4 to 7 days for the first single cells to adhere to the culture surface. The collagen coating improved the initial adherence of the cells, with more cells initially appearing compared to cultures on laminin-coated dishes. Before the first passage, the cultures contained cell debris which was difficult to remove but did not inhibit cell proliferation (Figure 19a). The newly dissociated cells showed a heterogenous morphology, often with numerous processes. This morphological diversity was more pronounced in cells cultured on collagen-coated plates (Figure 19a) than on laminin-coated plates (Figure 20a). By day 7 to 10, small groups of cells began to form on both collagen and laminin coatings. It was notable that cells reduced the formation of processes when

they came into contact with other cells. Another coating-specific phenomenon observed was that cells on collagen-coated plates were more evenly distributed over the plates, whereas cells on laminin-coated plates tended to grow in dense clusters (Figure 20b). These clusters grew steadily to form a dense monolayer with typical epithelial morphology in some areas of the plate (Figure 20c), while other areas of the laminin-coated dishes were cell-free (Figure 20b). After prolonged cultivation, this dense layer detached from the laminin-coated plates in some regions and retracted to an aggregated cell mass (Figure 20d). Once cells had detached from a region, this region was only slowly repopulated by cells. Therefore, some cultures were passaged before reaching full confluency. This phenomenon was not observed in all dissociation cultures on laminin. If the cells did not detach from the culture dish, the culture reached confluency after approximately 30 days (Figure 20c). In both cultures on laminin and collagen coating, the cells began to form small cell piles in some regions instead of growing as a monolayer (arrow in Figure 19b). The cultures on collagen-coated plates reached confluency and were passaged for the first time between days 25 and 30 (Figure 19b). After the first passage, cell morphology became less heterogenous and small groups of cells with a cuboidal morphology were observed after 2 days (Figure 19c). It took about one week for the cells to reach confluency when seeded at a concentration of approximately 10,000 cells per $cm^2$ (Figure 19d). Once established, the cultures remained stable for at least five subcultures before the proliferation rate decreased. Furthermore, it was examined whether the passaged cells could be cryopreserved for subsequent use. Remarkably, the proliferative capacity of the cells was effectively restored after cryopreservation at -80ºC.

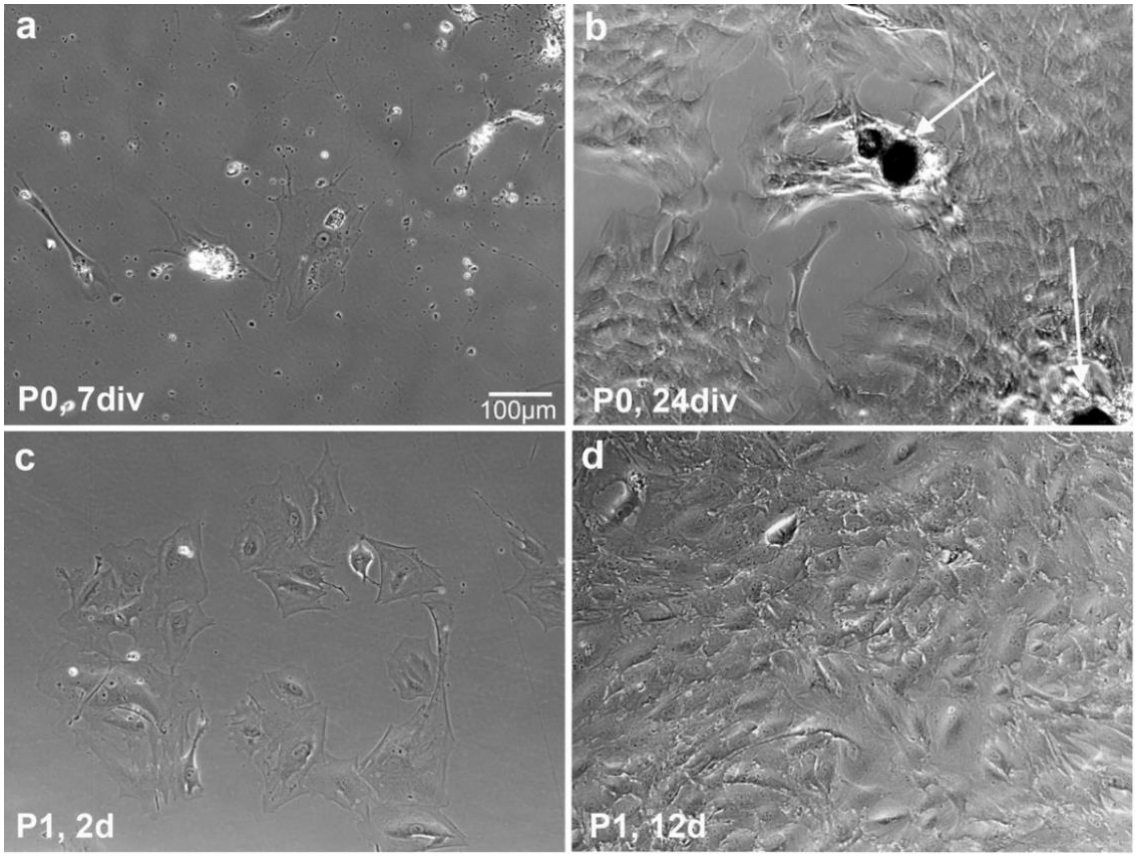


*Figure 19: Human primary CP dissociation culture on collagen coating.*
a. *Transmitted light image of newly seeded cells after 7 div showing heterogenous morphologies and several processes. The cultures contain cell debris after the initial plating, which is difficult to remove. b. Cells grow in groups, becoming more homogeneous and reducing cell processes upon contact with other cells. While cells continue to grow as a monolayer in some regions, in other regions aggregates of cells are observed (arrows). c. Transmitted light image of the cells, two days after the first passage, showing groups of cuboidal cells with less heterogenous morphologies than after the initial plating. d. After the first passage, cells grow evenly, forming a more homogeneous monolayer.*

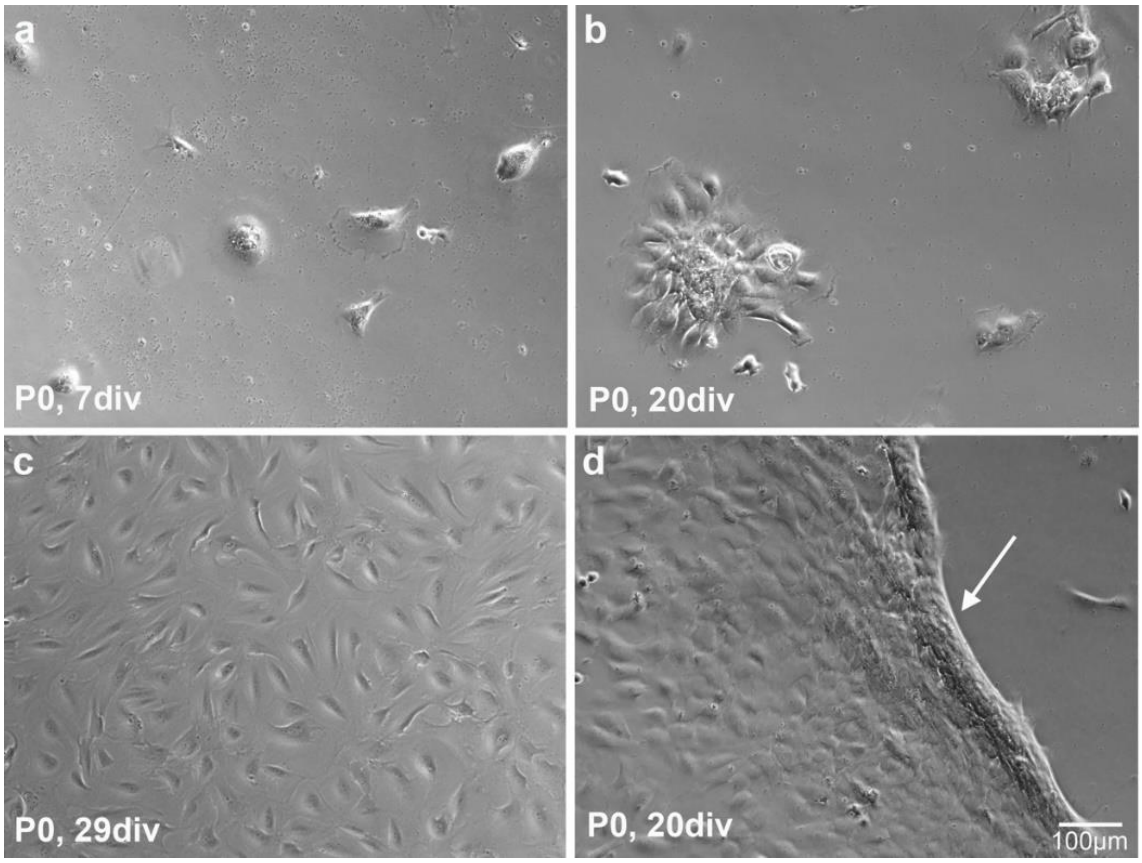


*Figure 20: Human primary CP dissociation culture on laminin coating.*
a. *Transmitted light image of newly seeded cells on laminin coating, showing a more homogeneous morphology with fewer processes than on collagen coating. b. Cells grow in dense groups, leaving cell-free areas in the dish, especially before the first passage. c. Transmitted light image of the culture building a dense monolayer and reaching confluency. d. Occasionally, the dense monolayer detaches from the laminin surface and retracts (arrow).*

### *4.5.3 Identification of cell types*

Due to the occasional heterogeneity observed in the morphology of cultured cells, we investigated the presence of other cell types within the dissociation cultures. As previously described, CP tissue contains several cell types, including epithelial, mesenchymal (fibroblasts), endothelial and immune cells (macrophages). Notably, GFAP staining on cryostat sections of human CP tissue had shown the presence of sporadic astrocytes near the transition zone (see Figure 4 above), which was therefore explicitly excluded from the dissociation process. Due to our selective dissection technique focusing on epithelial regions, the use of AraC to inhibit fibroblast growth and the observed morphology of the resulting cultures, we expected that the dissociated cells would be predominantly epithelial. To test this hypothesis, we initially confirmed the expression patterns of several markers on fixed human CP tissue. Subsequently, the same labeling was repeated on the dissociation cultures and compared to the reference tissue. To identify CPECs, we used TTR, a previously established marker that exhibited a cytoplasmatic expression pattern in CPECs on fixed human tissue (Figure 21a). Additionally, vimentin and phalloidin staining was performed, highlighting the cells' cytoskeleton and subsequently the CPEC-typical cuboidal morphology. In fixed CP tissue, vimentin staining for intermediate filaments showed a cytoplasmatic expression pattern and phalloidin, marking actin filaments, appeared concentrated at the cell membranes (Figure 21a). Performing the staining on human CP dissociation cultures of both collagen and laminin coated dishes, the cells showed similar expression patterns for TTR, vimentin, and actin as those observed in CPECs of the uncultured reference tissue (Figure 21b, c). The specificity of the stains was additionally verified by a staining control which showed no immunofluorescence signal. Together, these results strongly suggest that the vast majority of the cultured cells are epithelial. The expression of functional proteins characteristic of CPECs, such as ZO-1, will be presented in the next section.

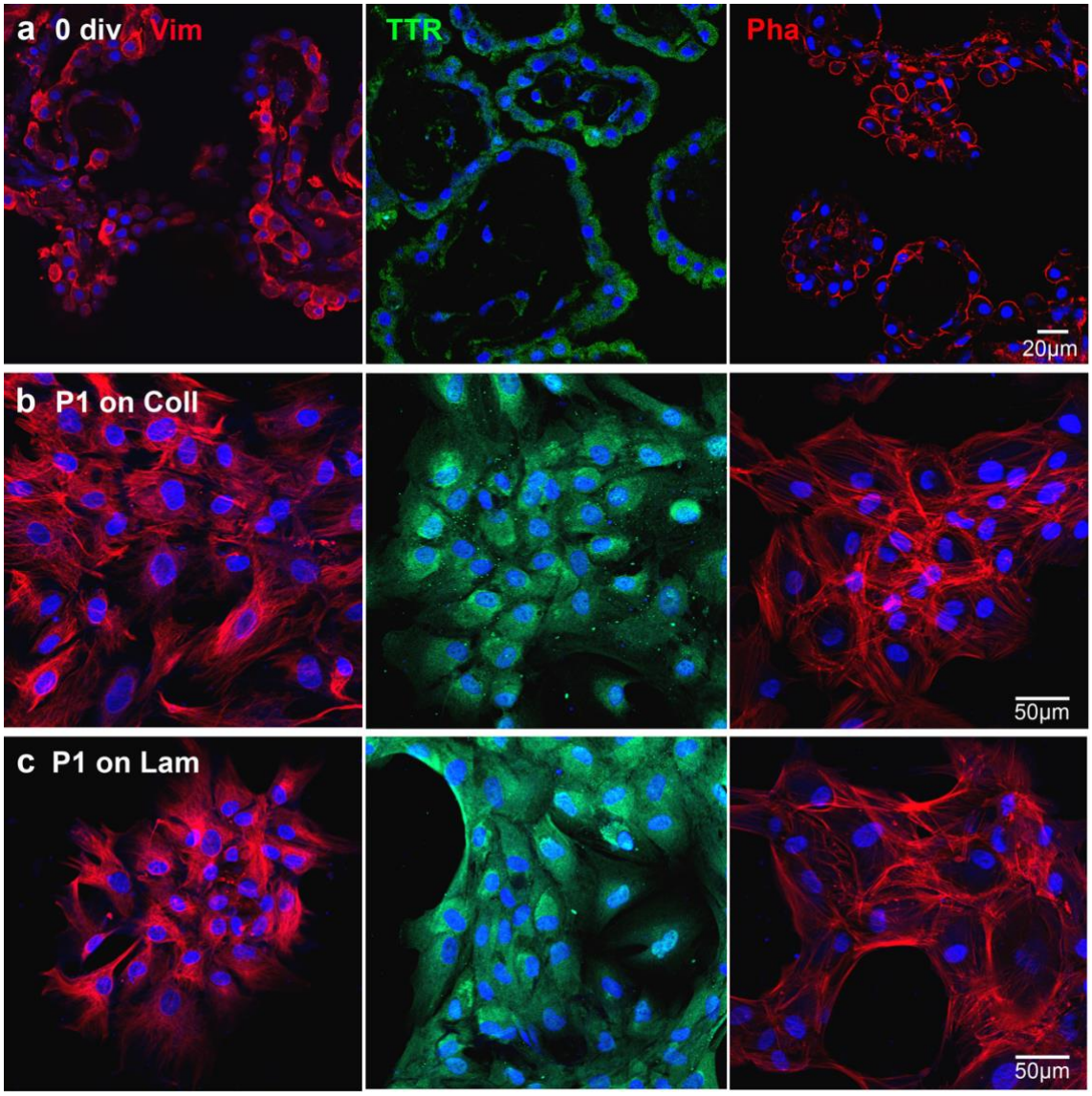


*Figure 21: Identification of CPECs.*
*a. Cryostat section of fixed human CP material stained with vimentin (Vim, red), transthyretin (TTR, green), and phalloidin (Pha, red) displaying cell-typical expression patterns. b. Primary human dissociation culture on collagen-coated dishes after the first passage displays similar staining patterns of Vim, TTR and Pha as CPEC of fixed tissue. c. Primary human dissociation culture on laminin-coated dishes after the first passage displays similar staining patterns of Vim, TTR and Pha. Nuclei are stained with DRAQ5 (blue).*

Furthermore, the presence of other cell types which are known to be present in CP tissue was investigated in the dissociation cultures. Therefore, the cultures were stained with the previously established markers of endothelial cells, astrocytes and macrophages (see Figure 4 and 5 above). Labeling the human dissociation cultures for GFAP, Iba-1 and CD-31, no positive cells were observed. To investigate possible neuronal differentiation in cell culture,

stainings with the neuronal marker HuCD were additionally performed. HuCD revealed no positive cells in the dissociation cultures.

### *4.5.4 Expression of functional proteins on CPECs in vitro*

A key feature of the CP epithelium *in vivo* is the formation of tight junctions. Immunostaining for the tight junction protein ZO-1 in dissociated primary human CPECs revealed positive signals localized to cell borders where cell contacts occur (Figure 22). The ZO-1 staining pattern showed varying degrees of continuity between cells, appearing either as separate dots or as a continuous line.

Remarkably, AQP4 was detected in primary human dissociated CPECs cultured on both collagen (Figure 22a) and laminin coatings (Figure 22b). AQP4 expression was generally heterogenous, with the number of positive cells varying between different regions of the same plate, across passages, and between cells from different body donors. At low resolution, AQP4 appeared to colocalize with ZO-1 at cell-cell contact sites in several CPECs (see arrows in Figure 22a). However, the two stainings showed distinct expression patterns at high resolution (see arrowheads in Figure 22b). Notably, no coating-specific impact on AQP4 expression was observed as AQP4 showed the same expression pattern in CPECs cultured on both laminin and collagen. Looking at the staining of AQP4 in Figure 22, an immunofluorescence signal was also observed in the nuclei which is false positive as demonstrated by a staining control (see Figure 28 below).

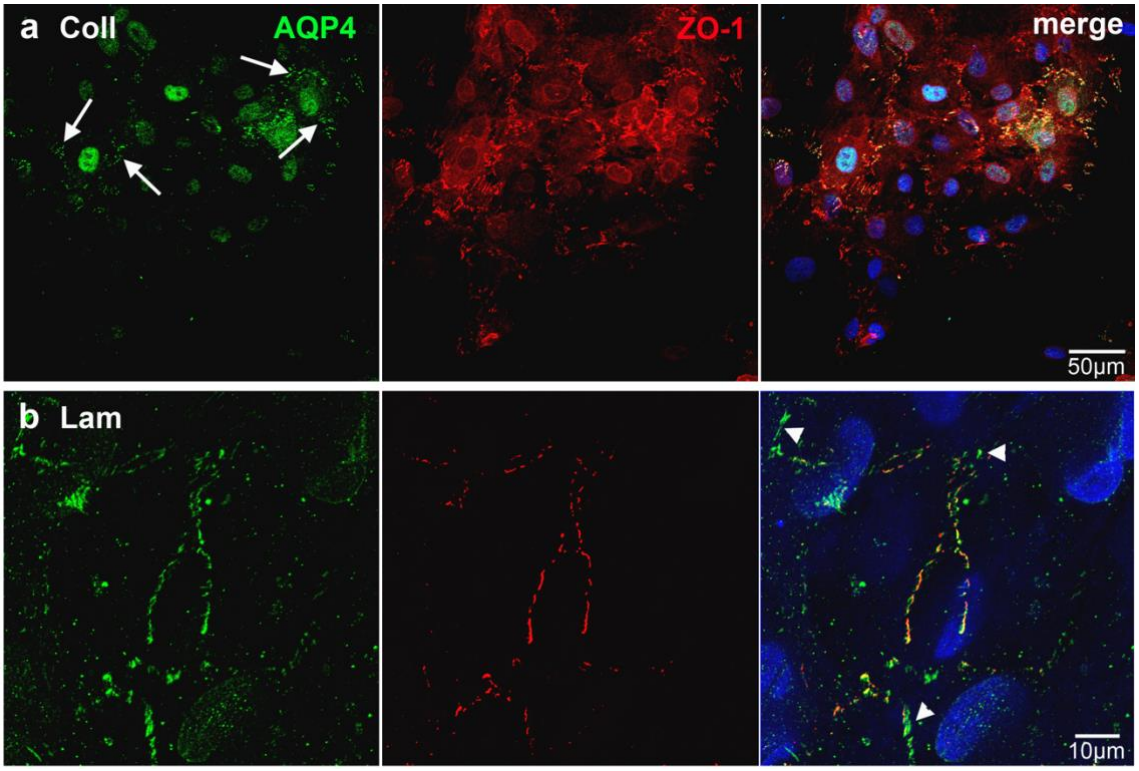


*Figure 22: Human primary dissociated CPECs cultured on both laminin and collagen express ZO-1 and AQP4 at cell-cell contact sites.*
*a. Primary human dissociation culture on collagen coating. The cells express membranous AQP4 (green) and ZO-1 (red) at cell-cell contact sites (arrows). The continuity of the ZO-1 expression pattern varies between cells, appearing either as separate dots or as a continuous line. b. High-resolution (Airy scan) image of primary human dissociation culture on laminin coating reveals that AQP4 (green) and ZO-1 (red) are expressed in close proximity but with distinct separate localization. The arrowheads indicate regions with a high concentration of AQP4 expression and a relatively low level of ZO-1 expression. Nuclei are stained with DRAQ5 (blue).*

The presence of three other functional proteins, AQP1, NKA and NKCC1, was also detected in these cells. In contrast to ZO-1 and AQP4, these proteins did not show a membranous distribution pattern (Figure 23). Interestingly, the intensity of the immunofluorescence signal for AQP1 expression varied significantly between cells, whereas the NKA staining showed consistent intensities across the cells (Figure 23).

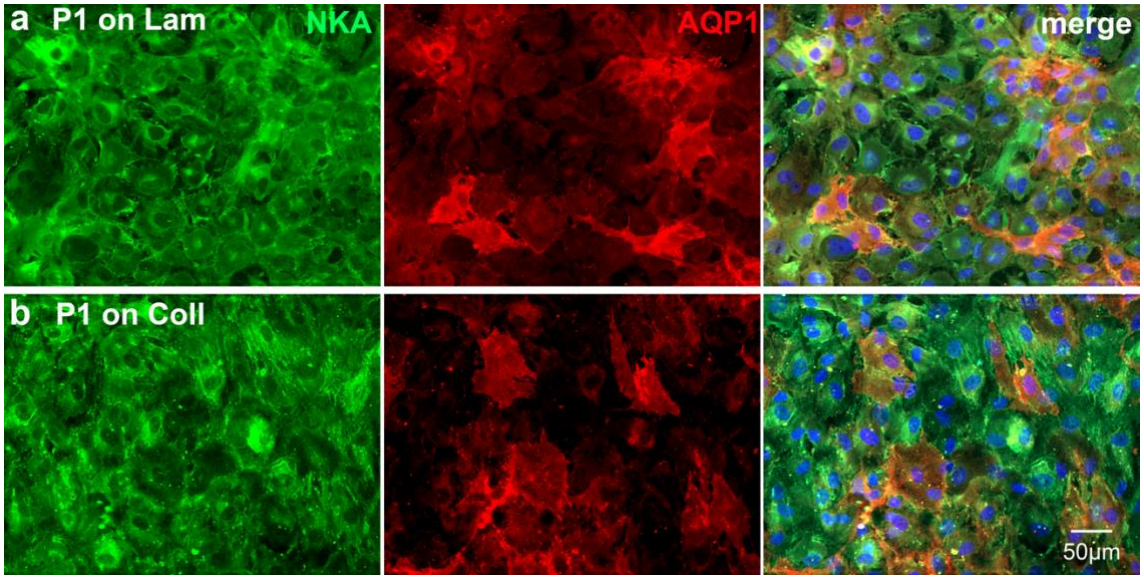


*Figure 23: Dissociated human primary CPECs cultured on both laminin and collagen coating express NKA and AQP1.*
*a. Human primary dissociation culture on laminin coating. CPECs express NKA (green) and AQP1 (red) with a cytoplasmatic expression pattern. AQP1 immunofluorescence intensity varies strongly between cells, whereas the NKA expression pattern is more homogenous. b. Human primary dissociation culture on collagen coating. CPECs express NKA and AQP1 with a cytoplasmatic expression pattern, showing the same differences as on laminin. Nuclei are stained with DAPI (blue).*

### *4.5.5 Effect of serum-free medium on protein expression*

As described above, human primary dissociation cultures exhibited optimal growth and proliferation when cultured in serum-supplemented medium. Nevertheless, it was possible to maintain cells in serum-free medium that had been cultivated in serum-supplemented medium before. Studies with primary porcine CPECs had indicated that cultivation in serum-free medium enhanced cell contacts and polarity (see discussion). We therefore examined the cultures that had been switched to and maintained in serum-free medium to determine whether there were any alterations in protein expression. Immunostaining for ZO-1, AQP1, AQP4, NKCC1, and NKA showed no apparently visible differences in our primary human CP culture model after serum withdrawal.

## 4.6 Effect of hypoxia on AQP4 expression

### *4.6.1 Hypoxia treatment of human CP explant cultures*

As hypoxia has been suggested to increase AQP4 levels in murine CPECs, we investigated possible effects of hypoxic conditions on AQP4 in human CPECs in the established culture models. First, the effect of hypoxia on AQP4 expression at 3, 4 and 5 days of treatment was investigated in the CP explant cultures. Remarkably, we observed that the majority of hypoxia-treated pieces exhibited intense AQP4 immunofluorescence signals (Figure 24b), while the control group exhibited less intense signals (Figure 24a).

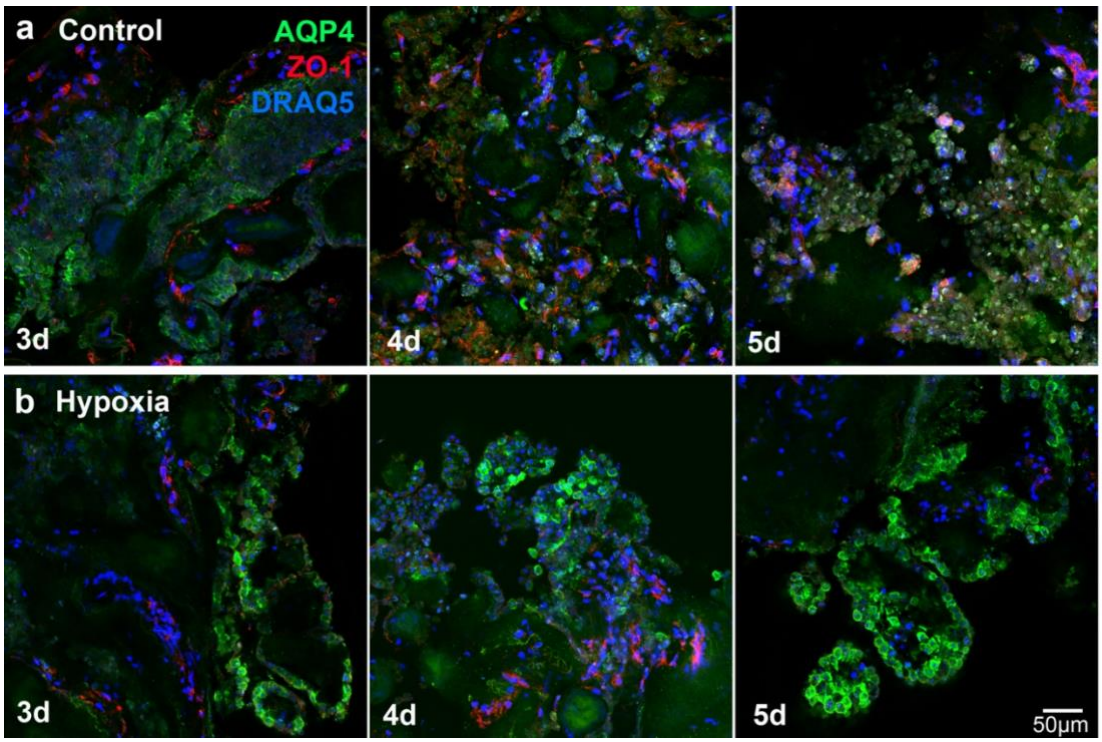


*Figure 24: Effect of hypoxia on AQP4 expression in human CP explant cultures.*
*The integrity of the CPECs, as indicated by ZO-1 staining (red), varies between regions and donors, making it sometimes difficult to evaluate the viability and to identify the cells. a. AQP4 expression (green) on the control group, cultured in normoxic conditions (20% $O_2$) after 3, 4 and 5 days of the experiment. AQP4 expression shows high variability in the number of positive cells and expression patterns. Notably, the AQP4 immunofluorescence signal appears less intense in most parts when compared to the control group b. AQP4 expression on CP explants cultured under hypoxic conditions after 3, 4, and 5 days of treatment. Several CPECs show strong AQP4 immunofluorescence signals, whereas others are immuno-negative. Nuclei are stained with DRAQ5 (blue).*

This observation was confirmed in a blinded experiment setting where a person not aware of the treatment evaluated the intensity and amount of AQP4 signal semi-quantitatively over the entire tissue culture pieces. However, it was not

possible to measure immunofluorescence signals over the entire tissue pieces as they exhibited large variations in the number of viable epithelial cells and age-related deposits which also showed false-positive immunofluorescence signals. To validate the semi-quantitative evaluation and investigate whether the number of AQP4-positive CPECs had increased by hypoxia treatment, cell counts were performed on randomly selected regions of the stained explant culture pieces (Table 11). Subsequently, the percentage of AQP4-positive cells of total number of epithelial cells was calculated (v1-12 in Table 11). Notably, the difference in immunofluorescence intensity was not taken into account in the collection of these data. Furthermore, tissue integrity varied between regions, resulting in areas that could not be evaluated. Note that tissue pieces from experimental groups were derived from the same CP region providing similar initial AQP4 levels. As described above, the amount of AQP4 expression varied substantially between CP regions, possibly resulting in different control values. The great variability of the data is also indicated by the large standard deviations (SD, Table 11) and visualized in Figure 25. However, a clearly higher number of AQP4-positive CPECs (in % of total CPECs per region) was counted after 5 days of hypoxia treatment (Figure 25, Table 11).

*Table 11: Numbers of AQP4-positive CPECs (in % of total CPECs per region) in human CP explant cultures treated with hypoxia compared to a control group.*

| ID | Type | Day | v1 (%) | v2 (%) | v3 (%) | v4 (%) | v5 (%) | v6 (%) | v7 (%) | v8 (%) | v9 (%) | v10 (%) | v11 (%) | v12 (%) | Mean (%) | SD |
|---|---|---|---|---|---|---|---|---|---|---|---|---|---|---|---|---|
| H102 | Hypoxia | 3 | 70 | 72.5 | 67.5 | 60 | - | - | - | - | - | - | - | - | 67.5 | 5.4 |
| H102 | Control | 3 | 45 | 57.5 | 95 | 95 | 87.5 | 90 | 90 | 85 | - | - | - | - | 80.63 | 18.74 |
| H102 | Hypoxia | 4 | 22.5 | 65 | 67.5 | 17.5 | 42.5 | 40 | 37.5 | 60 | - | - | - | - | 44.06 | 18.8 |
| H102 | Control | 4 | 30 | 25 | 30 | 50 | - | - | - | - | - | - | - | - | 33.75 | 11.09 |
| H102 | Hypoxia | 5 | 60 | 62.5 | 87.5 | 50 | 100 | 65 | 100 | 70 | - | - | - | - | 74.38 | 19.03 |
| H102 | Control | 5 | 27.5 | 32.5 | 35 | 40 | - | - | - | - | | | | | 33.75 | 5.2 |
| H103 | Hypoxia | 5 | 95 | 100 | 67.5 | 75 | 97.5 | 95 | 80 | 97.5 | 87.5 | 72.5 | 90 | 82.5 | 86.67 | 10.99 |
| H103 | Control | 5 | 97.5 | 95 | 100 | 90 | 87.5 | 97.5 | 95 | 95 | 52.5 | 62.5 | 57.5 | 62.5 | 82.71 | 18.17 |

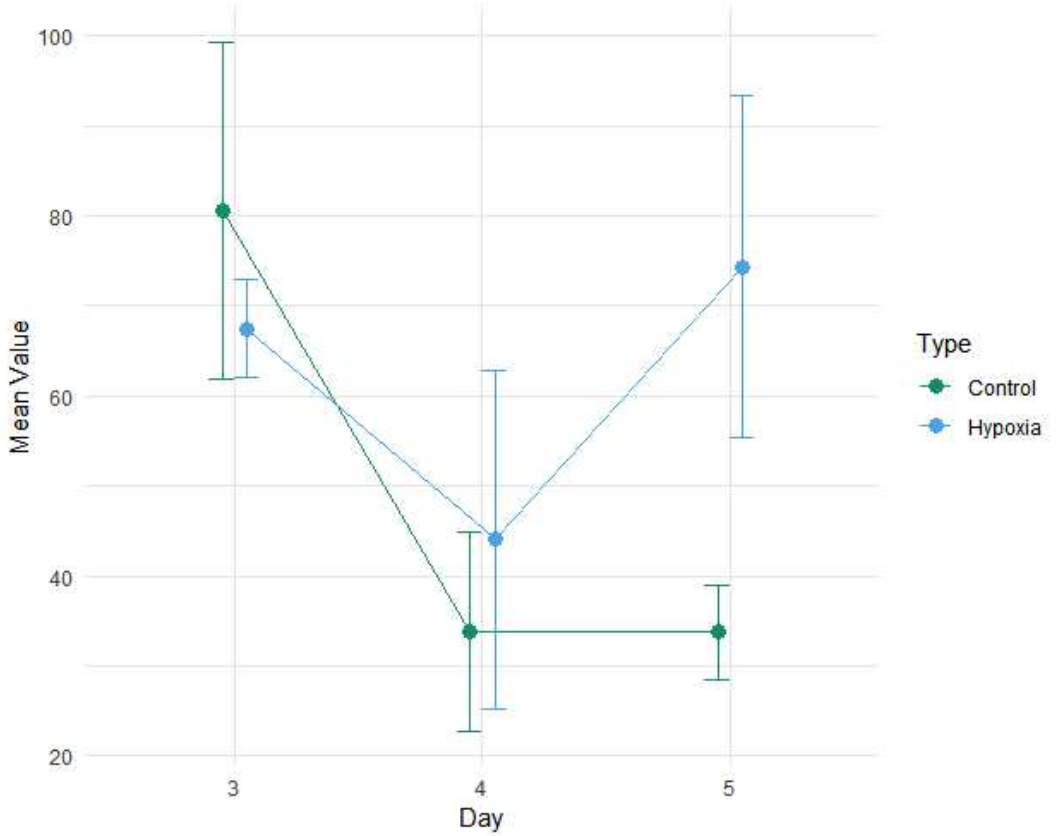


*Figure 25: Effect of hypoxia on AQP4 expression in human CP explant cultures over time.*
*Shown are the two types (control (green) and hypoxia (blue)) of human CP explant cultures over time in days following the mean values of CPECs with positive AQP4 expression (in % of total CPECs per region).*

The data were subsequently analyzed by performing a Wilcoxon test. Comparing the two groups hypoxia and control over all three days, the test revealed no statistically significant difference (p=0.50). Comparing the two groups hypoxia and control at day 5, the test showed a statistically significant difference (p=0.008). We repeated the experiment with explant cultures obtained from the following body donor (H103) and consequently restricted the hypoxia treatment to 5 days for all samples. Notably, cell counts revealed generally higher levels of AQP4-positive cells in H103 compared to H102 (Table 11) as visualized in Figure 26. Additionally, the values of AQP4-positive cells per region showed large variations, as already observed on ID H102 (see SD in Table 11 and Figure 26).

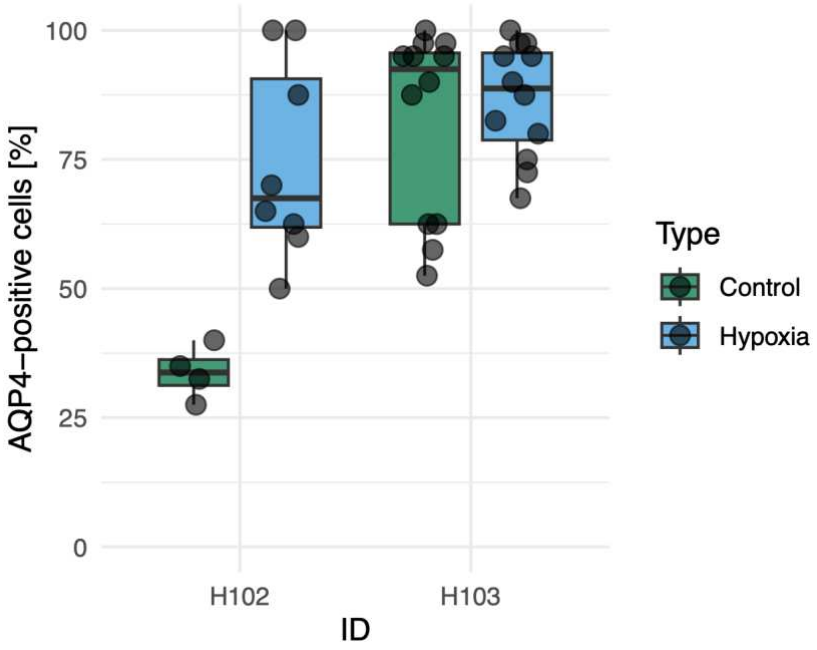


*Figure 26: Effect of hypoxia on AQP4 expression in human CP explant cultures of ID H102 and H103. Shown are the two types (control (green) and hypoxia (blue)) of human CP explant cultures of both IDs H102 and H103, following the values of CPECs with positive AQP4 expression (in % of total CPECs per region). Individual data measures are represented as black dots.*

A combined statistical analysis of both ID H102 and H103 data was performed by using a Wilcoxon test. Comparing the two groups (hypoxia and control) of all explant cultures at day 5 of treatment, no statistically significant difference was observed (p=0.24).

### *4.6.2 Hypoxia treatment of human primary CP dissociation culture*

In an attempt to obtain clearer results, hypoxia treatments were repeated on human CP dissociation cultures. In a first step, hypoxic *in vitro* conditions were verified using a hypoxia-sensitive marker (Figure 27).

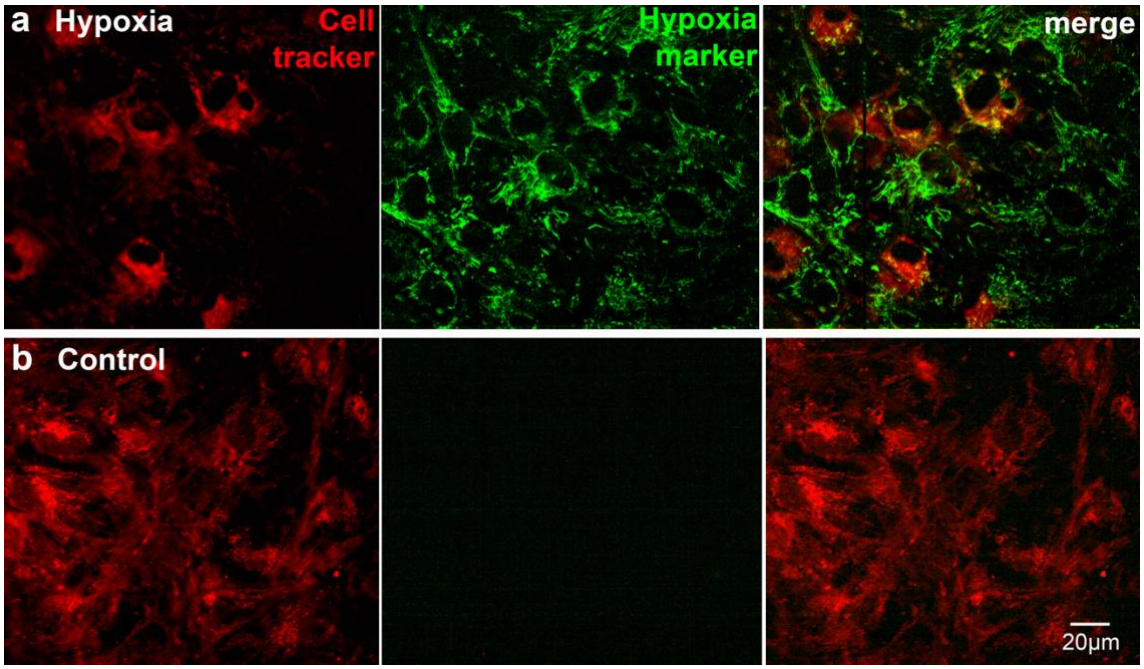


*Figure 27: Verification of hypoxic in vitro conditions in human primary CP dissociation culture. The cultures are stained with a cell tracker (CellTracker™ CM-DiI Dye) (red) and a hypoxia-sensitive marker (Image-iT™ Green Hypoxia Reagent) (green). a. The cells cultivated in hypoxic conditions (5% $O_2$) for 3 days show immunofluorescence signals when stained with the hypoxia-sensitive marker. b. The control group cultured under normoxic conditions (20% $O_2$) shows no immunofluorescence signal after exposure to the hypoxia-sensitive marker.*

Figure 28 shows an example of AQP4 staining results from CP dissociation cultures on collagen, showing untreated cells, cells treated with hypoxia for three days and a staining control. Notably, both hypoxia-treated and untreated CPECs showed similar AQP4 expression patterns (Figure 28). Although the variability in immunofluorescence signal intensity was much lower than the one observed in explant cultures, there were still substantial differences in the number of AQP4-positive cells between regions of the same plate in both hypoxia-treated and control groups (Figure 28).

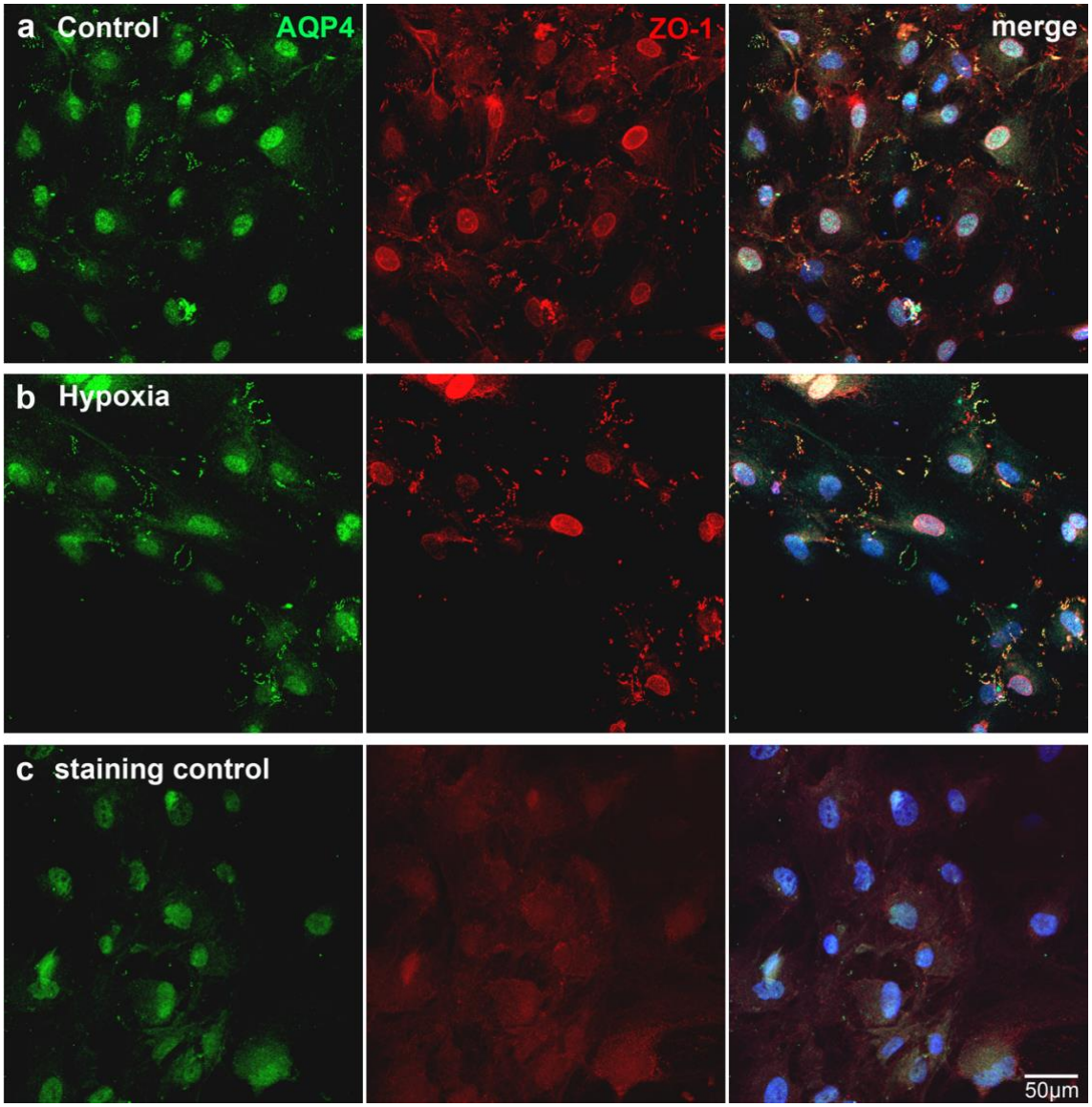


*Figure 28: Comparison of AQP4 and ZO-1 expression on hypoxia-treated human primary CP dissociation culture with a control group.*
*a. CPECs of the control group cultured under normoxic conditions demonstrate heterogenous expression of AQP4 (green) and ZO-1 (red) at cell-cell contacts as described above (Figure 22). b. CPECs cultured for 3 days under hypoxic conditions show similar AQP4 and ZO-1 expression patterns as the control group. c. Negative staining control using only secondary antibodies reveals an unspecific background signal in the nuclei from the green immunofluorescence staining on the cultures. Nuclei are stained with DAPI (blue).*

Cell counts were performed on randomly selected regions and cells were considered to be positive if they had at least one clearly identified region of AQP4 at the membrane border. Similar to the results of the explant cultures, great variability in the number of AQP4-positive cells between the body donors and between regions of the same cultures was observed (Table 12, Figure 29). The variabilities were visualized in a box plot in Figure 29.

*Table 12: Numbers of AQP4-positive CPECs (in % of total CPECs per region) in human primary CP dissociation cultures treated with hypoxia compared to a control group.*

| ID | Type | v1 (%) | v2 (%) | v3 (%) | v4 (%) | Mean | SD |
|---|---|---|---|---|---|---|---|
| H102 | Control | 25 | 45.5 | 37.5 | 67.6 | 43.9 | 17.91 |
| H102 | Hypoxia | 72.3 | 46.8 | 90 | 28.8 | 59.48 | 27.07 |
| H103 | Control | 9.8 | 17.5 | 8.6 | 13.5 | 12.35 | 4.02 |
| H103 | Hypoxia | 11.2 | 12.3 | 55.6 | 4.7 | 20.95 | 23.34 |

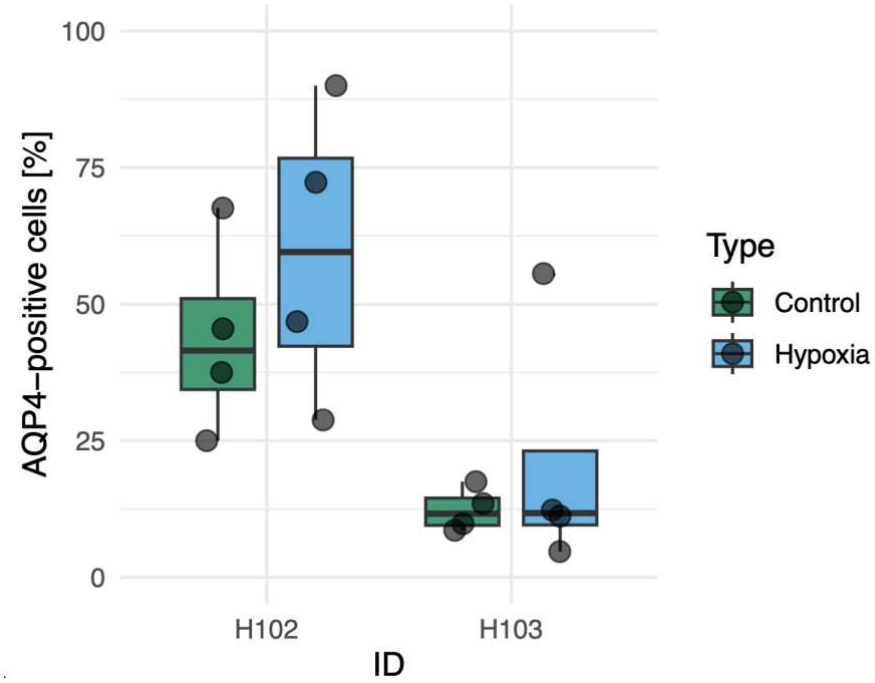


*Figure 29: Effect of hypoxia on AQP4 expression in human CP dissociation culture.*
*Shown are the two types (control (green) and hypoxia (blue)) of human CP dissociation cultures of both IDs H102 and H103, following the values (in % per region) of CPECs with positive AQP4 expression. Individual data measures are represented as black dots.*

For statistical analysis of the data, a Wilcoxon test was performed comparing the two groups (control and hypoxia) showing no statistically significant difference (p=0.51).

# 5 Discussion

This thesis work has explored and established different approaches to maintain and grow human CPECs in culture. Most remarkably, it shows that CNS tissue derived from *post mortem* human CP is viable enough to be maintained in explant cultures and expanded in dissociation cultures. These cultures provide a valuable tool for future research. While these cultures might serve different purposes concerning CPEC biology and BCSFB, our interest was to study the transport-related proteins, in particular the regulation of aquaporin expression. In the context of the recent discovery that the fast and most abundant water channel in the brain, AQP4, is not restricted to astrocytes and ependyma but also expressed in some but not all CPECs [69], we took first steps to identify regulating factors. Additionally, an extended histological characterization of the human CP and its attachment zone to the surrounding brain tissue was performed.

## 5.1 Establishment and characterization of the cultures

### *5.1.1 Cell proliferation*

Although there are not many data regarding proliferation in the adult CP, our results show that it is possible to stimulate human CPECs to expand in primary cultures, which implies cell division. CPECs are classified as macroglial cells, which, together with neurons are derived from neuroepithelial cells [115]. However, CPECs are unique to the CNS in exhibiting typical epithelial properties including the formation of a basal lamina and cell polarity. Although one characteristic of epithelial tissue in general is its regenerative capacity, proliferation in the CP epithelium is reported to occur only at a very low rate if at all [116, 117]. Our results suggest that the slow turnover rate of CPECs can be enhanced by proliferative culture conditions. Despite the longer time required for human CPEC cultures to proliferate and reach confluency after the initial seeding, they proliferated sufficiently to undergo multiple passages in medium supplemented with 10% FCS. Following studies demonstrating increased CPEC proliferation through growth factor supplementation, we added IGF-1 and EGF into our cultures [118]. As we did not observe any noticeable effect, this

additional variable was not included in our protocol, although we cannot rule out an impact due to the lack of quantified data. Notably, primary human CPEC dissociation cultures showed proliferative capacity even after cryopreservation at -80°C.

### *5.1.2 Characterization of CP cell types*

The process of obtaining primary cultures by tissue dissociation carries the risk of producing mixed cultures. Recently, Dani et al. provided a single-cell atlas of mouse CP, identifying six different cell types in the CP including epithelial, mesenchymal (fibroblasts), endothelial, immune (macrophages), neuronal and glial cells [119]. Additionally, the existence of cells with stem cell properties in the adult murine CP has been described, raising the question of whether proliferating cells are differentiated CPECs or progenitor cells [120]. In this study, human CP tissue was closely examined by immunohistochemical stainings. Investigating the stromal layer, astrocytes could be labeled with the marker GFAP, endothelial cells with CD-31 and macrophages with the marker Iba-1. Notably, astrocytes were exclusively present in proximity to the CP attachment zone whereas the rest of the human CP stroma showed no GFAP positive cells. Assessing the relative proportions of all non-epithelial CP cell types, we found a high number of macrophages in human CP stroma (up to 70%) besides abundant endothelial cells and some unlabeled cells. The high number of macrophages may be a species-related or an age-related phenomenon as it stands in contrast to the study of murine CP by Dani et al., who had identified fibroblasts as the second most abundant cell type after epithelial cells [119]. To prevent fibroblast contamination in CP dissociation culture both, a specific dissection technique and the use of an inhibitor of fibroblast growth such as AraC have been suggested [34, 121, 122]. Investigating the effect of AraC in our human CPEC culture model, we initially observed only small differences in the morphology of the cultures whereas after several weeks *in vitro*, the control group appeared overgrown. This observation indicates that AraC efficiently impairs fibroblast growth, and it correlates with our histological analyses suggesting the existence of few fibroblasts in human CP tissue. Interestingly, staining for Iba-1 on the control group revealed several

macrophages *in vitro*. However, no Iba-1 positive cells were found in cultures treated with AraC. Staining for endothelial (CD-31), glial (GFAP) and neuronal (HuCD) markers revealed no positive cells in both the control and AraC treated cultures. Characterizing the CPECs *in vitro*, we investigated the expression of a CPEC-specific marker, the morphology of the cultures and the expression of functional proteins. A protein that has been widely used as a specific marker for CPECs is transthyretin (TTR) [46, 48, 49, 53, 121, 123], which we found ubiquitously expressed in the human primary dissociation cultures. Additionally, the cells showed typical cuboidal morphology, which was further highlighted by labeling the cells' cytoskeleton. Investigating the expression of functional proteins, we found ZO-1 expressed at cell-cell contact sites, indicating the formation of tight junctions between the cells [45, 53]. Moreover, the cultured cells were also positive for AQP1, NKA and NKCC1. Taken together, these observations indicate that the proliferating cells in the newly established human dissociation cultures are differentiated CPECs. Interestingly, a study on primary porcine CP cultures suggested that the cultivation in serum-free medium enhanced cell contacts and polarity [124]. Exposing the human primary cultures to serum-free medium, we observed a decrease in cell proliferation, however, we did not observe substantial differences in the expression of characteristic CPEC-proteins compared to the control group. Therefore, we propose that serum withdrawal may not be necessary for the complete differentiation of primary human CPECs *in vitro*. In a review of CP culture models, Strazielle et al. note that the effect of serum-free medium has only been reported in porcine CP, whereas primary cultures from other species show differentiation in serum-supplemented medium [34]. Nonetheless, our results suggest that CPECs can be maintained in serum-free medium if they were previously cultured in serum-supplemented medium and reached sufficient cell numbers. This may be valuable for future research objectives.

### *5.1.3 Effects of collagen and laminin coating on the cultures*

Several notable differences were observed between the human dissociation cultures on different coatings. The first was the improved initial adherence of CPECs to collagen compared to laminin-coated surfaces. Additionally, the cells

exhibited a more heterogenous morphology on collagen coating compared to the predominantly cuboidal morphology observed on the laminin-coated surfaces. These findings are consistent with observations of previous CP culture studies [45, 53]. Nevertheless, immunofluorescence staining for functional proteins showed no substantial differences between cells cultured on collagen and laminin. While Strazielle et al. [45] suggest that laminin coating may favor the selection of epithelial cells, our observations imply that the type of coating primarily influences cell morphology and growth patterns rather than cell type selection. Consistently, Delery et al. reported a selective attachment of CPECs to collagen coating, with poor adherence for contaminating cells such as fibroblasts [53]. We suggest that both coatings are equally suitable for the investigation of functional mechanisms such as protein regulation, although the choice of coating may be relevant for investigations in other research fields such as barrier studies.

### 5.2 Advantages and challenges of primary cell cultures

As noted in the introduction, different types of cultures (primary cultures, cell lines, 3D-cultures, and organoids) are used in research, each with advantages and disadvantages that need to be considered based on the research objectives. Human CPECs have been cultured as cell lines derived from CP carcinoma and papilloma [40-42]. Cell lines offer advantages such as providing a pure and consistent population with reproducible results, easy handling, cost-effectiveness and, especially concerning CP material, accessibility [32]. However, it is important to recognize that cell lines, being genetically modified, are an artificial system. Genetic drift can occur spontaneously over time, leading to changes in phenotype such as protein expression, function and response to stimuli [125]. In particular, many immortalized CP cell line cultures have shown deviations from the characteristics of primary CPECs *in vitro*, exhibiting changes in morphology and properties, such as a lack of adherens junction proteins resulting in a poor barrier formation compared to primary cultures of rat or porcine CP [34, 126]. Observations regarding the properties of human CP cell lines vary among authors. For example, alterations in protein expression were reported in immortalized CPECs (HCPEpiC) compared to primary cells

[127]. Despite these challenges, certain cell lines, such as the HiBCPP cell line derived from human CP papilloma, have demonstrated expression of relevant marker genes and dense and continuous tight junctions under certain conditions, making them suitable for barrier studies [40-42].

While cell lines and organoids have proven to be valuable in various aspects of research, primary cultures are considered more relevant for addressing certain research questions, especially in studying molecular mechanisms of protein expression [128]. By establishing a primary culture model from human body donor CP, we provided an *in vitro* model that closely mimics the protein expression of the uncultured human cells. Both, fixed and cultured CPECs, showed positive immunofluorescence signals for the proteins TTR, actin, vimentin, ZO-1, AQP1, NKA, NKCC1 and, additionally, for AQP4. We therefore suggest this model to be a valuable tool to investigate functional mechanisms in human CPECs. Nevertheless, interpretation of the results obtained from primary culture models can be challenging as they exhibit substantial variability, for example concerning expression patterns. An additional issue of this culture model is the limited availability of human body donors, who also vary in *post mortem* time and age.

### 5.3 Regulation of AQP4 expression in CPECs

Although various molecular pathways of AQP4 regulation have been extensively studied, the understanding of this complex process remains incomplete. In addition to regulating AQP4 expression at the transcriptional and translational level, its functionality can be mediated by protein trafficking, modulations like phosphorylation, and interactions with other proteins, such as anchoring proteins [84]. While there exists a large body of literature on AQP4 regulation in astrocytes, it was long thought that CPECs exclusively express AQP1 as a water channel. However, recent evidence has shown that AQP4 can be upregulated in the CP epithelium under certain conditions such as hypoxia [63]. Based on these findings, we tested the effect of hypoxia on AQP4 in the newly established human CP cultures. Additionally, we investigated possible

correlations between AQP4 expression and changes in the basal lamina and the DGC, which is suggested to be the link between these components.

### *5.3.1 Regulation of AQP4 by the basal lamina and DGC anchoring*

In line with the results of Deffner et al. [69], we observed that several of the AQP4-positive CPECs displayed a basolateral, polar AQP4 expression pattern. Additionally, in our dissociation culture model, AQP4 expression was restricted to cell borders, in contrast to the cytoplasmatic expression pattern of AQP1, suggesting a potential interaction of AQP4 with specific membrane-associated proteins that do not interact with AQP1. Previous studies have shown that specific components of the basal lamina, such as agrin and laminin, induce AQP4 clustering in cell cultures [89, 90, 129, 130]. Additionally, silencing or knockout of β-DG and Dp, two components of the DGC, has been shown to disrupt AQP4 polarity on astrocytes [88-90, 131, 132]. In our study, CPECs were cultured on laminin and collagen coatings, the latter of which, to our knowledge, has not been reported to interact with the DGC. We therefore expected different AQP4 expression patterns on these coatings. Nevertheless, we found the membranous expression pattern of AQP4 at cell-cell contact sites on both laminin and collagen coatings. Additionally, co-stainings of AQP4 with laminin, β dystroglycan (DG) and dystrophin (Dp) were performed on thin sections of fixed human CP tissue. Laminin appeared regularly expressed at the basolateral side of the CP epithelium, without displaying any changes between AQP4-positive and AQP4-negative CPECs. This finding is consistent with the observation in the cultures, indicating a distinct underlying mechanism for AQP4 regulation in CPECs. The staining results for Dp were negative for both AQP4-positive and AQP4-negative CPECs, although outside the CP there was a strong reactivity. However, staining for β-DG showed a continuous basolateral expression along the entire human CP epithelium, also independent of AQP4 expression. The presence of β-DG suggests the existence of a DGC in the CP epithelium that is composed of homologue proteins. A possible candidate could be the Dp homologue utrophin, which has been described in the murine CP epithelium and may not have been recognized by our anti-Dp antibody [133]. Interestingly, the same study also reported negative results for β-DG in murine

CPECs, which is contrary to our findings in human CPECs. Therefore, the possibility of an additional species-related difference in the composition of the DGC should be considered. Nevertheless, our observation that β-DG expression in human CPECs is independent of AQP4 expression indicates a different regulation mechanism for AQP4 in these cells. Previous studies have shown the existence of both Dp-dependent and Dp-independent AQP4 clusters in the mouse brain [134], and heterogeneity in AQP4 anchoring mechanisms has been suggested by various researchers [68, 135]. For example, the role of AQP4 isoforms is discussed as an alternative regulation mechanism for AQP4 polarity. In earlier studies, the isoform M23 was identified as the predominant form in higher order aggregates known as OAPs and in astrocytic endfeet membranes [72]. It was suggested that M23-OAPs are responsible for AQP4 anchoring through their immobility [136]. Additionally, it has been suggested that OAP size, controlled by the compositions of the different AQP4 isoforms, is associated with different anchor proteins [137]. However, the recent discovery of the new AQP4ex isoform has led to new considerations as it has been shown to affect AQP4 polarization through interaction with α-syntrophin [77]. Recently, a complete loss of AQP4 polarity and mislocalization of α-syntrophin in astrocytic endfeet of AQP4ex-deficient mice was reported. The authors conclude that although the diffusional mobility of OAPs is indeed dependent on the OAP size, this effect is only minimally responsible for AQP4 polarization in astrocytes [138]. Whether these results apply to the CPECs remains to be determined.

Extending our investigations to the transitional zone between CP and brain tissue, we discovered a surprisingly strong and unpolarized AQP4 expression in astrocytes of this region. Interestingly, Dp staining showed a similarly strong unpolarized reactivity, meanwhile, β-DG was negative in these cells except in endfeet around blood vessels. These observations suggest that the membrane localization of AQP4 is differently regulated in perivascular astrocytes, astrocytes in the *Taenia choroidea* and CPECs. Functional implications of these observations are discussed in a subsequent part.

### *5.3.2 Effect of hypoxia on AQP4 expression*

An effect of hypoxic conditions on AQP4 expression has been suggested by several different studies in distinct cell types such as astrocytes [139] or cells in the placenta [140]. Most relevant for our study, Trillo-Contreras et al. were able to show a significant increase of AQP4 mRNA and protein levels in the CP epithelium when mice were kept under hypoxic conditions [63]. These observations are in line with the suggestion of an age-dependent underlying mechanism [69], as changes in the aged CP include stromal deposits and an enlarged diffusion pathway from the capillaries to the CP epithelium [106, 107]. Subsequently, CPECs may be impaired by hypoxia which has been suggested to effect AQP4 regulation on different levels. One molecular mechanism of hypoxia is the upregulation of the transcription factor HIF-1α, which has been shown to increase AQP4 mRNA and protein levels [78]. Additionally, hypoxia has been suggested to interfere with phosphorylation processes of AQP4 that cause conformational changes of the water channel protein, leading to its relocalization [80, 82]. In our study, exposing human CP explant cultures to hypoxia, we observed both a substantial increase in the intensity of the AQP4 immunofluorescence signal, especially after 5 days of treatment, and occasional shifting from a primarily membranous to a cytoplasmatic expression pattern. Changes in the pattern and intensity of AQP4 expression were also observed in a few samples of the control group, although much less pronounced. To investigate whether the number of AQP4-positive cells had increased in the hypoxia-treated cultures, cell counts were performed. Comparing the two groups (control and hypoxia treated) of the explant cultures obtained from the first body donor, we found a significantly higher number ($p=0.008$) of AQP4-positive cells after 5 days of hypoxia treatment. However, repeating the experiments with explant cultures from the second body donor did not yield the same results and over all did not result in a significant difference ($p=0.24$). This indicates that there might not be a direct effect of hypoxia and possibly other mechanisms involved in the expression of AQP4 in CPECs. Notably, we faced several challenges during cell counting. Variability of epithelial integrity and ZO-1 expression resulted in areas that could not be evaluated whereas other

regions were well maintained. Additionally, the initial number of AQP4-positive cells varied substantially between regions and body donors. We attempted to minimize this effect by splitting explant culture pieces and assigning one half to the control group and the other to the hypoxia treated group. However, on a microscopic scale there were still large differences that resulted in different control values. Notably, the explant culture of the second body donor showed very high numbers of AQP4 positive cells (up to 100%) that might conceal a possible effect. Furthermore, the difference in immunofluorescence intensity was not taken into account in the collection of this data as cells in the cell counts were considered positive when they showed any kind of AQP4 immunofluorescence signal. We thus conclude that further experiments are needed to evaluate whether or not there is an effect of hypoxia on AQP4 regulation in CPECs.

### *5.3.3 AQP4 on murine culture*

In previous studies, the presence of AQP4 at the protein level in murine CPECs under physiological conditions remained undetected. Although Deffner et al. showed an increase in AQP4 mRNA in aged mice compared to young mice, their immunofluorescence analyses showed no AQP4 expression in murine CPECs [69]. Surprisingly, our examination of murine explant cultures revealed the presence of several AQP4-positive CPECs. Co-staining with the proliferation marker Ki67 indicated that some of these AQP4-positive cells had undergone proliferation *in vitro*. As our study focused primarily on human CP cultures, we did not investigate this finding any further. Future studies on these cultures are needed and might contribute to the understanding of AQP4 regulation in CPECs.

## 5.4 Functional implications of AQP4 in the ageing CP and *Taenia choroidea*

In their study, Deffner et al. suggested that AQP4 expression on CPECs may be an age-related process as they were able to show an increase of AQP4 on the mRNA level in old mice compared to younger mice [69]. As water flow through aquaporins is not directed in one specific direction but driven by osmotic and hydrostatic gradients, they suggested two opposing theories about the effect of AQP4 on CSF production. The first theory implies an inward-directed water flow in which basolateral AQP4 enhances water entry into CPECs, which could facilitate CSF production. This would imply a compensatory mechanism in the aged brain, where the diffusion pathway between CP capillaries to CPECs is enlarged through stromal fibrosis and age-related deposits [69, 107]. This theory was supported by Trillo-Contreras et al., whose data showed that aging and hypoxia had a synergistical effect in increasing AQP4 levels, leading to hydrocephalus in mice [63].

The second theory describes an outward-directed water flow, where water leaks out of the CPECs, which would result in reduced CSF production. A decline in CSF secretion with age has been documented in rodents, sheep and humans [141-143]. Such increased water backflow into the CP stroma is likely to affect brain water homeostasis as there is no barrier between the CP stroma and the adjacent brain tissue [144]. This missing barrier between fenestrated blood-vessels in the CP stroma and the brain parenchyma has previously been suggested as entry route for viral CNS infection [145] and immune cells [146]. Extending our investigation on this CP to brain tissue transition zone, we observed a substantially high AQP4 expression on astrocytes in this region on the human body donor tissue. We thus hypothesize that astrocytes in this region might form a cuff between the CP stroma and brain tissue, limiting water transition between these tissues (Figure 30) [113]. Additionally, high levels of AQP4 on these astrocytes might contribute to enhanced water re-absorbance capacity for both, fluids coming from the CP and the interstitial fluid from the brain parenchyma, with a subsequent drainage into the fenestrated blood-vessels. Thereby, these astrocytes in the *Taenia choroidea* may contribute to

the clearance of metabolites from the brain parenchyma and thus be part of the glymphatic drainage pathway. Whether this phenomenon may also be age-related remains to be shown.

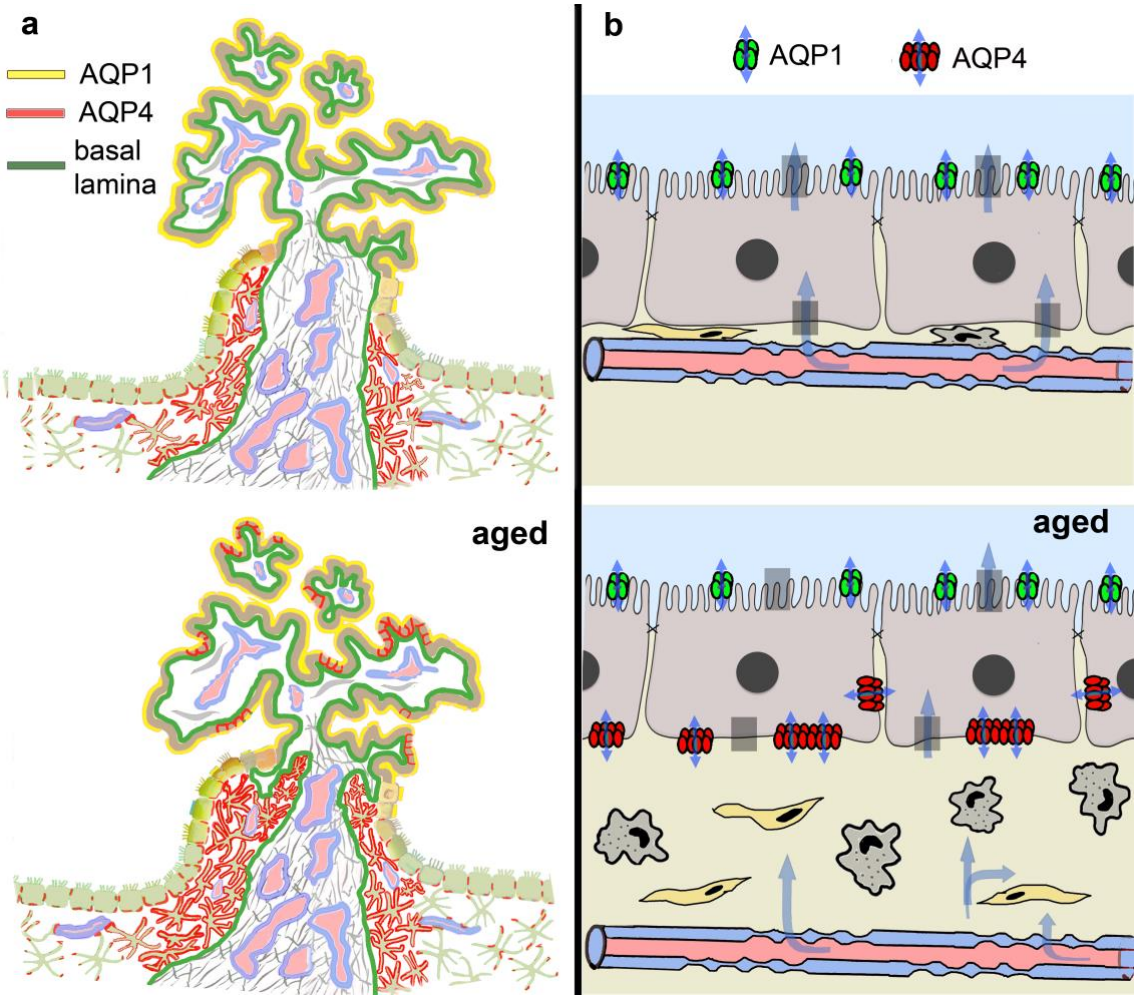


*Figure 30: Schematic illustrations summarizing AQP expression in the ependyma, the CP and the trans-itional zone, in addition to changes that occur during ageing*
*A, the blood vessels entering the CP are surrounded by meningeal tissue forming the CP stroma. They are surrounded by a subpial/perivascular basal lamina continuous with the CP epithelial basal lamina. In the trans-ition zone, this basal lamina is covered by strongly AQP4-expressing astrocytic processes, forming a glial plate. B, capillaries in the CP stroma are fenestrated, facilitating CSF secretion by CPEs through transporters and channels, including apical AQP1. The capillary fenestration also implies the lack of a barrier between the stroma and the glial plate in the transition zone. In the ageing CP, the stroma is enlarged by thicker connective tissue and infiltrated immune cells, such as macrophages. Also, many CPEs express AQP4 basolaterally, possibly compensating for obstructed diffusion. We hypothesize that the high density of AQP4 water channels in the glial plate provides a possible clearance pathway for metabolites from brain parenchyma, draining into stromal blood vessels. Abbreviations: AQP1, aquaporin-1; AQP4, aquaporin-4; CP, choroid plexus; CPEs, choroid plexus epithelial cells. Modified with permission from Deffner et al. (2022) and Bihlmaier et al. (2023).*
*Figure from [113]*

## 5.5 Implications for Alzheimer's disease

Alzheimer's disease (AD) dementia is a very burdensome disease, with a worldwide steadily increasing disease burden according to the Global Burden of Disease (GBD) classification system [147, 148]. It is characterized by an age-related particular progression of cognitive and functional decline combined with a specific neuropathology [109]. Although the precise pathophysiological mechanisms of this disease are still under debate, it is generally accepted that neuronal decline is caused by the accumulation of proteins in the brain, such as β-amyloid (Aβ) [109, 149, 150]. Several changes in CP tissue have been associated with this Aβ accumulation and with AD. In particular, age-related changes observed in the CP such as epithelial cell atrophy, thickening of the basal lamina, increased deposits (as Biondi ring tangles) and stromal fibrosis are significantly more pronounced in AD [151-153]. Additionally, a recent MRI study showed that a larger CP volume and reduced CP permeability correlate with the severity of cognitive impairment in AD [154]. Investigations of both Aβ production and clearance rate in AD patients found that the Aβ production rate was not different compared to controls, whereas the Aβ clearance rate was significantly reduced in the AD group [155]. Together with the original description of the glymphatic pathway, Iliff et al. demonstrated that a reduction in CSF production leads to impaired clearance of Aβ [7]. In their study, reduced CSF flow was induced in mouse models by knocking out AQP4. This effect of AQP4 on the glymphatic pathway was primarily attributed to facilitated CSF absorption in astrocytic endfeet [7]. However, the discovery of AQP4 expression on CPECs and the observed correlations with age and hypoxia suggest an additional role for AQP4 in these cells in CSF homeostasis in AD [69, 156].

# 6 Conclusion

The CSF system has recently gained increased attention as an important part of the brain's clearance and water homeostasis system. This is referred to as the glymphatic pathway theory and has been suggested to involve the water channel AQP4 and to be an important component in understanding the pathogenesis of neurodegenerative diseases. CP culture models are a valuable tool for investigating the regulation and production of CSF, as well as for BCSFB studies. Although many primary culture models, cell lines and 3D culture models exist from different animal species, human CP culture models are not readily available except for a few studies on cell lines and organoids. In this study, we have successfully established two primary CP culture models from human body donors, providing new opportunities to perform studies in a less artificial system. Human primary CP cultures showed optimal growth in serum-supplemented medium conditions and benefited from the use of AraC to suppress fibroblast and macrophage subcultures. The addition of growth factors had no apparent effect and was not pursued in this study. Tissue integrity was maintained in most explant cultures throughout the cultivation period, with positive immunofluorescence signals for CPEC-typical proteins. Nevertheless, alterations in the expression patterns were observed, indicating a loss of polarization. Human primary dissociation cultures were identified as epithelial, showing positive immunofluorescence signals for CPEC-typical proteins. The cultures were cultivated on both laminin and collagen coatings exhibiting differences in growth and morphology but showing similar protein expression patterns. Cultures could be passaged up to 6 times and proliferative capacity was restored after cryopreservation at -80ºC. Although access to human body donor tissue is limited and varies in *post mortem* time and age, we suggest these cultures to be a valuable tool for future research.

The water channel AQP4 has been reported to play a central role in the functionality of the glymphatic system and consequently in brain water homeostasis and health. Following the recent discovery of AQP4 expression in human body donor CPECs, the new culture models were subsequently used for first investigations of regulatory mechanisms behind this phenomenon.

Comparing AQP4 expression on CPECs cultured on laminin, a coating known to induce AQP4 clustering in astrocyte cultures, we observed no difference to the expression pattern on collagen coating. Another possible mechanism that may induce AQP4 in CPECs is hypoxia, as previous studies found AQP4 expression in CPECs of hypoxia treated mice. CP tissue undergoes age-related changes, which include stromal fibrosis and a subsequently enlarged diffusion pathway, which are even more pronounced in AD. Subsequently, CPECs may experience oxygen deficits in these tissues. Investigating the effect of hypoxic conditions on the AQP4 expression in human CP explant cultures, we observed increased AQP4 intensity after 5 days of hypoxia treatment and cell counts revealed a significantly increased number of AQP4-positive cells compared to the control group. However, repeating the hypoxia experiments in cultures obtained from another body donor did not show a statistically significant difference, providing overall no definite effect of hypoxia treatment. It should be noted that we faced several challenges during cell counting. Firstly, there was substantial variability in the initial AQP4 levels between regions and body donors. We attempted to minimize this effect by splitting explant culture pieces and assigning one half to the control group and the other to the hypoxia treated group. However, on a microscopical level there were still significant differences observed. Secondly, cell viability and tissue integrity varied between the pieces, resulting in areas that could not be evaluated. Finally, the intensity of the immunofluorescence signal was not considered in the cell counting. We therefore suggest that further experiments should be carried out to determine whether or not there is an effect of hypoxia on AQP4 expression in these cells. If a hypoxic state induced AQP4 expression in CPECs, this could either compensate and increase CSF production, or act as a functional leak, thereby decreasing CSF production in the ageing brain.

As a second aim of this study, an extended histological characterization of the human CP and its attachment zone was performed, providing new insights into water homeostasis in this contact zone between the CSF and the blood system. Therefore, the potential role of the DGC, a structure involved in AQP4 anchoring, was investigated by immunofluorescence staining on cryostat

sections of fixed human CP tissue. In the CP epithelium, Dp staining was negative whereas DG showed a positive immunofluorescence signal that was independent of AQP4 expression in CPECs. These results, combined with the observation that laminin substrate had no effect on AQP4 expression *in vitro,* indicate a distinct underlying regulatory mechanism in CPECs. Interestingly, astrocytes in the *Taenia choroidea* showed a strongly increased and unpolarized AQP4 and Dp immunofluorescence signal whereas DG was negative. This suggests that these astrocytes also have a different AQP4 regulation than the astrocytes in the brain parenchyma. Based on these observations, we propose that astrocytes in this transition zone may play a unique role in water absorption in this region, thereby participating in the control of a functional leakage between the CP tissue and the adjacent brain tissue. Subsequently, this process may contribute substantially to the glymphatic pathway.

Dysfunction of the brain’s clearance system plays an important role in the pathogenesis of neurodegenerative diseases such as AD. It is therefore highly relevant to do further research in order to gain a deeper understanding of underlying mechanisms.

# 7 Deutsche Zusammenfassung

Der *Plexus choroideus* ist ein Gewebe in den Ventrikeln des inneren Liquorsystems des Gehirns, dessen zentrale Aufgaben die Produktion von Liquor und der Aufbau der Blut-Liquor-Schranke sind. Mit der Entdeckung, dass Liquor über den perivaskulären Raum mit dem Interstitium des Gehirnparenchyms kommuniziert und so zur Beseitigung von Abfallprodukten aus dem Gehirn beiträgt, erhielt das Liquorsystem eine neue Relevanz, da Ablagerungen im Gehirn zu dessen Funktionsverlust führen und ein zentrales Merkmal vieler neurodegenerativer Erkrankungen, wie z.B. der Alzheimer-Krankheit, sind. Da Lymphgefäße im Gehirn fehlen und diese Drainagefunktion dort von Gliazellen übernommen wird, insbesondere durch Kanalproteine wie dem Wasserkanal Aquaporin-4 (AQP4), entstand die neue Bezeichnung „glymphatisches“ System. Ziel dieser Arbeit war es, humanen *Plexus choroideus* weiter zu charakterisieren und ein *in vitro* Modell zu etablieren, um Regulationsmechanismen der Liquorproduktion untersuchen zu können. Während es etliche Primärkulturmodelle, Zelllinien und 3D-Kulturmodelle von verschiedenen Tierarten gibt, sind menschliche *Plexus choroideus* Kulturmodelle, mit Ausnahme einiger weniger Studien an Zelllinien und Organoiden, kaum verfügbar. Im Rahmen dieser Arbeit wurden zwei Primärkulturmodelle für humane *Plexus choroideus* Epithelzellen etabliert, die neue Möglichkeiten für Studien in einem näher an der menschlichen Realität liegenden System bieten. Dafür wurde das Wachstum humaner *Plexus choroideus* Epithelzellen aus dem Gehirn von Körperspendern unter verschiedenen Kulturbedingungen untersucht. Die Kulturen zeigten optimales Wachstum in serumhaltigem Medium. Die Behandlung mit Cytarabin (AraC) inhibierte das Wachstum von Fibroblasten und Makrophagen, wohingegen der Zusatz von Wachstumsfaktoren keinen sichtbaren Effekt zeigte. Explantatkulturen wiesen in den meisten Regionen einen guten Gewebeerhalt auf und bewahrten eine ähnliche Proteinexpression wie die des nativen Gewebes. In Dissoziationskulturen zeigten Zellen die spezifische Proteinexpression von *Plexus choroideus* Epithelzellen und entwickelten morphologische Charakteristika von Epithelzellkulturen. Die Dissoziationskulturen wurden parallel auf Laminin- und Kollagenbeschichtung

kultiviert und wiesen Unterschiede in Wachstum und Morphologie, nicht jedoch in den Expressionsmustern der untersuchten Proteine auf. Die humanen *Plexus choroideus* Primärkulturen konnten bis zu sechs Mal passagiert werden und zeigten selbst nach Kryokonservierung bei -80ºC Proliferationsfähigkeit. Obwohl der Zugang zu menschlichem Körperspendergewebe begrenzt ist und sowohl das Alter als auch das *post-mortem* Intervall variiert, sind diese humanen *Plexus choroideus* Primärkulturmodelle ein wichtiges Werkzeug für zukünftige Studien im Bereich der Liquor- und Blut-Hirn-Schrankenforschung.

AQP4 ist das wichtigste Wasserkanalprotein des Gehirns und hat große Bedeutung für den Wasserhaushalt und somit auch die Funktionalität des Gehirns. Die jüngste Entdeckung von Deffner et. al., dass AQP4 in manchen *Plexus choroideus* Epithelzellen des humanen Gehirns exprimiert wird, wirft Fragen über die Regulation und Funktionalität der AQP4 Expression in diesen Zellen auf. Die Regulation von AQP4 ist bis heute nicht vollständig verstanden und umfasst verschiedene Aspekte, von denen wir uns in dieser Studie auf zwei konzentriert haben: die Bedeutung des Dystrophin-Glykoprotein-Komplexes im Bereich des *Plexus choroideus* und den Einfluss von hypoxischen Bedingungen in kultivierten Epithelzellen. Studien haben gezeigt, dass spezifische Komponenten der Basallamina die AQP4 Expression beeinflussen, indem sie mit dem Dystrophin-Glykoprotein-Komplex interagieren. Um zu untersuchen, ob dieser Regulationsmechanismus auch für die AQP4 Expression in humanen *Plexus choroideus* Epithelzellen gilt, wurde die AQP4 Expression auf Laminin, eine Basallamina Komponente, die mit dem Dystrophin-Glykoprotein-Komplex interagiert, mit der auf Kollagen, einer Komponente, für die keine solche Interaktion bekannt ist, in den neu etablierten Kulturen verglichen. Zusätzlich wurden die Expressionsmuster von AQP4 und Laminin, sowie von Proteinen des Dystrophin-Glykoprotein-Komplexes auf fixiertem *Plexus choroideus* Gewebe verglichen. Unsere Ergebnisse deuten darauf hin, dass die Regulation von AQP4 in humanen Plexus choroideus Epithelzellen unabhängig von dessen Interaktion mit dem Dystrophin-Glykoprotein Komplex und der Basallamina ist.

Da vor kurzem gezeigt wurde, dass hypoxische Bedingungen in Mäusen eine AQP4 Produktion in *Plexus choroideus* Epithelzellen auslösen, setzten wir die

humanen *Plexus choroideus* Kulturen solchen Bedingungen aus und verglichen die AQP4 Expression mit einer Kontrollgruppe. Interessanterweise zeigten die unter hypoxischen Bedingungen kultivierten Explantatstücke in vielen Regionen ein sehr stark positives Immunofluoreszenzsignal. Um ausschließlich das spezifische Signal in *Plexus choroideus* Epithelzellen zu bewerten, wurden Zellzählungen durchgeführt. Dabei wurde in verschiedenen zufällig ausgewählten Regionen der Prozentsatz an AQP4-positiven Epithelzellen pro Gesamtzahl der Epithelzellen ermittelt. Die Ergebnisse deuteten auf einen Stimulationseffekt nach 5 Tagen Hypoxie Behandlung hin. Die Wiederholung des Experiments mit Kulturen eines anderen Körperspenders ergab jedoch insgesamt keinen statistisch signifikanten Unterschied. Weitere Experimente sind notwendig, um einen Effekt der Hypoxiebehandlung auf die AQP4-Expression nachzuweisen oder zu widerlegen.

In einer erweiterten histologischen Charakterisierung des humanen *Plexus choroideus* wurde dessen Übergangszone zum Gehirnparenchym, welche auch als *Taenia choroidea* bezeichnet wird, untersucht. Diese Region ist von besonderem Interesse, da im Stroma des *Plexus choroideus* die Blut-Hirn-Schranke unterbrochen ist und somit an dieser Stelle eine mögliche Eintrittspforte von Wasser aber auch von Erregern in das Gehirnparenchym besteht. Interessanterweise beobachteten wir, dass Astrozyten in der Übergangszone eine veränderte Expression von AQP4 und dem Dystrophin-Glykoprotein Komplex aufwiesen. Die sehr starke und unpolare Expression von AQP4 an dieser Stelle lässt vermuten, dass Astrozyten in dieser Region eine wichtige resorptive und damit schrankenähnliche Funktion für die Wasser-Homöostase und -drainage im Sinne des glymphatischen Systems einnehmen könnten.

Erkenntnisse über die AQP4 Expression und Regulation in humanem Plexus choroideus und dessen Übergangszone können einen wichtigen Beitrag zum Verständnis des Reinigungssystems des Gehirns und damit zum Verständnis des Pathomechanismus neurodegenerativer Erkrankungen wie der Alzheimer-Krankheit leisten.

# 8 Literaturverzeichnis


1. Daneman, R. and A. Prat, *The Blood–Brain Barrier.* Cold Spring Harbor Perspectives in Biology, 2015. **7**(1): p. a020412.
2. Rasmussen, M.K., H. Mestre, and M. Nedergaard, *Fluid transport in the brain.* Physiol Rev, 2022. **102**(2): p. 1025-1151.
3. Engelhardt, B. and L. Sorokin, *The blood-brain and the blood-cerebrospinal fluid barriers: function and dysfunction.* Seminars in Immunopathology, 2009. **31**(4): p. 497-511.
4. Segal, M.B., *Extracellular and cerebrospinal fluids.* Journal of Inherited Metabolic Disease, 1993. **16**(4): p. 617-638.
5. Stern, L. and R. Gautier, *Recherches sur Le liquide céphalo-rachidien: I.–Les rapports entre Le liquide céphalo-rachidien et la circulation sanguine.* Archives Internationales de Physiologie, 1921. **17**(2): p. 138-192.
6. Spector, R. and C.E. Johanson, *The nexus of vitamin homeostasis and DNA synthesis and modification in mammalian brain.* Molecular Brain, 2014. **7**(1): p. 3.
7. Iliff, J.J., et al., *A Paravascular Pathway Facilitates CSF Flow Through the Brain Parenchyma and the Clearance of Interstitial Solutes, Including Amyloid β.* Science Translational Medicine, 2012. **4**(147): p. 147ra111-147ra1.
8. Bohr, T., et al., *The glymphatic system: Current understanding and modeling.* iScience, 2022. **25**(9): p. 104987.
9. Spector, R., S. Robert Snodgrass, and C.E. Johanson, *A balanced view of the cerebrospinal fluid composition and functions: Focus on adult humans.* Exp Neurol, 2015. **273**: p. 57-68.
10. Sakka, L., G. Coll, and J. Chazal, *Anatomy and physiology of cerebrospinal fluid.* Eur Ann Otorhinolaryngol Head Neck Dis, 2011. **128**(6): p. 309-16.
11. Davson, H. and M.B. Segal, *Physiology of the CSF and blood-brain barriers.* (No Title), 1996.
12. Nilsson, C., et al., *Circadian variation in human cerebrospinal fluid production measured by magnetic resonance imaging.* American Journal of Physiology-Regulatory, Integrative and Comparative Physiology, 1992. **262**(1): p. R20-R24.
13. Xie, L., et al., *Sleep Drives Metabolite Clearance from the Adult Brain.* Science, 2013. **342**(6156): p. 373-377.
14. Orešković, D., M. Radoš, and M. Klarica, *Role of choroid plexus in cerebrospinal fluid hydrodynamics.* Neuroscience, 2017. **354**: p. 69-87.
15. Damkier, H.H., P.D. Brown, and J. Praetorius, *Cerebrospinal Fluid Secretion by the Choroid Plexus.* Physiological Reviews, 2013. **93**(4): p. 1847-1892.
16. Iliff, J.J., et al., *Brain-wide pathway for waste clearance captured by contrast-enhanced MRI.* Journal of Clinical Investigation, 2013. **123**(3): p. 1299-1309.
17. Mott, F., *The Oliver-Sharpey lectures on the cerebrospinal fluid.* Lancet, 1910. **2**(1): p. 79.

18. Jessen, N.A., et al., *The Glymphatic System: A Beginner's Guide.* Neurochemical Research, 2015. **40**(12): p. 2583-2599.
19. Proulx, S.T., *Cerebrospinal fluid outflow: a review of the historical and contemporary evidence for arachnoid villi, perineural routes, and dural lymphatics.* Cellular and Molecular Life Sciences, 2021. **78**(6): p. 2429-2457.
20. Louveau, A., et al., *Structural and functional features of central nervous system lymphatic vessels.* Nature, 2015. **523**(7560): p. 337-341.
21. Bohr, T., et al., *The glymphatic system: Current understanding and modeling.* iScience, 2022. **25**(9): p. 104987.
22. Brown, P.D., et al., *Molecular mechanisms of cerebrospinal fluid production.* Neuroscience, 2004. **129**(4): p. 955-968.
23. Kierdorf, K., et al., *Macrophages at CNS interfaces: ontogeny and function in health and disease.* Nature Reviews Neuroscience, 2019. **20**(9): p. 547-562.
24. Spector, R., et al., *A balanced view of choroid plexus structure and function: Focus on adult humans.* Experimental Neurology, 2015. **267**(Supplement C): p. 78-86.
25. Kratzer, I., J. Ek, and H. Stolp, *The molecular anatomy and functions of the choroid plexus in healthy and diseased brain.* Biochimica et Biophysica Acta (BBA) - Biomembranes, 2020. **1862**(11): p. 183430.
26. Wolburg, K., et al., *Ultrastructural localization of adhesion molecules in the healthy and inflamed choroid plexus of the mouse.* Cell and Tissue Research, 1999. **296**(2): p. 259-269.
27. Quintela, T., et al., *Gender associated circadian oscillations of the clock genes in rat choroid plexus.* Brain Structure and Function, 2015. **220**(3): p. 1251-1262.
28. Zlokovic, B.V., et al., *Differential Regulation of Leptin Transport by the Choroid Plexus and Blood-Brain Barrier and High Affinity Transport Systems for Entry into Hypothalamus and Across the Blood-Cerebrospinal Fluid Barrier*.* Endocrinology, 2000. **141**(4): p. 1434-1441.
29. Ghersi-Egea, J.F., et al., *Molecular anatomy and functions of the choroidal blood-cerebrospinal fluid barrier in health and disease.* Acta Neuropathologica, 2018. **135**(3): p. 337-361.
30. Wolburg, H., et al., *Ependymal Cells☆*, in *Reference Module in Biomedical Sciences*. 2015, Elsevier.
31. Christensen, I.B., et al., *Choroid plexus epithelial cells express the adhesion protein P-cadherin at cell-cell contacts and syntaxin-4 in the luminal membrane domain.* American Journal of Physiology-Cell Physiology, 2018. **314**(5): p. C519-C533.
32. Kaur, G. and J.M. Dufour, *Cell lines.* Spermatogenesis, 2012. **2**(1): p. 1-5.
33. Huch, M., et al., *The hope and the hype of organoid research.* Development, 2017. **144**(6): p. 938-941.
34. Strazielle, N. and J.-F. Ghersi-Egea, *In Vitro Models of the Blood–Cerebrospinal Fluid Barrier and Their Use in Neurotoxicological Research*. 2011, Humana Press. p. 161-184.

35. Dabbagh, F., H. Schroten, and C. Schwerk, *In Vitro Models of the Blood–Cerebrospinal Fluid Barrier and Their Applications in the Development and Research of (Neuro)Pharmaceuticals.* Pharmaceutics, 2022. **14**(8): p. 1729.
36. Hogue, M.J., *Human fetal choroid plexus cells in tissue cultures.* The Anatomical Record, 1949. **103**(3): p. 381-399.
37. Wroblewska, Z., et al., *Human brain in tissue culture. II. Studies of long-term cultures.* Journal of Comparative Neurology, 1975. **161**(3): p. 307-316.
38. Wroblewska, Z., et al., *Comparison of human cytomegalovirus growth in MRC-5 human fibroblasts, brain, and choroid plexus cells in vitro.* J Med Virol, 1981. **8**(4): p. 245-56.
39. Redzic, Z.B., *Studies on the human choroid plexus in vitro.* Fluids and Barriers of the CNS, 2013. **10**(1): p. 10.
40. Ishiwata, I., et al., *Establishment and characterization of a human malignant choroids plexus papilloma cell line (HIBCPP).* Human Cell, 2008. **18**(1): p. 67-72.
41. Schwerk, C., et al., *Polar Invasion and Translocation of Neisseria meningitidis and Streptococcus suis in a Novel Human Model of the Blood-Cerebrospinal Fluid Barrier.* PLoS ONE, 2012. **7**(1): p. e30069.
42. Speidel, A., et al., *Transmigration of Trypanosoma brucei across an in vitro blood-cerebrospinal fluid barrier.* iScience, 2022. **25**(4): p. 104014.
43. Pellegrini, L., et al., *Human CNS barrier-forming organoids with cerebrospinal fluid production.* Science, 2020: p. eaaz5626.
44. Villalobos, A.R., J.T. Parmelee, and J.B. Pritchard, *Functional Characterization of Choroid Plexus Epithelial Cells in Primary Culture.* Journal of Pharmacology and Experimental Therapeutics, 1997. **282**(2): p. 1109-1116.
45. Strazielle, N. and J.-F. Ghersi-Egea, *Demonstration of a Coupled Metabolism–Efflux Process at the Choroid Plexus as a Mechanism of Brain Protection Toward Xenobiotics.* The Journal of Neuroscience, 1999. **19**(15): p. 6275-6289.
46. Southwell, B.R., et al., *Thyroxine transport to the brain: role of protein synthesis by the choroid plexus.* Endocrinology, 1993. **133**(5): p. 2116-2126.
47. Lallai, V., A. Ahmed, and C. Fowler, *Method for Primary Epithelial Cell Culture from the Rat Choroid Plexus.* BIO-PROTOCOL, 2020. **10**(4).
48. Monnot, A.D. and W. Zheng, *Culture of Choroid Plexus Epithelial Cells and In Vitro Model of Blood–CSF Barrier*. 2012, Humana Press. p. 13-29.
49. Zheng, W., Q. Zhao, and J.H. Graziano, *Primary culture of choroidal epithelial cells: Characterization of an in vitro model of blood-CSF barrier.* In Vitro Cellular & Developmental Biology - Animal, 1998. **34**(1): p. 40-45.
50. Crook, R.B., H. Kasagami, and S.B. Prusiner, *Culture and Characterization of Epithelial Cells from Bovine Choroid Plexus.* Journal of Neurochemistry, 1981. **37**(4): p. 845-854.

51. Haselbach, M., et al., *Porcine choroid plexus epithelial cells in culture: Regulation of barrier properties and transport processes.* Microscopy Research and Technique, 2001. **52**(1): p. 137-152.
52. Lauer, A.N., et al., *Optimized cultivation of porcine choroid plexus epithelial cells, a blood-cerebrospinal fluid barrier model, for studying granulocyte transmigration.* Laboratory Investigation, 2019. **99**(8): p. 1245-1255.
53. Delery, E.C. and A.G. MacLean, *Culture Model for Non-human Primate Choroid Plexus.* Frontiers in Cellular Neuroscience, 2019. **13**(396).
54. Aldred, A.R., C.M. Brack, and G. Schreiber, *The cerebral expression of plasma protein genes in different species.* Comparative Biochemistry and Physiology Part B: Biochemistry and Molecular Biology, 1995. **111**(1): p. 1-15.
55. Denker, B.M., et al., *Identification, purification, and partial characterization of a novel Mr 28,000 integral membrane protein from erythrocytes and renal tubules.* Journal of Biological Chemistry, 1988. **263**(30): p. 15634-15642.
56. Agre, P., S. Sasaki, and M.J. Chrispeels, *Aquaporins: a family of water channel proteins.* Am J Physiol, 1993. **265**(3 Pt 2): p. F461.
57. Agre, P., et al., *Aquaporin CHIP: the archetypal molecular water channel.* American Journal of Physiology-Renal Physiology, 1993. **265**(4): p. F463-F476.
58. Trillo-Contreras, J.L., et al., *Cellular Distribution of Brain Aquaporins and Their Contribution to Cerebrospinal Fluid Homeostasis and Hydrocephalus.* Biomolecules, 2022. **12**(4).
59. Walz, T., et al., *Biologically active two-dimensional crystals of aquaporin CHIP.* J Biol Chem, 1994. **269**(3): p. 1583-6.
60. Gonen, T., et al., *Lipid-protein interactions in double-layered two-dimensional AQP0 crystals.* Nature, 2005. **438**(7068): p. 633-8.
61. Zelenina, M., *Regulation of brain aquaporins.* Neurochemistry International, 2010. **57**(4): p. 468-488.
62. Ishibashi, K., Y. Tanaka, and Y. Morishita, *The role of mammalian superaquaporins inside the cell.* Biochimica et Biophysica Acta (BBA) - General Subjects, 2014. **1840**(5): p. 1507-1512.
63. Trillo-Contreras, J.L., et al., *Combined effects of aquaporin-4 and hypoxia produce age-related hydrocephalus.* Biochimica Et Biophysica Acta-Molecular Basis of Disease, 2018. **1864**(10): p. 3515-3526.
64. Nielsen, S., et al., *Distribution of the Aquaporin Chip in Secretory and Resorptive Epithelia and Capillary Endothelia.* Proc Natl Acad Sci USA, 1993. **90**(15): p. 7275-7279.
65. Praetorius, J. and S. Nielsen, *Distribution of sodium transporters and aquaporin-1 in the human choroid plexus.* American Journal of Physiology-Cell Physiology, 2006. **291**(1): p. C59-C67.
66. Oshio, K., et al., *Reduced cerebrospinal fluid production and intracranial pressure in mice lacking choroid plexus water channel Aquaporin-1.* The FASEB Journal, 2005. **19**(1): p. 76-78.
67. Jung, J.S., et al., *Molecular characterization of an aquaporin cDNA from brain: candidate osmoreceptor and regulator of water balance.*

Proceedings of the National Academy of Sciences, 1994. **91**(26): p. 13052-13056.
68. Nagelhus, E.A. and O.P. Ottersen, *Physiological roles of aquaporin-4 in brain.* Physiol Rev, 2013. **93**(4): p. 1543-62.
69. Deffner, F., et al., *Aquaporin-4 expression in the human choroid plexus.* Cellular and Molecular Life Sciences, 2022. **79**(2): p. 90.
70. Rash, J.E., et al., *Direct immunogold labeling of aquaporin-4 in square arrays of astrocyte and ependymocyte plasma membranes in rat brain and spinal cord.* Proceedings of the National Academy of Sciences, 1998. **95**(20): p. 11981-11986.
71. Wolburg, H., *Orthogonal arrays of intramembranous particles: a review with special reference to astrocytes.* Journal fur Hirnforschung, 1995. **36**(2): p. 239-258.
72. Wolburg, H., et al., *Chapter one - Structure and Functions of Aquaporin-4-Based Orthogonal Arrays of Particles*, in *International Review of Cell and Molecular Biology*, K.W. Jeon, Editor. 2011, Academic Press. p. 1-41.
73. Mack, A., J. Neuhaus, and H. Wolburg, *Relationship between orthogonal arrays of particles and tight junctions as demonstrated in cells of the ventricular wall of the rat brain.* Cell Tissue Res, 1987. **248**(3): p. 619-25.
74. Rossi, A., et al., *Evidences for a Leaky Scanning Mechanism for the Synthesis of the Shorter M23 Protein Isoform of Aquaporin-4.* Journal of Biological Chemistry, 2010. **285**(7): p. 4562-4569.
75. Pisani, F., et al., *Regulation of aquaporin-4 expression in the central nervous system investigated using M23-AQP4 null mouse.* Glia, 2021. **69**(9): p. 2235-2251.
76. Furman, C.S., et al., *Aquaporin-4 square array assembly: Opposing actions of M1 and M23 isoforms.* Proceedings of the National Academy of Sciences, 2003. **100**(23): p. 13609-13614.
77. De Bellis, M., et al., *Translational readthrough generates new astrocyte AQP4 isoforms that modulate supramolecular clustering, glial endfeet localization, and water transport.* Glia, 2017. **65**(5): p. 790-803.
78. Ding, J.Y., et al., *Hypoxia-inducible factor-1α signaling in aquaporin upregulation after traumatic brain injury.* Neuroscience Letters, 2009. **453**(1): p. 68-72.
79. Gomes, A., et al., *The Emerging Role of microRNAs in Aquaporin Regulation.* Front Chem, 2018. **6**: p. 238.
80. Kitchen, P., et al., *Targeting Aquaporin-4 Subcellular Localization to Treat Central Nervous System Edema.* Cell, 2020. **181**(4): p. 784-799.e19.
81. Nesverova, V. and S. Törnroth-Horsefield, *Phosphorylation-Dependent Regulation of Mammalian Aquaporins.* Cells, 2019. **8**(2): p. 82.
82. Kitchen, P., et al., *Identification and Molecular Mechanisms of the Rapid Tonicity-induced Relocalization of the Aquaporin 4 Channel.* Journal of Biological Chemistry, 2015. **290**(27): p. 16873-16881.
83. Fazzina, G., et al., *The Protein Kinase C Activator Phorbol Myristate Acetate Decreases Brain Edema by Aquaporin 4 Downregulation after*

*Middle Cerebral Artery Occlusion in the Rat.* Journal of Neurotrauma, 2010. **27**(2): p. 453-461.
84. Vandebroek, A. and M. Yasui, *Regulation of AQP4 in the Central Nervous System.* International Journal of Molecular Sciences, 2020. **21**(5): p. 1603.
85. Nagelhus, E.A., et al., *Aquaporin-4 Water Channel Protein in the Rat Retina and Optic Nerve: Polarized Expression in Müller Cells and Fibrous Astrocytes.* The Journal of Neuroscience, 1998. **18**(7): p. 2506-2519.
86. Amiry-Moghaddam, M., D.S. Frydenlund, and O.P. Ottersen, *Anchoring of aquaporin-4 in brain: Molecular mechanisms and implications for the physiology and pathophysiology of water transport.* Neuroscience, 2004. **129**(4): p. 997-1008.
87. Kröger, S., H. Wolburg, and A. Warth, *Redistribution of aquaporin-4 in human glioblastoma correlates with loss of agrin immunoreactivity from brain capillary basal laminae.* Acta Neuropathologica, 2004. **107**(4): p. 311-318.
88. Nico, B., et al., *Altered blood–brain barrier development in dystrophic MDX mice.* Neuroscience, 2004. **125**(4): p. 921-935.
89. Noël, G., et al., *The Laminin-Induced Phosphorylation of PKCδ Regulates AQP4 Distribution and Water Permeability in Rat Astrocytes.* Cellular and Molecular Neurobiology, 2021. **41**(8): p. 1743-1757.
90. Noël, G., D.K.L. Tham, and H. Moukhles, *Interdependence of Laminin-mediated Clustering of Lipid Rafts and the Dystrophin Complex in Astrocytes.* Journal of Biological Chemistry, 2009. **284**(29): p. 19694-19704.
91. Zaccaria, M.L., et al., *Dystroglycan distribution in adult mouse brain: a light and electron microscopy study.* Neuroscience, 2001. **104**(2): p. 311-324.
92. Neely, J.D., et al., *Syntrophin-dependent expression and localization of Aquaporin-4 water channel protein.* Proc Natl Acad Sci U S A, 2001. **98**(24): p. 14108-13.
93. Quinton, P.M., E.M. Wright, and J.M. Tormey, *Localization of sodium pumps in the choroid plexus epithelium.* J Cell Biol, 1973. **58**(3): p. 724-30.
94. Gregoriades, J.M.C., et al., *Genetic and pharmacological inactivation of apical Na+-K+-2Cl(-) cotransporter 1 in choroid plexus epithelial cells reveals the physiological function of the cotransporter.* American Journal of Physiology-Cell Physiology, 2019. **316**(4): p. C525-C544.
95. Wright, E.M. and Y. Saito, *The Choroid Plexus as a Route from Blood to Brain.* Annals of the New York Academy of Sciences, 1986. **481**(1 The Neuronal): p. 214-220.
96. Alvarez-Leefmans, F.J., *CrossTalk proposal: Apical NKCC1 of choroid plexus epithelial cells works in the net inward flux mode under basal conditions, maintaining intracellular Cl- and cell volume.* Journal of Physiology-London, 2020. **598**(21): p. 4733-4736.
97. MacAulay, N. and C.R. Rose, *CrossTalk opposing view: NKCC1 in the luminal membrane of choroid plexus is outwardly directed under basal*

*conditions and contributes directly to cerebrospinal fluid secretion.* The Journal of Physiology, 2020. **598**(21): p. 4737-4739.
98. Husted, R.F. and D.J. Reed, *Regulation of cerebrospinal fluid potassium by the cat choroid plexus.* The Journal of Physiology, 1976. **259**(1): p. 213-221.
99. Wu, Q., et al., *Functional demonstration of Na+-K+-2Cl- cotransporter activity in isolated, polarized choroid plexus cells.* Am J Physiol, 1998. **275**(6): p. C1565-72.
100. Fröhlich, F., et al., *Potassium Dynamics in the Epileptic Cortex: New Insights on an Old Topic.* The Neuroscientist, 2008. **14**(5): p. 422-433.
101. Steffensen, A.B., et al., *Cotransporter-mediated water transport underlying cerebrospinal fluid formation.* Nature Communications, 2018. **9**(1): p. 2167.
102. Venero, J.L., et al., *Detailed localization of aquaporin-4 messenger RNA in the CNS: preferential expression in periventricular organs.* Neuroscience, 1999. **94**(1): p. 239-250.
103. Speake, T., L.J. Freeman, and P.D. Brown, *Expression of aquaporin 1 and aquaporin 4 water channels in rat choroid plexus.* Biochimica et Biophysica Acta (BBA) - Biomembranes, 2003. **1609**(1): p. 80-86.
104. Trillo-Contreras, J., et al., *AQP1 and AQP4 Contribution to Cerebrospinal Fluid Homeostasis.* Cells, 2019. **8**(2): p. 197.
105. Masseguin, C., et al., *Aging affects choroidal proteins involved in CSF production in Sprague-Dawley rats.* Neurobiology of Aging, 2005. **26**(6): p. 917-927.
106. Shuangshoti, S. and M.G. Netsky, *Human choroid plexus: Morphologic and histochemical alterations with age.* American Journal of Anatomy, 1970. **128**(1): p. 73-95.
107. Serot, J.M., et al., *Choroid plexus and ageing in rats: a morphometric and ultrastructural study.* European Journal of Neuroscience, 2001. **14**(5): p. 794-798.
108. Emerich, D.F., et al., *The choroid plexus in the rise, fall and repair of the brain.* BioEssays, 2005. **27**(3): p. 262-274.
109. Soria Lopez, J.A., H.M. González, and G.C. Léger, *Chapter 13 - Alzheimer's disease*, in *Handbook of Clinical Neurology*, S.T. Dekosky and S. Asthana, Editors. 2019, Elsevier. p. 231-255.
110. Xu, Z., et al., *Deletion of aquaporin-4 in APP/PS1 mice exacerbates brain Aβ accumulation and memory deficits.* Molecular Neurodegeneration, 2015. **10**(1).
111. Feng, W., et al., *Microglia prevent beta-amyloid plaque formation in the early stage of an Alzheimer's disease mouse model with suppression of glymphatic clearance.* Alzheimer's Research & Therapy, 2020. **12**(1).
112. Peng, W., et al., *Suppression of glymphatic fluid transport in a mouse model of Alzheimer's disease.* Neurobiology of Disease, 2016. **93**: p. 215-225.
113. Mack, A.F., R. Bihlmaier, and F. Deffner, *Shifting from ependyma to choroid plexus epithelium and the changing expressions of aquaporin-1 and aquaporin-4.* The Journal of Physiology, 2023.

114. Bihlmaier, R., et al., *Aquaporin-1 and Aquaporin-4 Expression in Ependyma, Choroid Plexus and Surrounding Transition Zones in the Human Brain.* Biomolecules, 2023. **13**(2): p. 212.
115. Rowitch, D.H. and A.R. Kriegstein, *Developmental genetics of vertebrate glial–cell specification.* Nature, 2010. **468**(7321): p. 214-222.
116. Liddelow, S.A., *Development of the choroid plexus and blood-CSF barrier.* Frontiers in Neuroscience, 2015. **9**.
117. Korzhevskii, D.É., *Proliferative zones in the epithelium of the choroid plexuses of the human embryo brain.* Neuroscience and Behavioral Physiology, 2000. **30**(5): p. 509-512.
118. Barkho, B.Z. and E.S. Monuki, *Proliferation of Cultured Mouse Choroid Plexus Epithelial Cells.* Plos One, 2015. **10**(3).
119. Dani, N., et al., *A cellular and spatial map of the choroid plexus across brain ventricles and ages.* Cell, 2021. **184**(11): p. 3056-3074.e21.
120. Li, Y., J. Chen, and M. Chopp, *Cell proliferation and differentiation from ependymal, subependymal and choroid plexus cells in response to stroke in rats.* Journal of the Neurological Sciences, 2002. **193**(2): p. 137-146.
121. Tsutsumi, M., M.K. Skinner, and E. Sanders-Bush, *Transferrin gene expression and synthesis by cultured choroid plexus epithelial cells: Regulation by Serotonin and Cyclic Adenosine 3',5'-Monophosphate.* Journal of Biological Chemistry, 1989. **264**(16): p. 9626-9631.
122. Schroten, M., et al., *A Novel Porcine In Vitro Model of the Blood-Cerebrospinal Fluid Barrier with Strong Barrier Function.* PLoS ONE, 2012. **7**(6): p. e39835.
123. Herbert, J., et al., *Transthyretin.* Neurology, 1986. **36**(7): p. 900-900.
124. Hakvoort, A., et al., *The Polarity of Choroid Plexus Epithelial Cells In Vitro Is Improved in Serum Free Medium.* Journal of Neurochemistry, 1998. **71**.
125. Boassa, D., W.D. Stamer, and A.J. Yool, *Ion channel function of aquaporin-1 natively expressed in choroid plexus.* J Neurosci, 2006. **26**(30): p. 7811-9.
126. Szmydynger-Chodobska, J., et al., *Expression of junctional proteins in choroid plexus epithelial cell lines: a comparative study.* Cerebrospinal fluid research, 2007. **4**: p. 11-11.
127. Lallai, V., et al., *Nicotine Acts on Cholinergic Signaling Mechanisms to Directly Modulate Choroid Plexus Function.* eNeuro, 2019. **6**(2): p. ENEURO.0051-19.2019.
128. Segeritz, C.P. and L. Vallier, *Cell Culture: Growing Cells as Model Systems In Vitro.* Basic Science Methods for Clinical Researchers, 2017: p. 151-72.
129. Noell, S., et al., *Effects of agrin on the expression and distribution of the water channel protein aquaporin-4 and volume regulation in cultured astrocytes.* European Journal of Neuroscience, 2007. **26**(8): p. 2109-2118.
130. Noël, G., et al., *Agrin plays a major role in the coalescence of the aquaporin-4 clusters induced by gamma-1-containing laminin.* Journal of Comparative Neurology, 2020. **528**(3): p. 407-418.

131. Rurak, J., et al., *Distribution of potassium ion and water permeable channels at perivascular glia in brain and retina of the Large<sup>myd</sup> mouse.* Journal of Neurochemistry, 2007. **103**(5): p. 1940-1953.
132. Belmaati Cherkaoui, M., et al., *Dp71 contribution to the molecular scaffold anchoring aquaporine-4 channels in brain macroglial cells.* Glia, 2021. **69**(4): p. 954-970.
133. Haenggi, T., et al., *The role of utrophin and Dp71 for assembly of different dystrophin-associated protein complexes (DPCS) in the choroid plexus and microvasculature of the brain.* Neuroscience, 2004. **129**(2): p. 403-413.
134. Nicchia, G.P., et al., *Dystrophin-dependent and -independent AQP4 pools are expressed in the mouse brain.* Glia, 2008. **56**(8): p. 869-876.
135. Enger, R., et al., *Molecular scaffolds underpinning macroglial polarization: An analysis of retinal Müller cells and brain astrocytes in mouse.* Glia, 2012. **60**(12): p. 2018-2026.
136. Smith, A.J., et al., *Aggregation state determines the localization and function of M1– and M23–aquaporin-4 in astrocytes.* Journal of Cell Biology, 2014. **204**(4): p. 559-573.
137. Nicchia, G.P., et al., *Expression of multiple AQP4 pools in the plasma membrane and their association with the dystrophin complex.* Journal of Neurochemistry, 2008. **105**(6): p. 2156-2165.
138. Palazzo, C., et al., *AQP4ex is crucial for the anchoring of AQP4 at the astrocyte end-feet and for neuromyelitis optica antibody binding.* Acta Neuropathologica Communications, 2019. **7**(1).
139. Wang, C., et al., *Mechanism of aquaporin 4 (AQP 4) up-regulation in rat cerebral edema under hypobaric hypoxia and the preventative effect of puerarin.* Life Sciences, 2018. **193**: p. 270-281.
140. Szpilbarg, N., et al., *Oxygen regulation of aquaporin-4 in human placenta.* Reproductive BioMedicine Online, 2018. **37**(5): p. 601-612.
141. Evans, P.G., et al., *Non-Invasive MRI of Blood–Cerebrospinal Fluid Barrier Function.* Nature Communications, 2020. **11**(1).
142. Chen, R.L., et al., *Age-related changes in choroid plexus and blood–cerebrospinal fluid barrier function in the sheep.* Experimental Gerontology, 2009. **44**(4): p. 289-296.
143. May, C., et al., *Cerebrospinal fluid production is reduced in healthy aging.* Neurology, 1990. **40**(3_part_1): p. 500-500.
144. Pfeiffer, F., A.F. Mack, and H. Wolburg, *Topological Aspects of the Blood–Brain and Blood–Cerebrospinal Fluid Barriers and Their Relevance in Inflammation*, in *The Blood Brain Barrier and Inflammation*, R. Lyck and G. Enzmann, Editors. 2017, Springer International Publishing: Cham. p. 23-48.
145. Deffner, F., et al., *Histological Evidence for the Enteric Nervous System and the Choroid Plexus as Alternative Routes of Neuroinvasion by SARS-CoV2.* Frontiers in Neuroanatomy, 2020. **14**(74).
146. Lazarevic, I., et al., *The choroid plexus acts as an immune cell reservoir and brain entry site in experimental autoimmune encephalomyelitis.* Fluids and Barriers of the CNS, 2023. **20**(1).

147. Association, A.s., *2019 Alzheimer's disease facts and figures.* Alzheimer's & Dementia, 2019. **15**(3): p. 321-387.
148. Li, X., et al., *Global, regional, and national burden of Alzheimer's disease and other dementias, 1990–2019.* Frontiers in Aging Neuroscience, 2022. **14**.
149. Perl, D.P., *Neuropathology of Alzheimer's Disease.* Mount Sinai Journal of Medicine: A Journal of Translational and Personalized Medicine, 2010. **77**(1): p. 32-42.
150. Scheltens, P., et al., *Alzheimer's disease.* The Lancet, 2021. **397**(10284): p. 1577-1590.
151. Serot, J.-M., et al., *Morphological alterations of the choroid plexus in late-onset Alzheimer's disease.* Acta Neuropathologica, 2000. **99**(2): p. 105-108.
152. Serot, J.M., M.C. Bene, and G.C. Faure, *Choroid plexus, ageing of the brain, and Alzheimer's disease.* Frontiers in Bioscience-Landmark, 2003. **8**: p. S515-S521.
153. Wen, G.Y., H.M. Wisniewski, and R.J. Kascsak, *Biondi ring tangles in the choroid plexus of Alzheimer's disease and normal aging brains: a quantitative study.* Brain Research, 1999. **832**(1): p. 40-46.
154. Choi, J.D., et al., *Choroid Plexus Volume and Permeability at Brain MRI within the Alzheimer Disease Clinical Spectrum.* Radiology, 2022. **304**(3): p. 635-645.
155. Mawuenyega, K.G., et al., *Decreased Clearance of CNS β-Amyloid in Alzheimer's Disease.* Science, 2010. **330**(6012): p. 1774-1774.
156. Municio, C., et al., *Choroid Plexus Aquaporins in CSF Homeostasis and the Glymphatic System: Their Relevance for Alzheimer's Disease.* International Journal of Molecular Sciences, 2023. **24**(1): p. 878.

# 9 Erklärung zum Eigenanteil

Die Arbeit wurde am Institut für Klinische Anatomie und Zellanalytik unter Betreuung von Herrn Professor Dr. med. Bernhard Hirt und Herrn Dr. Andreas Mack durchgeführt.

Die Konzeption der Studie erfolgte durch Herrn Dr. Andreas Mack.

Die Euthanasie und Dekapitation der Mäuse erfolgte durch Frau Melanie Scharr und Herrn Dr. rer. nat. Peter Neckel.

Die Entnahme des humanen Gewebes wurde von mir mit Unterstützung durch Herrn Dr. rer. nat. Peter Neckel, Herrn Jürgen Papp und Herrn Dr. Andreas Mack durchgeführt.

Die Feinpräparation des *Plexus choroideus* wurde von mir nach Einarbeitung durch Herrn Dr. Andreas Mack und in Zusammenarbeit mit Herrn Dr. Andreas Mack durchgeführt.

Die Einbettung der Gewebe und das Schneiden am Kryostat wurde von Herrn Ulrich Mattheus durchgeführt.

Die Arbeit mit den Zell- und Organkulturen wurde nach Einarbeitung durch Frau Melanie Scharr, Frau Sarah Frosch und Frau Karin Seid von mir eigenständig durchgeführt.

Die Hypoxie Versuche und Zellzählungen wurden nach Einarbeitung durch Herrn Dr. Andreas Mack von mir eigenständig durchgeführt.

Die immunhistologischen Färbungen wurden nach Einarbeitung durch Herrn Ulrich Mattheus von mir eigenständig durchgeführt.

Die Mikroskopie wurde nach Einarbeitung durch Herrn Dr. Andreas Mack von mir eigenständig durchgeführt.

Die in dieser Arbeit enthaltene Abbildung 1 wurde mit Erlaubnis (open access) entnommen aus: „The glymphatic system: Current understanding and modeling“, Bohr et al., iScience, 2022.

Die in dieser Arbeit enthaltene Abbildung 2 wurde mit Erlaubnis (License Number: 5764860012218) entnommen aus: M. Amiry-Moghaddam,D.S. Frydenlund,O.P. Ottersen, Anchoring of aquaporin-4 in brain: Molecular mechanisms and implications for the physiology and pathophysiology of water transport. Neuroscience. 2004.

Die in dieser Arbeit enthaltenen Abbildungen 3, 4 und 30 wurden von mir in Zusammenarbeit mit Herrn Dr. Andreas Mack erstellt und aus unseren gemeinsamen Veröffentlichungen entnommen.

Die restlichen in dieser Arbeit enthaltenen Abbildungen 5-29 wurden von mir nach Einarbeitung durch Herrn Dr. Andreas Mack eigenständig erstellt.

Die statistische Auswertung erfolgte nach Anleitung durch Herrn Dr. Andreas Mack und Beratung durch das Institut für Klinische Epidemiologie und angewandte Biometrie durch mich.

Ich versichere, das Manuskript selbständig nach Anleitung durch Herrn Dr. Andreas Mack verfasst zu haben und keine weiteren als die von mir angegebenen Quellen verwendet zu haben.

Teile dieser Arbeit sind in vorherigen Veröffentlichungen (Bihlmaier et al. 2023, Mack et al. 2023) verwendet worden.

Tübingen, den 17.06.2024

Ronja Bihlmaier

# 10 Veröffentlichungen

Teile der vorliegenden Dissertationsschrift wurden bereits in den folgenden Publikationen veröffentlicht:

**Bihlmaier R**., Deffner F., Mattheus U., Neckel P., Hirt B., Mack A., Aquaporin-1 and Aquaporin-4 Expression in Ependyma, Choroid Plexus and Surrounding Transition Zones in the Human Brain. Biomolecules. 2023. doi: 10.3390/biom13020212.

Mack A., **Bihlmaier R**., Deffner F., Shifting from ependyma to choroid plexus epithelium and the changing expression of aquaporin-1 and aquaporin-4. Journal of Physiology. 2023. doi: 10.1113/JP284196.

# 11 Danksagung

Mein erster Dank gilt meinem Betreuer Andreas Mack, der mich weit über meine Erwartungen hinaus bei allen Schritten dieser Arbeit unterstützte. Er hat seine langjährige Erfahrung und sein Wissen in zahlreichen Diskussionen mit mir geteilt, mich für die Wissenschaft begeistert und mir ermöglicht, all meine Ideen umzusetzen. Vielen Dank, dass du so viel Zeit und Arbeit in dieses spannende Projekt investiert hast.

Als nächstes möchte ich einen besonderen Dank an meinen Doktorvater Prof. Dr. med. Bernhard Hirt richten, der dieses Projekt von Anfang an unterstützte und möglich machte, und der sich in besonderem Maße für mich bei der Bewerbung für das IZKF-Stipendium einsetzte.

Ich möchte mich herzlich beim gesamten Team des Instituts für Klinische Anatomie und Zellanalytik für die schöne und spannende Zeit bedanken. Danke, dass ihr mich so herzlich aufgenommen habt, immer wieder für mich mitgekocht habt, während ich noch in den Experimenten steckte, euch nach meiner Arbeit erkundigt und eure wissenschaftliche Erfahrung mit mir geteilt habt. Ich habe mich immer sehr wohl gefühlt und das Miteinander sehr genossen.

Im Speziellen möchte ich mich bei Melanie Scharr bedanken, die eine wichtige Ansprechpartnerin für mich war und sich sehr viel Zeit nahm, um mich in die Arbeit mit den Zellkulturen einzulernen. Ihre Unterstützung ermöglichte mir einen schnellen Einstieg und ein gutes Vorankommen mit den Experimenten.

Des Weiteren danke ich Ulrich Mattheus, der mich mit viel Zeit und Geduld in die Histologie einführte und darüber hinaus mit seiner herzlichen Art immer für mich da war und mir bei allen möglichen Problemen weiterhalf.

Peter Neckel danke ich für seine Unterstützung bei der Entnahme des Körperspendermaterials und für seinen wertvollen Beitrag zu den Veröffentlichungen und Experimenten sowie für seine Einschätzungen bezüglich der Zellkulturen.

Auch Karin Seid und Sarah Frosch möchte ich für ihre Anleitung im Umgang mit den Kulturen und Unterstützung bei weiteren Anliegen unterschiedlichster Art danken.

Ein besonderer Dank gilt meiner forschungsbegeisterten Freundin Nicole Neuser, die mir neben emotionalem Beistand auch bei einigen Fragestellungen weiterhalf.

Dem Promotionskolleg des IZKFs möchte ich meinen herzlichen Dank aussprechen für die Betreuung, die vielen Ratschläge und die Möglichkeit, einen umfassenderen Einblick in die Wissenschaftswelt und ganz unterschiedliche Forschungsbereiche zu erhalten.

Ich möchte mich ebenfalls bei den anonymen Körperspenderinnen und Körperspendern für ihr Vertrauen und ihren wichtigen Beitrag zur Forschung bedanken.

Den Verantwortlichen des Instituts für Klinische Epidemiologie und angewandte Biometrie danke ich für ihre Unterstützung und Beratung bezüglich der statistischen Auswertung.

Zuletzt möchte ich mich bei meiner Familie, meinen Freundinnen und Freunden und meinem Partner Jakob Krenn bedanken, die mich bei dieser Arbeit begleitet haben. Neben Anregungen, Hilfestellungen und Verbesserungsvorschlägen waren sie emotionale Stützen für mich und haben viel Verständnis dafür aufgebracht, wenn ich diese Arbeit in meinem Zeitmanagement priorisiert habe. Danke für euren Zuspruch, euer Vertrauen in mich und dafür, dass ihr immer für mich da seid.